UNIVERSITY OF CALIFORNIA, SAN DIEGO

Polarity Regulation During Neuronal Migration and Differentiation

A Dissertation submitted in partial satisfaction of the Requirements for the degree Doctor of Philosophy

in

Biomedical Sciences

by

Holden Richard Higginbotham

Committee in charge:

Professor Joseph Gleeson, Chair
Professor Don Cleveland
Professor Bruce Hamilton
Professor Karen Oegema
Professor Dennis O'Leary

2008

The Dissertation of Holden Richard Higginbotham is approved, and it is acceptable in quality and form for publication on microfilm:

_____

_____

_____

_____

_____

Chair

University of California, San Diego

2008

DEDICATION

To my Wife, Nicole, who's a super support and a delight.

TABLE OF CONTENTS

LIST OF FIGURES

ACKNOWLEDGEMENTS

I would like to acknowledge Professor Joseph Gleeson for his enthusiastic and motivating support and mentorship.

I would also like to thank the Gleeson Lab for stimulating discussions and support.

Work in Chapter II was published as: Higginbotham, Holden; Bielas, Stephanie; Tanaka, Teruyuki; Gleeson, Joseph G. Transgenic mouse line with green-fluorescent protein-labeled Centrin 2 allows visualization of the centrosome in living cells. Transgenic Research, **13**: 155-164, 2004.

Part of work in Chapter III was published as: Higginbotham, Holden; Tanaka, Teruyuki; Brinkman, Brendan; Gleeson, Joseph G. GSK3beta and PKCzeta function in centrosome localization and process stabilization during Slit-mediated neuronal repolarization. Mol Cell Neurosci. **32**(1-2): 118-32, 2006.

Part of work in Chapter IV was published as: Koizumi, Hiroyuki; Higginbotham, Holden; Poon, Tiffany; Brinkman, Brendan; Gleeson, Joseph G. Doublecortin maintains bipolar shape and nuclear translocation during migration in the adult forebrain. Nat Neurosci. **9**(6): 779-86. 2006.

VITA

2000	Bachelor of Science, Magna Cum Laude, Brigham Young University, Provo, UT
2008	Doctor of Philosophy, University of California, San Diego

PUBLICATIONS

Higginbotham, Holden; Bielas, Stephanie; Tanaka, Teruyuki; Gleeson, Joseph G. Transgenic mouse line with green-fluorescent protein-labeled Centrin 2 allows visualization of the centrosome in living cells. Transgenic Research, 13: 155-164, 2004.

Higginbotham, Holden; Tanaka, Teruyuki; Brinkman, Brendan; Gleeson, Joseph G. GSK3beta and PKCzeta function in centrosome localization and process stabilization during Slit-mediated neuronal repolarization. Mol Cell Neurosci. 32(1-2): 118-32, 2006.

Koizumi, Hiroyuki; Higginbotham, Holden; Poon, Tiffany; Brinkman, Brendan; Gleeson, Joseph G. Doublecortin maintains bipolar shape and nuclear translocation during migration in the adult forebrain. Nat Neurosci. 9(6): 779-86. 2006.

Higginbotham, Holden; Gleeson, Joseph G. The centrosome in neuronal development. Trends in Neurosci. 30(6): 276-83, 2007.

FIELDS OF STUDY

Major Field: Biomedical Science

Studies in Cell Biology and Developmental Neuroscience
Professor Joseph Gleeson

ABSTRACT OF THE DISSERTATION

Polarity Regulation During Neuronal Migration and Differentiation

by

Holden Richard Higginbotham

Doctor of Philosophy in Biomedical Sciences

University of California, San Diego, 2008

Professor Joseph Gleeson, Chair

A key requirement of normal brain development is that during their proliferation, migration and differentiation precursors and daughter neurons establish and maintain a specific cell polarity, defined as having one or more axes of symmetry. Cell polarization divides the cell into different functional domains and facilitates the orientation of neurons within the overall brain framework, allowing functional connections to be established. In this dissertation I will describe work I have performed to address the question of how cell

polarity is regulated during neuron migration and differentiation. I will address how the cytoskeleton and cell polarity are dynamically regulated in migrating neurons of the embryonic and adult forebrain. Specifically, I will investigate how the position of the centrosome is regulated in response to guidance cues in tangentially migrating neurons. To visualize the centrosome I have generated a transgenic mouse line that expresses a GFP-tagged centrosomal protein. *In vitro* studies were conducted using tangentially migrating neurons from postnatal transgenic mice to determine what molecules regulate the centrosome's position. I found that the polarity molecules GSK-3β and aPKCζ regulate the centrosome's position and that repolarization in response to guidance cues depends the activity of these factors. Additionally, I analyze centrosomal position during radial migration in the embryonic cortex and report on the effect of disrupting polarity factors during migration. Next I report on the role of the microtubule-associated protein Doublecortin (DCX) in tangentially migrating neurons and show that loss of DCX results in inefficient consolidation of a single leading process during migration. Lastly, I show that during radial migration in embryogenesis, DCX cooperates with its gene-family member DCK1 to exit the multipolar stage of migration and assume a bipolar morphology.

I. INTRODUCTION

The mammalian brain, with its anatomical intricacy, complex chemistry, electrical properties, and cellular diversity is a remarkable structure that regulates most organ and sensory systems, memory and behavior. Concomitant with its complexity, however, is a considerable susceptibility to aberrations that can occur either during development, after injury, or with aging. In humans, some of the resulting changes fall within the spectrum of normal human experience, while others are more severe, significantly disrupting a person's quality of life, like epilepsy, autism, and schizophrenia.

Although the brain can dynamically respond to new conditions by generating additional neurons and reforming connections, many defects that result from injury or developmental abnormalities are long-lasting and intractable, demonstrating that in many ways the brain is a relatively static structure after development is completed. For this reason, understanding how normal neuronal development proceeds is crucial not only for characterizing and treating disorders early on, but also for generating therapeutic strategies for older individuals that restore some of the developing brain's plasticity.

A key requirement of normal brain development is that during their proliferation, migration and differentiation individual neurons and their precursors establish and maintain a specific cell polarity, defined as having one or more axes of symmetry. Cell polarization divides the cell into different functional domains and facilitates the orientation of neurons within the overall brain framework, which is necessary for establishing cell-cell connections. In this dissertation I will describe work I have performed to address the question of how cell polarity is regulated during neuron migration and differentiation.

Embryonic Neurogenesis

The earliest initial event in the formation of the vertebrate CNS is gastrulation of the blastula to form three germ layers: the endoderm, mesoderm, and ectoderm. A structure termed the notochord arises from the mesoderm along the future anterior-posterior (A-P) axis of the embryo and produces molecular signals that induce the overlying ectoderm to adopt a neural fate. This process, known as neurulation, occurs around embryonic day 8 and 9 (E8,9) in mouse and E20-25 in humans. The induced neural plate then undergoes morphological changes where its lateral margins fold inward and close off to form the neural tube (Bystron et al., 2008). At E9 in mouse and E25 in humans, the anterior portion of the neural tube becomes subdivided into vesicle-like structures that will be endowed with forebrain, midbrain and hindbrain character, termed the prosencephalon, mesencephalon, and rhombencehalon. The rostral end of the prosencephalon becomes the telencephalon, which after development is complete is composed of the dorsal neocortex and its associated structures together with the ventral basal ganglia (Takahashi and Liu, 2006).

Neocortical Development

The cortex has increased in size and complexity throughout evolution to become in mammals a highly organized structure that contains hundreds of different neuronal and glial cell types (Molyneaux et al., 2007). The outermost region of the mammalian cortex, the neocortex, is unique to mammals and is responsible for their higher cognitive functions like sensory perception, consciousness, generation of motor commands and language. While other regions of the brain are organized into cellular clusters called

nuclei, the neocortex is organized into six sheet-like layers. These laminae are composed of two major classes of neurons: interneurons that transmit signals via gamma-aminobutyric acid (GABA) and cortical projection neurons that use glutamate (Molyneaux et al., 2007). In general, interneurons make local connections and generate primarily inhibitory neurotransmissions while projection neurons extend axons to distant targets outside the cortex and whose neurotransmissions are excitatory. Projection neurons are generated within the neocortex from progenitors that divide in the germinal zone that lines the inner fluid-filled lateral ventricles of the neocortex, termed the ventricular zone (VZ), while interneurons are primarily generated from progenitors located in the ventral telencephalon.

The hippocampus and olfactory cortex (known collectively as the "allocortex") are phylogenetically older structures than the neocortex whose primary functions are short-term memory/spatial navigation and olfaction, respectively. While they are also composed of both interneurons and projection neurons, allocortical neurons are generated in regions distinct from neocortical neurons and they arise later in development. Interestingly, it is only in the allocortex where adult neurogenesis is known to occur (Zhao et al., 2008). The evidence for adult neurogenesis in the neocortex is disputed (Gould et al., 1999; Rakic, 2002) and the evolutionary reasons for the lower neurogenic capacity of the neocortex are not known.

Neuronal Proliferation in the Cortex

The neocortex forms at the rostral end of the neural tube as a single sheet of pseudostratified neuroepithelial cells that are derived from the neural plate (Bystron et al.,

2008; Molyneaux et al., 2007). Neuroepithelial cells reside immediately adjacent to the fluid-filled lateral ventricles, (a region termed the ventricular zone [VZ]) and divide symmetrically, with the cleavage plane perpendicular to the ventricular surface, generating identical daughter cells. After expansion of the progenitor pool, self-renewing asymmetric divisions commence that generate a daughter progenitor cell and a daughter neuron. Asymmetric divisions begin around E10 in mice and E33 in humans and they mark the onset of neurogenesis, or the birth of projection neurons destined for the cortical plate (CP). Soon after neurogenesis begins a cell layer known as the primordial plexiform layer or preplate begins to form between the progenitor layer and the pial surface. The preplate contains a heterogeneous, transient population of cells that is derived both from the underlying neuroepithelial progenitors and extra-cortical locations. In addition to contributing to the preplate, neuroepithelial cells and their progeny will produce all of the projections neurons of the CP.

As neurogenesis proceeds, neuroepithelial cells downregulate their epithelial characteristics and become radial glial cells (RGCs), which share some molecular similarities with neuroepithelia, although most radial glial cells are restricted in their fate to either astrocytes, oligodendrocytes or neurons (Bystron et al., 2008; Gotz and Huttner, 2005). Possessing long processes that extend from the VZ to the pial surface, RGCs are highly polarized cells that have long been known to serve as migratory guides to projection neurons migrating from the VZ into the CP (Rakic, 1972). More recently, it has become well-accepted that RGCs have an additional function as progenitor cells that make major contributions to cortical neurogenesis (Anthony et al., 2004; Noctor et al., 2001). Radial glial cells divide multiple times during their lifetime, either dividing

symmetrically to produce two radial glial cells or asymmetrically to produce a radial glial daughter and either an intermediate progenitor or a neuron. In late stages of neurogenesis the radial glial scaffold is dismantled and RGCs are transformed into astrocytes (Schmechel and Rakic, 1979). However, there is evidence that some RGCs remain postnatally to play a role in adult neurogenesis (Merkle et al., 2004).

One peculiar feature of RGCs and neuroepithelial cells bears mentioning. During S-phase of the cell cycle the nucleus moves through the thin apical (pial) process into the upper VZ. Later, just before metaphase and cytokinesis, the nucleus moves rapidly towards the ventricle where it completes mitosis. The purpose of this movement termed 'interkinetic nuclear migration' (INM) isn't understood, but some genetic disruptions that alter cortical formation also disrupt INM (Gambello et al., 2003). It has been suggested that a structural link between the centrosome and nucleus is required for INM (Xie et al., 2007).

Around the time that projection neurons begin to accumulate in the CP (E13 in mice), an additional proliferative layer known as the subventricular zone (SVZ) forms above the VZ and is composed of cells called intermediate progenitors (IPs), or basal progenitors (Dehay and Kennedy, 2007). IPs are initially generated by asymmetric division of radial glia, but at later stages of development the IP pool expands internally by self-renewing symmetric divisions (Noctor et al., 2004). Unlike RGCs, IPs do not contact the ventricle nor do they act as a migratory scaffold for neurons. Instead they adopt a multipolar morphology and divide symmetrically to either self-renew or generate two postmitotic daughter neurons (Noctor et al., 2004; Noctor et al., 2008).

The importance of IPs to overall neocorticogenesis is not well understood. The SVZ has increased in size and complexity during the course of evolution and the cellular organization of the SVZ in primates is distinct from that of any other species (Bystron et al., 2008). The SVZ also expands during neurogenesis as progenitors in the VZ are depleted, suggesting IPs cells play an important role in the generation of late-born neurons. For example, in humans the SVZ becomes the principle source of upper-layer neurons in late neurogenesis after the VZ has been reduced to a one-cell layer. Since upper-layer neurons are a recent evolutionary addition, it has been proposed that the SVZ in primates has expanded to increase the number of cortical neurons (Molyneaux et al., 2007).

How are the identities of projection neurons of the different cortical layers indicated? In large measure cell fate is determined in a temporal manner, where early cell divisions generate neurons of the deep layers and later divisions the upper layers. This timing appears to be intrinsic to the precursors (Shen et al., 2006), but environment can also influence call fate. Transplantation experiments show that earlier born neurons can respond to their environment to generate pyramidal neurons of all layers, but as development proceeds transplanted progenitors become more restricted in their potential (Frantz and McConnell, 1996; McConnell and Kaznowski, 1991).

The embryonic ventral telencephalon consists of the medial and lateral ganglionic eminences (MGE and LGE) in which reside the progenitors of cortical GABAergic interneurons (de Carlos et al., 1996; Wichterle et al., 1999). The ventral LGE contains progenitors of the GABAergic projection neurons of the striatum and nucleus accumbens, while the dorsal LGE contains progenitors for neurons destined for the olfactory bulb.

The MGE contains interneuron precursors bound for the cortex, hippocampus, and globus pallidus.

Adult Neurogenesis

Long thought to be a static structure after development was complete, it came as a surprise to neuroscientists to discover that neurogenesis occurs in adult rodents and humans (Altman and Das, 1966; Eriksson et al., 1998). This has been clearly demonstrated in two locations: the subventricular zone (SVZ) near the lateral ventricles and the subgranular zone (SGZ) in the hippocampus. Neurons generated in the adult SVZ migrate rostrally into the olfactory bulbs where they become granule and periglomerular neurons while the SGZ gives rise to granule cells of the dentate gyrus. The newborn neurons can integrate into the adult tissue and establish functional circuitry (Zhao et al., 2008).

The multipotent stem cells of the adult SVZ have their embryonic origin in the MGE and LGE (Young et al., 2007). In the SVZ there are three types of precursor cells: type C transit amplifying precursor cells, type A migrating neuroblasts and type B GFAP-positive astrocytes (Doetsch et al., 1997). Type A cells divide as they migrate from the SVZ into the olfactory bulb through the rostral migratory stream (RMS) (Lois and Alvarez-Buylla, 1994). Clusters of rapidly dividing immature precursors (type C cells) are scattered along the chain of migrating cells and contribute to the type A pool while type B astrocytes ensheath the pathway in a tube-like structure (Lim and Alvarez-Buylla, 1999). Type B astrocytes not only stimulate the proliferation of type C cells, but they also can act as neural stem cells themselves (Doetsch et al., 1999) and have been proposed to

be derived from embryonic radial glial cells (Tramontin et al., 2003). More recently it has been shown that precursors in the SVZ have different embryonic origins and produce different neuronal progeny when heterotopically grafted or cultured, suggesting that adult neural stems cells have a more restricted fate than their embryonic precursors (Merkle et al., 2007; Young et al., 2007).

What signaling pathways regulate progenitor division during embryonic and adult neurogenesis? One important aspect of neurogenesis is the propagation of progenitor identity during division to prevent a premature depletion of the progenitor pool. Two basic mechanisms seem to be at work to achieve this: the asymmetric segregation of cell fate determinants into only one of two daughter cells and the orientation of the cleavage plane so that one of the daughter cells maintains contact with the proliferative niche (Knoblich, 2008). Both mechanisms require the exquisite regulation of polarity factors and the cytoskeleton.

In addition, several signaling pathways promote a radial glial identity including the Wnt, Shh, Notch, neuregulin/ErbB, and FGF pathways (Anton et al., 1997; Dang et al., 2006; Gaiano et al., 2000; Machon et al., 2003; Yoon et al., 2004; Zhou et al., 2004a). Interestingly, signaling from daughter neurons migrating along radial glial fibers can also promote a radial glial identity, presumably as a mechanism to maintain the glial scaffold during migration (Anton et al., 1997). In addition to ligand/receptor interactions, calcium signaling can modulate proliferation in the neocortex as waves of calcium influx propagate through RGCs (Weissman et al., 2004). In the adult, transplantation experiments have revealed the crucial role of the local environment in controlling the proliferation, migration and differentiation of precursors. Many of the signaling pathways

described in embryonic development continue to function in the adult brain (Ninkovic and Gotz, 2007).

Perturbation in the regulation of progenitor division causes disease in both rodents and humans. Under-proliferation or over-proliferation in neuropeithelial cells and RGCs results in microcaphaly and macrocephaly, repectively. Focal disruptions in proliferation can lead to focal cortical dysplasia (Pang et al., 2008). Interestingly, many of the genes implicated in proliferative disease encode for proteins associated with the centrosome, a cellular organelle of paramount importance in cell polarity (Chae and Walsh, 2007).

Neuron Migration

Disruptions in proliferation can also adversely affect another important stage of neurogenesis: neuron migration, where newly-born neurons migrate from proliferative zones to their final positions within the laminae of the cortex. Mistiming or mispolarization of cell division can change the cellular milieu to the extent that neurons are unable to navigate correctly. For example, loss of polarity in RGCs by Numb and Numbl inactivation leads to progenitor dispersion and disorganized cortical lamination (Rasin et al., 2007).

During development the waves of neuron migration that occur in different regions of the brain differ both in their timing, mode of movement, and response to guidance cues. When migrating neurons with distinct cell fates and destinations spatiotemporally intersect, it becomes apparent that their directionality and movement is predetermined to some degree. How neurons differentially respond to environmental cues is a key question of neurobiology. From a cell biological perspective, neuron migration can be categorized

into two different modes: radial and tangential migration. Radial migration occurs primarily in projections neurons of the cortex and granule neurons of the olfactory bulb, cerebellum, and hippocampus. Tangential migration is primarily employed by interneurons generated in the ventral telencephalon and SVZ and migrating to the cortex and olfactory bulbs, respectively.

Radial Migration

In the cortex, pyramidal or projection neurons migrate radially into the CP along radial glial fibers. Around E14 in mice, the first wave of projection neurons leaves the VZ and enters the preplate area, effectively splitting the preplate into the upper marginal zone and a lower subplate (Marin-Padilla, 1998). Subsequent migration proceeds in an inside-out fashion, where early progeny become established in the lower layers and subsequent neurons migrate past them into the upper layers (Angevine and Sidman, 1961; Rakic, 1974).

As has been mentioned, radial glial fibers guide migrating neurons into the cortical plate, implying that adhesion between RGCs and neurons must be regulated so that neurons will remain attached to RGCs until they reach their destined layer. The importance of the RGC-neuron interaction is best illustrated by work investigating the protein Reelin. This molecule is secreted by Cajal-Retzius cells in the marginal zone (MZ) located below the pial surface (Ogawa et al., 1995) and it regulates glial-neuronal adhesion. Defects in Reelin signaling result in an inverted cortex (Caviness, 1976), where neurons prematurely detach from the RGCs before reaching the uppermost layers of the CP (Cooper, 2008). Reelin signaling is also required to maintain RGC polarity (Hartfuss

et al., 2003; Weiss et al., 2003). Interestingly, in the RMS Reelin promotes the detachment of type A cells from each other as they terminate tangential chain migration and radially migrate into the olfactory bulb (Hack et al., 2002). Gap junctions on RGCs and neurons are also required for radial migration. However, the mechanism employed doesn't rely on cell-cell communication between the gap junctions as might be predicted from their traditional role, but rather on their function as adhesive structures (Elias et al., 2007).

Time-lapse imaging of radially migrating projection neurons has shown that a neuron's path to the CP is not as straightforward as previously thought. They can exhibit at least three modes of migration: somal translocation, locomotion, and multipolar migration, which can be interrupted by multiple reversals of migration direction. Which mode a cell adopts depends in large part on its contact with RGCs and the pial surface while guidance cues can alter their directionality. Early in development while the cortical wall is still thin, neurons extend an apical process to the pial surface and then in one movement translocate the nucleus through the process into the cortical plate, independent of RGCs (Hatanaka et al., 2004; Nadarajah et al., 2001). As the cortical wall thickens with the addition of new neurons, cells rely increasingly on RGCs for guidance and move along them in a manner termed locomotion where the leading process wraps around the RGC fiber and remains a relatively constant length while the nucleus makes small, incremental jumps forward (Edmondson and Hatten, 1987; Rivas and Hatten, 1995).

Multipolar migration is a migratory phase that most locomoting cells undergo as they pass through the SVZ where they detach from RGCs and extend multiple transient processes for ~24 hours before readopting a bipolar morphology and resuming

locomotion into the CP (Noctor et al., 2004; Tabata and Nakajima, 2003). The purpose of this apparent delay in migration in not known, but the return to a bipolar morphology from a multipolar one is clearly important and depends on the activity of several cytoskeletal factors, including Doublecortin, Lis-1, and Cdk5. RNAi-mediated knockdown of any of these factors causes cells to arrest in a multipolar mode and not reach the CP (Bai et al., 2003; Ohshima et al., 2007; Tsai et al., 2005).

It is likely that at least some of the cells in the multipolar phase are IPs and the and the migration arrest might reflect a cell's preparation for mitosis. In addition, during the multipolar phase axon extension occurs (Noctor et al., 2004; Shoukimas and Hinds, 1978), so the multipolar morphology may actually reflect a mixed polarity response to axon guidance cues that orient the axon down and migration cues that orient the leading process up. Whatever the purpose of the multipolar stage and the identity of the cues that trigger it, it is clear that cells experience drastic restructuring of the cytoskeleton as they enter and leave the SVZ. How this occurs is an important neurodevelopmental question.

Tangential Migration

Tangential migration is defined as following a migratory path that runs parallel to the pial surface. In general this occurs without the use of glial guides. There are two principle groups of tangentially migrating neurons in the cortex: cortical interneurons generated embryonically in the subpallium (LGE and MGE) and type A olfactory bulb neuroblasts generated in the anterior SVZ (SVZa) in both embryonic and adult stages.

SVZa neuron migration through the RMS into the olfactory bulb (OB) begins in late embryogenesis and peaks during the first week after birth, but continues throughout

life. Upon arriving in the OB, SVZa neurons turn orthogonally and migrate radially into the granule and periglomerular layers where they become integrated into the circuitry (Alvarez-Buylla and Garcia-Verdugo, 2002). OB neuroblasts can travel up to 5mm in mice and 17mm in humans. Migration through the RMS has been described as chain migration, where cells move closely apposed to each other and are connected by membrane specializations (Lois et al., 1996). A layer of astrocytes ensheaths the migrating cells until they arrive in the OB and may be involved in modulating the speed of migration (Zhao et al., 2008).

Guidance Cues and Polarity

One area of significant interest had been how guidance cues regulate cell directionality. Migrating neurons are highly polarized cells and their directionality directly corresponds to their polarity. Response to chemoattractive and chemorepellant factors results in a shift or reversal of polarity, which occurs through the formation and selection of neuronal processes (Ward et al., 2005). In the cortex, glial guides provide a migratory path and influence cell polarity, but secreted molecules also play a role in regulating polarity by eliciting cytoskeletal restructuring (Chen et al., 2008; Deng, 2002).

The role of guidance cues is even clearer in tangential migration where SVZa neurons are guided to the OB by the actions of integrin, astrocyte-derived factors, members of the ephrin-B and Slit families of secreted proteins (Lledo and Saghatelyan, 2005). In fact, neurons in the SVZa have been observed to reverse their migration direction multiple times en route to the OB (Murase and Horwitz, 2004), suggesting that

both attractive and repulsive cues impinge upon neuronal polarity *in vivo* and that net movement in one direction results from a biased response to one cue.

Slit1 and Slit2 are members of an evolutionarily conserved family of large secreted glycoproteins that were first described as guidance molecules that repel axons crossing the midline in Drosophila (Battye et al., 1999; Kidd et al., 1999; Rothberg et al., 1990). Slit chemorepulsion is mediated by members of the Roundabout (Robo) receptor family, immunoglobulin cell adhesion molecules that are expressed in crossing axons (Kidd et al., 1998). Four Robos have been identified in mammals and they contain five Ig domains (two only in Robo4), three type III fibronectin motifs, a transmembrane segment, and a cytoplasmic tail containing four conserved signalling motifs which are thought to interact with downstream signaling molecules (Andrews et al., 2007).

In the cortex, Slit1 and Slit2 are expressed in the septum and diffuse to form a concentration gradient from the septum to the OB. SVZa neuroblasts expressing Robo2 and Robo3 are directed to the OB by migrating along the Slit gradient (Hu, 1999; Nguyen-Ba-Charvet et al., 2004; Wu et al., 1999). *In vitro* studies show that Slit elicits a repulsive response that causes cells to repolarize and migrate away from the source of Slit (Ward et al., 2003) and this repulsion depends on regulation of the RhoGTPase Cdc42 (Wong et al., 2001), a molecule known for its role in cell polarity in *C. elegans* and in other migrating cells (Nobes and Hall, 1999). In Slit1/2-deficient mice some SVZa neurons migrate caudally instead of rostrally, supporting the idea that Slits confer directionality *in vivo* (Nguyen-Ba-Charvet et al., 2004). Interestingly this study also showed that SVZa cells themselves express Slit and may regulate the migration of neighboring cells. In explant studies of the Slit1/2-deficient mice, greater migration from

the explant in the absence of Slit suggested a possible attractive effect of Slit in addition to its repulsive effect. How Slit controls directionality through the neuronal cytoskeleton is not known.

Interestingly, as with radial glial division, calcium signaling seems to play an important role in neuron migration. Waves of intracellular calcium transients control the stepwise process of migration that consists of leading neurite extension, nuclear translocation, and trailing process retraction. In cerebellar granule neurons, the frequency of Ca^{2+} transients in the cell soma controls the speed of migration and loss of Ca^{2+} transients triggers the completion of migration at the cell's final destination (Komuro and Kumada, 2005; Komuro and Rakic, 1998). In tangentially migrating interneurons from the MGE, a transient elevation in Ca^{2+} within the proximal end of the leading process directly proceeded nuclear translocation (Moya and Valdeolmillos, 2004). Slit2-induced reversal of migration in cerebellar granule neurons is mediated by a wave of Ca^{2+} that emanates from the distal end of the leading process nearest the source of Slit (Guan et al., 2007; Xu et al., 2004). The reversal in polarity is accompanied by a reversal in RhoA distribution, a RhoGTPase known to have a role in nuclear translocation and trailing process retraction (Causeret et al., 2004; Ridley et al., 2003).

Later I will discuss the possible roles in neuron migration and differentiation of the IQGAP family of proteins and DCK1, a member of the Dcx family, both of which may integrate signals from Ca^{2+} transients into cytoskeletal dynamics (Briggs and Sacks, 2003a; Lin et al., 2000). IQGAP1 is an effector of Cdc42 and contains four IQ motifs that can bind calmodulin, the primary mediator of Ca^{2+} signaling and DCK1 has structural similarity to Ca^{2+}/calmodulin kinases suggesting its kinase activity may be regulated by

Ca^{2+} signaling. Both IQGAP and DCX-family proteins have well-established roles in cytoskeletal regulation (Briggs and Sacks, 2003b; Kawauchi and Hoshino, 2008).

Migrating neurons are highly polarized. Early electron micrograph studies of developing monkey neocortex described a close apposition between migrating neurons and radial glial fibers (Rakic, 1971). Neurons have an elongated, pear-shaped form and a spindle-shaped nucleus. The leading process is voluminous near the soma but tapers distally and is rich in cytoplasmic organelles. The leading process terminates with a branching growth cone that probes the extracellular environment. The trailing process displays fewer organelles and becomes uniformly slender immediately after the nucleus. As mentioned earlier, migration occurs in a step-wise fashion with leading process extension followed by nuclear translocation and trailing process retraction (Edmondson and Hatten, 1987; Tsai and Gleeson, 2005). Microtubules (MTs) in the leading process are oriented with their plus ends towards the growth cone while MTs that extend rearward to the nucleus are of mixed polarity (Rakic et al., 1996). The rearward MTs surround the nucleus in a cage-like structure that contracts and elongates during nuclear translocation (hattRivas and Hatten, 1995; Solecki et al., 2004). It is likely that forces generated in the leading process are transmitted to the nucleus via this MT cage structure to advance the nucleus within the leading process.

Initial observations of migrating cortical and cerebellar granule neurons revealed another interesting pattern: typically, the centrosome is located ahead of the nucleus in the direction of migration (Gregory et al., 1988; Rakic, 1972; Tanaka et al., 2004). Its purpose there is unknown and will be a primary focus of this dissertation.

Migration Disorders

Several developmental brain disorders have been linked to defects in migration in humans. Mutations in genes that direct migration initiation (*Filamin-A)* give rise to periventricular heterotopia, while mutations in genes involved in later stages of migration (*Doublecortin, Lis-1, Tub1A*) result in type I lissencephaly (smooth brain) and subcortical band heterotopia (band of neurons ectopically located in the white matter). Mutations in genes that regulate the termination of radial migration (dystrophin) lead to type II lissencephaly (i.e. cobblestone lissencepahly—clusters of neurons along the surface of a lissencephalic brain) (Kerjan and Gleeson, 2007; Lian and Sheen, 2006; Ross, 2002).

Aberrant development of the inhibitory GABAergic circuits has been implicated in disorders such as schizophrenia, autism, and Tourette's syndrome (Di Cristo, 2007). The most prominent pathology in the dorsolateral prefrontal cortex in patients with schizophrenia is a deficit in the interneuronal neuropil (Selemon et al., 2007). Accordingly, Neuregulin1, a secreted guidance cue that acts through its receptor ErbB to promote migration of cortical interneurons into the cortex, has been implicated in susceptibility to schizophrenia (Corfas et al., 2004). Additionally, schizophrenic individuals with deficits in olfaction have been reported, hinting at disruptions in tangential migration of SVZa cells into the OBs (Moberg et al., 1999). All of this suggests that deficits in interneuronal response to guidance cues during migration may underlie these developmental disorders. Thus it remains an important issue to determine how response to guidance cues is regulated.

Neuronal Differentiation

Once migrating neurons reach their appropriate laminar targets they differentiate by extending axons and dendrites, expressing different complements of transcription factors, and serving different functions (Molyneaux et al., 2007). The ability of cells to polarize correctly during migration impinges directly on their ability to elaborate functional axonal and dendritic arbors.

In the cortex, mature projection neurons are pyramidal in shape with a fusiform, apically oriented dendrite and a thin axon that extends basally towards what was embryonically the subplate, where it turns and grows tangentially to synapse either with other cortical neurons or subcortical regions. Elegant studies of migrating neurons have shown that axon elongation actually begins during migration as neurons pause in the SVZ and become multipolar (Noctor et al., 2004; Rakic, 1972; Shoukimas and Hinds, 1978). The apical dendrite likely forms from the migratory leading process (Barnes et al., 2008).

Axon and dendrite formation is regulated by guidance cues in a similar manner to the leading process during migration. Localized calcium gradients can regulate cytoskeletal elements to control axon growth cone steering. The secreted guidance cue Semaphorin 3a is an attractant for apical dendrites and a repellant for axons (Polleux et al., 1998; Polleux et al., 2000). Wnt, netrins, Shh, and TGF-beta/BMP signaling also play a role in axon guidance in other systems, but their role in cortical development has not been addressed (Charron and Tessier-Lavigne, 2007; Dickson, 2002).

Disorders resulting from defects in differentiation are numerous. Synaptic spine dysmorphology is found in patients with mental retardation. Corpus callosum defects result from axon guidance problems and alterations in dendritic morphology probably

underlie epilepsy (Jiang et al., 1998). These disorders emphasize the important role that cell polarity plays in normal brain development.

The Centrosome in Neuronal Development

A central component of the neuronal cytoskeletal structure is the microtubule (MT) array, and the centrosome or MT-organizing center lies at its hub. The centrosome is an evolutionarily-conserved structure that can be traced to the basal body/axoneme of unicellular organisms (Azimzadeh and Bornens, 2004). During interphase the centrosome organizes an astral array of MTs that confers polarity to the cell and functions in movement, intracellular transport, and cell-cell interactions (Azimzadeh and Bornens, 2007). The centrosome also plays a central role in mitosis, where it becomes the center of the spindle pole body that nucleates the mitotic asters of MTs that separate the chromatids in anaphase.

The centrosome consists of a pair of centrioles that are composed of cylindrical arrays of triplet MTs organized with nine-fold radial symmetry (Azimzadeh and Bornens, 2007). The centrioles are oriented orthogonally to each other and are linked by fibers containing the proteins centrin, γ-tubulin and pericentrin. Surrounding the core centrioles is the pericentriolar matrix (PCM), which is involved in MT nucleation and anchoring.

During S-phase the centrioles separate and replicate using themselves as a template. Centrin, a member of a family of ancient proteins associated with the centriole/basal bodies, is required for centriole duplication and is recruited to the vicinity of the separated centrioles. After replication, the older centriole is designated the mother centriole and is 20% larger than the daughter centriole (Chretien et al., 1997). Although

the PCM surrounding both the mother and daughter centrioles can nucleate MTs, only the mother is able to anchor them on its centriole-associated sub-distal appendages (Piel et al., 2000). Complete daughter centriole maturation takes two complete mitoses, when it finally acquires the sub-distal appendages of the mother centriole.

Considering the fundamental role of the centrosome in establishing cell polarity, an important unanswered question in neurobiology is how the cytoskeleton is regulated during neuronal proliferation, migration, and differentiation. Since many neurodevelopmental disorders are a result of mutations in cytoskeletal genes, this work will have important implications in the understanding and potential treatment of human disease. Studying the cytoskeleton from the perspective of the centrosome provides a simple model for investigating how both cell intrinsic and extrinsic factors influence the cytoskeleton and cell polarity. Also, because most genes that have been identified in humans as responsible for cortical malformations have also proved functionally relevant to development in mice, the mouse is a useful model for studying the pathophysiological mechanisms of these human diseases (Pombero et al., 2007). For these reasons, we have developed a mouse model in which the centrosome can be visualized in living cells. This will be described in Chapter II. In Chapter III, the mouse model will be used to investigate the role of the centrosome in migration and differentation in tangentially and radially migrating neurons. Chapter IV will focus on the role of *Doublecortin* family of microtubule-associated proteins *DCX* and *DCK1* in radial and tangential migration.

II. TRANSGENIC MOUSE LINE WITH GREEN-FLUORESCENT PROTEIN-LABELED CENTRIN 2 ALLOWS VISUALIZATION OF THE CENTROSOME IN LIVING CELLS

ABSTRACT

The centrosome plays diverse roles throughout the cellular mitotic cycle and in postmitotic cells. Analysis of centrosome position and dynamics in living murine cells has been limited due to a lack of adequate reporters and currently requires either cell fixation/immunostaining or transfection with centrosome reporters. Here we describe the generation and characterization of a transgenic mouse line that constitutively expresses green fluorescent protein-labeled Centrin-2 (GFP-CETN2). The phenotype of the mouse is indistinguishable from wild-type and it displays a single pair of fluorescent centrioles in cells of every organ and time point examined. This model will be helpful for visualizing the centrosome in multiple experimental conditions.

INTRODUCTION

The centrosome was defined on the basis of its central position in the cell and as the focus of cytoplasmic fibers. Subsequent characterization has determined that the main constituents include a pair of centrioles, pericentriolar material (PCM), and microtubules that emanate from this structure (Doxsey, 2001). The centrosome is the major microtubule (MT) organizing center of the cell, thought to determine the distribution and polarity of the MT array. Subsequently, the role of the centrosome in various cellular processes has expanded beyond this classical view. Genetic and molecular techniques have implicated the centrosome and centrosomal-associated proteins in various processes

including cell cycle regulation (Hinchcliffe et al., 2001), signal transduction (Diviani and Scott, 2001), cell migration (Danowski et al., 2001; Schliwa et al., 1982; Yvon et al., 2002), transcription activation, and DNA damage repair (Araki et al., 2001; Deng, 2002; Meraldi et al., 1999; Stevenson et al., 2001). However, much concerning the structure, function, and regulation of the centrosome remains to be discovered, creating the need for suitable models allowing for the observation and manipulation of centrosomes in living tissue and cells.

The centrosome is composed of two centrioles that are symmetrical, tubular structures made of nine triplet blades of α and β tubulin. The surrounding PCM is located at the centrosome during interphase, and is composed of various proteins including γ-tubulin (which also localizes to the centrioles) and pericentrin. Similar in structure and content to centrioles, basal bodies are formed from similar proteins and act at the membrane to form primary flagellum and cilia (Beisson and Wright, 2003). Centrin-2 (CETN2), which localizes to the centrioles, PCM, and basal bodies is an X-linked gene in mice and humans with a predicted product of 172 amino acids and a molecular mass of 20 kD (Errabolu et al., 1994; Hart et al., 2001). CETN2 presumably functions in cell cleavage and recent evidence suggests that it is required for centriole duplication in mammalian cells (Paoletti et al., 1996; Salisbury et al., 2002).

Current methods for visualizing centrosomes in murine cells, including electron microscopy or immunocytochemistry with γ-tubulin (Stearns et al., 1991; Zheng et al., 1991) or pericentrin (Doxsey et al., 1994) antibodies, do not allow observation in live cells. An alternative strategy is ectopic gene expression by transfection or viral infection

with a constitutive centrosomal marker, which has limitations including possible toxic effects of transfection and low numbers of labeled cells of a restricted type.

Here we report the generation of a line of mice that expresses a constitutive green fluorescent protein-labeled centrosome. This GFP-CETN2 mouse line provides a model for observing the centrosome in live cells and tissue, eliminating the need for further manipulation. The mouse has no identifiable phenotype, and a pair of labeled centrioles was observed in every organ and every time point examined.

RESULTS

Generation Of Transgenic Line

Fourteen transgenic founder lines were derived by pronuclear injection of the pCX-GFP-CETN2 construct (Fig. II.1) into fertilized ova from CB6 mice. The GFP-CETN2 transgene contains an internal CMV enhancer and is driven by a chicken β-actin promoter (Okabe et al., 1997) to produce constitutive, ubiquitous expression. All the mice that were PCR-positive for the transgene (14 of 28 lines) developed normally and had no aberrant phenotype that was detectable by 12 months of age. They also expressed GFP-CETN2, based on the presence of fluorescent signal emanating from the pair of centrioles in acutely dissociated cerebellar granule neurons isolated from postnatal day 5 (P5) pups (data not shown). We chose to maintain two lines, 3-4 and 18-1, based on their consistent and robust expression of GFP-positive centrosomes in these granule cells.

Transgene Characterization

To ensure that our transgene was correctly expressed at the centrosome, we stained tissue from the 18-1 transgenic line with anti-pericentrin and anti-γ-tubulin antibodies, both of which are established markers for centrosomes. This analysis was performed in skeletal muscle and dissociatedfrom a postnatal day 0 (P0) mouse and mouse embryonic fibroblasts (MEFs) from embryonic day 14.5 mice (E14.5), where the low density of centrosomes allowed for a clear indication of overlapping localization.

We observed co-localization of the GFP signal with γ-tubulin and pericentrin, suggesting that the product of the transgene correctly targeted to the centrosome (Fig. II.2B,C). However not all GFP-positive centrosomes were reactive with anti-pericentrin (Fig. II.2C, arrows), consistent with previous observations that pericentrin localizes to centrosomes in a cell-cycle-dependent manner (Dictenberg et al., 1998). This suggests that localization of GFP-CETN2 labels centrosomes in cells independent of cell cycle stage, a finding that supports earlier observations by White et al. that the GFP-CETN2 localizes to the centrosome in all stages of the cell cycle (White et al., 2000). In addition, MEFs from the transgenic line displayed GFP-positive centrosomes in virtually every cell observed (Fig. II.2A), with correct GFP-CETN2 localization confirmed with an anti-γ-tubulin antibody (Fig. II.2B). As expected, not all of the GFP signal was isolated to the centrosome in the dissociated MEFs (Fig. II.2A), consistent with previous observations by Paoletti, et al. that most cellular centrin is not centrosome-associated (Paoletti et al., 1996). Occasional fibroblasts with relatively larger nuclei were found with multiple centrosomes, but these were also observed in wild-type fibroblasts at similar levels (Fig.

II.2D,E). These data suggest that the GFP-CETN2 transgene is localizes to a pair of centrioles, but otherwise produces no cellular phenotype.

The advantage of using this model for accurate resolution of individual centrioles was made apparent when the GFP signal was compared with γ-tubulin staining in the MEFs. For example, two pairs of GFP-positive centrioles were occasionally identified in transgenic MEF cells, but when visualized with anti-γ-tubulin, these four centrioles appear as two poorly resolved centrioles (Fig. II.2F-H). A similar observation was made previously by Paoletti et al. where they found that an anti-centrin antibody often provided more discreet staining of the individuals centrioles than γ-tubulin staining (Paoletti et al., 1996).

Though the GFP-CETN2 mice have no observable phenotype throughout the twelve-month time course examined, there remained the possibility that overexpression of CETN2 might have an effect on centrosome number, because it plays a critical role in centrosome duplication (Salisbury et al., 2002). Therefore, we tested whether centrosome number was similar in cells derived from the GFP-CETN2 line and control strain. We quantitated the number of centrioles in several hundred low-density low-passage MEFs from the transgenic line and from wild-type mice stained with anti-γ-tubulin antibody, and determined the percentage of nuclei with greater than a single pair of centrioles in close approximation. The number of centrioles per nucleus in transgenic fibroblasts was not significantly different from that of non-transgenic fibroblasts ($p>0.1$, Chi-squared) (Fig. II.3). We conclude that the GFP-CETN2 transgene does not have a major effect on

centrosome number in at least one type of primary cultured cells from the transgenic model.

Developmental Expression of GFP-CETN2

We next analyzed GFP-CETN2 expression in various tissues at specific developmental time points in the two transgenic lines. Because the 18-1 and the 3-4 line showed identical results (data now shown), we focused our attention on just one line, 18-1, for further analysis. GFP-CENT2 expression was identified in all tissues analyzed at E14.5, P0, and adult (Figs. II.4-6). A pair of GFP-positive centrioles of uniform size and shape in close proximity to the nucleus was identified in nearly every cell from embryonic and perinatal tissue. In adult tissue, however, fewer nuclei had adjacent centrosomes that were visible, but at least a fraction of cells contained centrosomes in every tissue section examined.

Embryo (E14.5)

In the embryonic central nervous system cortex, proliferating cells in the ventricular zone displayed a typical polarized morphology, with a more superficial nucleus and centrosomes located adjacent to the lumen as described (Chenn et al., 1998) (Fig. II.4A,B). In the epithelial tissue of the retina, intestine, lungs and kidney, GPF-CETN2 localized to the apical region of the cell lining the lumen, indicating the location of the basal body at the base of microvilli and cilia (Beisson and Wright, 2003; Laoukili et al., 2000) (data not shown). A much lower percentage of hepatocytes displayed GFP-positive centrioles compared with other epithelial tissue (data not shown).

In cardiac and skeletal muscle, centrosomes were less apparent than was observed in epithelial tissue (data not shown). We were able to identify a centrosome adjacent to virtually every isolated nucleus in embryonic bone (Fig. II.4C,D). It was not clear if the difference in ability to identify the centrosome was a reflection of a greater dispersion in tissue such as bone, or whether other tissues had lower percentages of cells with labeled centrosomes. It has previously been observed that in skeletal muscle grown *in vitro*, myotubes lose their centrosomes as they fuse into myofibers (Connolly et al., 1986; Tassin et al., 1985a; Tassin et al., 1985b), and this same phenomenon may occur *in vivo* in other tissue types as differentiation progresses, providing a potential explanation as to why the percentage of cells with visible centrosomes in the adult was relatively reduced when compared to embryogenesis. To verify that the GFP signal was properly localized to a centrosomal structure, we co-stained tissue from the transgenic mouse with an anti-γ-tubulin antibody. We found co-localization of the GFP signal with γ-tubulin in a similar pattern to that described previously (Paoletti et al., 1996), where the γ-tubulin signal was slightly offset from the GFP signal (Fig. II.4A,C).

A question of particular importance regarding the generation of a transgenic line is whether the transgene's expression pattern reliably parallels the expression pattern of the endogenous gene, in this case CETN2. To address this question, we co-stained wild-type littermates with an anti-CETN2 antibody. We found similar localization in all tissues where we detected endogenous CETN2, including bone, ventricular zone of the developing brain, lung and kidney (Fig. II.4B,D; II.5B,D), suggesting that our transgene accurately reports the endogenous localization of CETN2.

Other groups have previously reported that the GFP-CETN2 construct driven from a different promoter produces fluorescent signal at the pair of centrioles where one centriole (the mother centriole) is consistently brighter than the daughter. Examination of fixed tissue and MEFs revealed that not all cells in the GFP-CETN2 mouse exhibited this differential intensity in GFP signal (Fig. II.2A,B; II.4A,B; II.5A,B). Similarly, staining of wild-type tissue with anti-centrin antibodies did not show a difference in intensity between the two centrioles (Fig. II.4B,D; II.5B,D). These results suggest that this model may not be optimal for differentiating between mother and daughter centrioles.

In all tissues examined, we occasionally observed cells with brighter than normal centrosomes and/or brighter cytoplasmic GFP signal relative to centrosome signal (see Fig. II.2A and data not shown). The cytoplasmic GFP signal was not unexpected based on earlier studies in HeLa cells that found that more than 90% of centrin is not associated with centrosomes (Paoletti et al., 1996). A specific cell-cycle event or selective stabilization of the GFP-CETN2 mRNA or protein product during certain stages of the cell cycle may give rise to this brighter signal.

Postnatal Day 0 (P0)

At the completion of gestation, we found that the centrosome was visible in a comparable percentage of cells and at similar expression levels when compared to embryonic time points. The epithelia of the cerebral ventricle, small intestine, retina, kidney, lung, muscle, liver, dermis and bone all displayed GFP-positive centrosomes in similar patterns (Fig. II.5A,C and data not shown). Co-staining with γ-tubulin showed

almost complete co-localization with GFP-CETN2. Occasional centrosomes with GFP signal were observed that lacked any apparent co-localization of γ-tubulin (Fig. II.5A, arrow). However, increasing the intensity of the γ-tubulin signal revealed some expression in nearly all GFP-CETN2 positive structures, suggesting that these structures were centrosomes and suggesting some variability in the sensitivity of the anti-γ-tubulin antibody. Very rarely, paired γ-tubulin signal was observed without any apparent GFP signal in close proximity (Fig. II.5A,C, arrowheads), suggesting that GFP-CETN2 did not localize to the same region as γ-tubulin in that particular cell. These differences were seen in less than 1% of cells, and likely represent subtle variability of these different methods to detect signal.

Adult

We observed a lower percentage of nuclei with adjacent visible centrosomes in adult, but still found GFP-positive centrosomes in all tissue analyzed. Epithelial tissue of the small intestine and stomach displayed a polarized distribution of centrosomes as seen in developing tissue, but they were found at a much lower density (data not shown). In contrast to earlier time points, in the adult retina we observed comet-like tails extending from centrioles/basal bodies in the photoreceptor cell layer, where connecting cilia link the inner and outer segments of photoreceptors (Fig. II.6A) (Wolfrum et al., 2002). As with earlier time points, liver displayed a very low density of visible centrosomes (data not shown). In the kidney, centrosome density was highest in the Bowman's capsule region, though centrosomes were seen throughout the entire organ (data not shown). We observed a very low number of centrosomes in adult skeletal muscle, which was expected

based on earlier studies showing a loss of centrosomes during myoblast differentiation (Connolly et al., 1986; Ralston, 1993; Tassin et al., 1985a; Tassin et al., 1985b) (Fig. II.6C). Similarly, in cardiac muscle we observed very few localized GFP signals (data not shown).

Bright fluorescent signals from what appear to be intracellular GFP-aggregates emanated from specific regions exclusively in the adult brain, particularly the pyramidal cell layer of the hippocampus and granule cell layer of the cerebellum, and randomly throughout the molecular layer and cortical plate region of the cerebral telencephalon in a small subset of cells (Fig. II.6C and data not shown). These aggregates were unpaired, with rounded or ovoid morphology approximately 5-20 μM in diameter. This signal did not overlap with centrosomes, which were still visible in many adjacent cells, but normal centrosomes were not readily apparent in the cells that contained the aggregates (Fig. II.6C, insert). The appearance of the aggregates raised a concern that they may reflect an inability in the adult to deal with the protein aggregates or protein toxicity as effectively as in the embryo. An examination of regions in the cerebellum and ventricular zone for pyknotic nuclei and evidence of increased apoptosis revealed no difference between transgenic and wild-type embryos (Hacker, 2000) (data not shown).

DISCUSSION

The centrosome plays a diverse set of roles throughout the cellular cycle, and visualization of its location and number in both living and fixed tissue will become increasingly important for numerous biological questions. White et al. previously created

HeLa and Syrian Hamster cell lines stably expressing GFP-CETN2 that localized to the centrioles and the PCM (White et al., 2000). These cell lines were demonstrated to have normal cell cycle dynamics and apparently normal centrosome function, suggesting no untoward effects of expression of GFP-CETN2 in cells. Other groups have used a similar approach to examine centrosome dynamics in living cells (Piel et al., 2000; Piel et al., 2001). We here report the generation of a GFP-CETN2 transgenic mouse that will facilitate the study of centrosome function at all stages of development in most tissues of the mouse. These mice have no observable phenotype up to one year of age, suggesting the absence of major defects in cell function. This transgenic mouse model will provide a tool to observe centrosome dynamics in numerous cell types for different applications (Chenn et al., 1998; Hinds and Ruffett, 1971).

Centrin is a well-characterized centrosomal protein that localizes to the distal lumen of centrioles, the linker material between two adjacent centrosomes, and basal bodies in ciliated cells (Klotz et al., 1997; Laoukili et al., 2000; Paoletti et al., 1996). It likely functions in the duplication of centrioles during S phase and their subsequent separation during mitosis. Newly generated centrosomes incorporate cytoplasmic centrin into their distal lumen during their formation, and a mutation in centrin slows the template-mediated assembly of centrioles (Araki et al., 2001; Baron et al., 1992; D'Assoro et al., 2001; Marshall et al., 2001).

We have established that CETN2 fused to GFP is a suitable reporter for the centrosome by co-staining several transgenic tissues with anti-γ-tubulin and anti-pericentrin antibodies. Two distinct, uniform GFP signals corresponding to the two

centrioles of the centrosome were found in all tissues at all time points examined. We have shown that the transgene does not visibly alter the phenotype of the mouse or the average number of centrosomes per cell. Further, we have shown that this reporter may offer improved resolution over immunostaining for visualizing individual centrioles.

Previous studies examining centrin found greater resolution of individual centrioles using an anti-centrin antibody than with an anti-γ-tubulin antibody (Paoletti et al., 1996). We found similar results, but the model presented here has a distinct advantage over using antibodies to stain centrosome in that we detected extremely low GFP background signal that might confound the correct localization of the centrosome. GFP signal is present in the cytoplasm, as expected based on previous results (Paoletti et al., 1996), but two centrioles could always be clearly distinguished in the vast majority of dispersed cells.

In a few instances where transgenic tissue was co-stained with anti-γ-tubulin antibodies, GFP-CETN2 signal was found without corresponding γ-tubulin signal. We found that in many instances, the missing γ-tubulin signal was actually present, but at very low intensity, suggesting some non-uniformity in immunostaining. In dispersed cells, this situation was rarely encountered, suggesting that antibody penetration may have been a limiting factor in the staining of frozen fixed tissue. Additionally, some of this difference might relate to the difference in γ-tubulin and centrin localization to different regions of the centrosome, giving an incomplete image of the entire centrosome. The observation that the vast majority of GFP-CETN2 signal co-localized with pericentrin and γ-tubulin, taken together with the high signal: noise ratio of the transgene

product leads us to conclude that our model faithfully reports the location of a single centrosome and may be superior to staining with centrosomal antibodies in many applications.

We have shown that the GFP-CETN2 signal is visible in all tissues analyzed at embryonic, perinatal, and adult stages in mouse. We have shown that this expression is similar to that observed in wild-type tissue stained for centrin, suggesting that this model does not cause observable changes in the endogenous behavior of centrin. Centrosome distribution varies, however, according to tissue and cell type. Centrosomes were found at relatively high densities in tissue undergoing cell division, such as the endothelia of vasculature and epithelial cells, which have a polarized phenotype with a high density of GFP-positive centrosomes at the apical region bordering the lumen. The only exception was in the liver, where we did not observe a polarized centrosome distribution, in contrast to earlier observations (Meads and Schroer, 1995). In addition to their function as MT organizing centers, centrosomes or centrosome-like structures may act as basal bodies at the base of cilia that line the epithelial lumen in various tissues (Beisson and Wright, 2003; Laoukili et al., 2000). The high density of centrosomes that we observed in epithelial cells suggests that many of the GFP-positive structures that we observed may actually be basal bodies.

In analyzing frozen tissue, we found occasional cells that appeared to express GFP-CETN2 at higher levels than neighboring cells, where both the diffuse cytoplasmic and centrosomal GFP signals were evident. The cause of this increased expression was not clarified in this study. These bright cells were rare and did not display abnormal

number or structure of the centrosome. Some cytoplasmic GFP-CETN2 signal is not unexpected, as one study showed that less than 10% of the centrin is localized at the centrosome in HeLa cells and human lymphocytes (Paoletti et al., 1996). Occasional cells were found with supernumerary centrosomes, but we found no evidence that the prevalence of this anomaly was increased in cells from GFP-CETN2 mice. It does not appear that these supernumerary centrosome cells are a result of aberrant transgene expression as we and others also found them in wild-type cells with a similar frequency (Mussman et al., 2000; Xu et al., 1999).

We observed a lower percentage of cells with identifiable centrosomes in adult tissue. In muscle, myotubes lose centrosomes during cell fusion (Connolly et al., 1986; Tassin et al., 1985a; Tassin et al., 1985b), but comprehensive analyses of centrosome distribution in fully differentiated adult tissue do not exist. It may be that non-dividing tissue ceases production of the centrosome at a certain developmental stage. It has been shown that the MT nucleating capacity of the cell does not require the centrosome and cells without centrosomes survive and can even undergo mitosis (Bobinnec et al., 1998; de Saint Phalle and Sullivan, 1998; Debec et al., 1995; Sluder et al., 1989). Because we used a constitutive promoter, we would expect the GFP-CETN2 to be produced at all cells and in all tissue. Therefore it is possible that some post-mitotic cells no longer contain centrosomes so the GFP-CETN2 accumulates and subsequently degrades. The bright green fluorescent signals we observed in the pyramidal cell layers of the hippocampus, cortex and cerebellum may be the result of an aggregation of the GFP-CETN2 fusion protein due to failed or slowed protein degradation. Because of this finding, we caution against the use of this model in studying the centrosome in the adult

brain. We saw no evidence, however, that this was toxic to cells, but may be the result of an aggregation of the GFP-CETN2 fusion protein due to failed or slowed protein degradation.

The generation of the GFP-CETN2 transgenic mouse provides many advantages over cell lines with labeled centrosomes in that it will allow the investigation of the role of the centrosome in several types of living tissue without further manipulation. The role of the centrosome in primary cell cultures can be investigated with this model. It will be useful in studies ranging from cell cycle regulation and signal transduction to cell migration and generation of aneuploidy in tumor cells.

MATERIALS AND METHODS

Generation of GFP-CETN2 Construct

The pCX-GFP-CETN2 construct (Fig. II.1) was created by ligating a GFP-CETN2 insert into the pCX vector. The GFP-CETN2 insert (White et al., 2000)(kind gift of J. Salisbury) was created by PCR amplification of GFP-CETN2 with the forward primer 5'-CGCTAGCGCTACCGGTCGCC-3' and reverse primer 5'-TTATTAATAGAGGCGGTCTTTTTCATC-3' in order to introduce a stop codon following the last amino acid of CETN2. Pfu Gold polymerase (Stratagene) amplification of this product was followed by treatment with T4 polynucleotide kinase for 15 minutes to ensure 5' and 3' end phosphorylation. The construct was then gel purified using GeneClene (BIO101). The pCX-GFP vector (Okabe et al., 1997) containing the CMV-internal enhancer, chick beta-actin promoter, beta-actin intron and bovine globin poly-

adenylation signal was digested with EcoRI to remove GFP, treated with Klenow to achieve blunt ends followed by calf alkaline phosphatase treatment. It was gel purified and ligated with the insert. Clones were screened for orientation by restriction digestion with PstI. The open-reading-frame of CETN2 was sequenced in its entirety to verify that there were no PCR-mutations. The pCX-GFP-CETN2 construct was transfected into 293T cells to verify that the centrioles were visible under indirect fluorescence.

Generation of Transgenic Mouse

The Centrin2-GFP construct was prepared for pronuclear injection by isolating centrin-GFP plasmid DNA by CsCl centrifugation. The construct was removed from the pCX plasmid with BamHI and SalI and was electroeluted from the agarose gel overnight at 80-100V with Schleicher and Schuell Elutrap. Centrin-GFP DNA was recovered from the elute with a Qiagen midi column followed by ethanol precipitation. DNA was dissolved in injection buffer and dialyzed for 20 min against injection buffer using the Millipore “drop dialysis” technique.

At the UCSD Transgenic Mouse and Gene Targeting Core, the construct was injected into the pronucleus of a fertilized ovum from the hybrid strain CB6, which is a hybrid between BalbC and C57 Bl6. The ovum was subsequently implanted into pseudopregnant females. Offspring were analyzed for insertion of the construct by PCR, using the primers forward: 5’-AGAAGAACGGCATCAAGGTG-3’ reverse: 5’-GAACTCCAGCAGGACCATGT-3’, which amplifies a 200 base product across the carboxy end of GFP. All 14 founder lines were fertile and healthy and none exhibited extraneous phenotypes. These lines were further characterized by analysis of dissociated

cerebellar granule neurons at P5 to test for labeled centrioles. Two lines were selected (18-1 and 3-4) for further characterization based upon high GFP expression levels.

Frozen Tissue Sections

Wild-type and transgenic adult (120 days) mice taken from the 18-1 line were sacrificed by cervical dislocation and immediately perfused with PBS followed by 4% paraformaldehyde (PFA) in PBS. Selected tissues and organs were removed and drop fixed in 4% PFA 24-48 hours and the cryoprotected 24 hours in 25% sucrose solution. The neonatal (from 3-4 line) and embryonic tissue (from 18-1 line) was not perfusion fixed, but drop fixed in 4% PFA for 24 hours then cryoprotected 24 hours in 25% sucrose. The tissue was then frozen in OCT compound (Tissue-Tek, Sakura Finetek USA) and sliced into 5-10 μm sections (cryostat kindly provided by Rappaport Lab).

Immunofluorescence

Anti-γ-tubulin (DQ-19, Sigma) and anti-CETN2 (kindly provided by J Salisbury) were used at 1:500 and 1:1000 dilution, respectively. GFP-CETN2, γ-tubulin, and centrin were visualized with an epifluorescent microscope and images were taken from compressed deconvolved z-stack images (Applied Precision). Pericentrin was visualized using a confocal microscope stained with a rabbit anti-pericentrin polyclonal antibody (Covance Research Products PRB-432C) at 1:100 dilution and secondary Alexa Flour® 568 goat anti-rabbit IgG (Molecular Probes Eugene, Oregon, USA) at 1:200 in 1% BSA, 0.1% Triton-X and PBS. Nuclear counterstaining was achieved by propidium iodide in the adult tissue and Hoechst in the P0 and embryonic specimens.

MEF Preparation

Mouse embryonic fibroblasts were isolated following the protocol provided by TJ Bowen from Wynshaw-Boris lab. Briefly, a timed pregnant female was sacrificed at day 14.5. Under sterile conditions, embryos were separated and their organs removed. Fibroblasts were isolated by repeated trypsinization of minced tissue (0.04% Trypsin in DMEM). Cells were grown in DMEM, 15% FBS, and penicillin/streptomycin at 37°. For immunocytochemistry, MEFs were fixed 10 minutes in –20C methanol and stained with rabbit anti-γ-tubulin (Sigma T3559) and secondary Alexa Flour 594 goat anti-rabbit. Cells were viewed with fluorescent microscope.

Statistical analysis

Standard statistical methods were utilized to analyze centrosome number in MEFs (Glantz, 1996).

ACKNOWLEDGEMENTS

We thank Jeffrey Salisbury, Mayo Clinic, for the GFP-CETN2 construct and CETN2 antibody; Jun-ichi Miyazaki, Osaka University Medical School, for the pCX-EGFP plasmid; UCSD Transgenic Core, for derivation of the transgenic lines; TJ Bowen of the Wynshaw-Boris lab, UCSD, for the MEF protocol; David Rappaport, UCSD, for use of his cryostat; Arshad Desai, Karen Oegema, and Alex Dammermann for their helpful suggestions.

This work was supported by the Neuroplasticity of Aging Training Grant (H.H.), the Genetics Training Grant (S.B.), and the NINDS (J.G.G.).

This chapter was published as Higginbotham, Holden; Bielas, Stephanie; Tanaka, Teruyuki; Gleeson, Joseph G. Transgenic mouse line with green-fluorescent protein-labeled Centrin 2 allows visualization of the centrosome in living cells. Transgenic Research, **13**: 155-164, 2004.

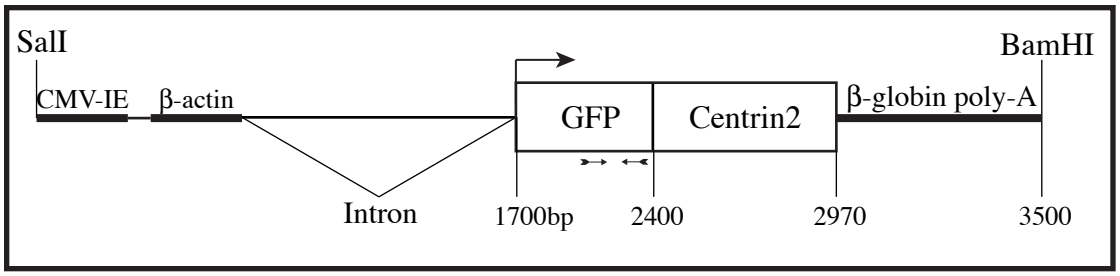

Figure II.1: GFP-CETN2 construct. The expression of the GFP-CETN2 transgene is under the regulation of a CMV-Immediate Early (IE) enhancer and a chicken b-actin promoter from the pCX vector. The arrows indicate the forward and reverse primers used for PCR-based genotyping.

Figure II.2: Transgene characterization. (A) MEFs showing GFP-CETN2 localization to centrosome and cytoplasm. Arrowheads show supernumerary centrosomes in one cell. Differential cytoplasmic GFP signal intensity from cell to cell is apparent. (B) MEFs labeled with γ-tubulin antibody (red) showing co-localization with GFP-CETN2. Typically one centrosome (2 centrioles) is associated with each nucleus. (C) Skeletal muscle from P0 transgenic mouse labeled with anti-pericentrin antibody (red), showing overlapping localization with GFP-CETN2. There are some pairs of centrioles (arrows) that are not positive for pericentrin, possibly due to the cell-cycle-dependent localization of pericentrin to the centrosome. (D) GFP-CETN2 transgenic fibroblast with large nucleus displaying multiple centrosomes. (E) Similar non-transgenic cell stained with anti-γ-tubulin antibody showing similar supernumerary centrosomes. (F) Two closely apposed pairs of centrioles that appear as a single pair when labeled with anti-γ-tubulin antibody (G). (H) Merged image of (F) and (G). Scale bar=5 microns.

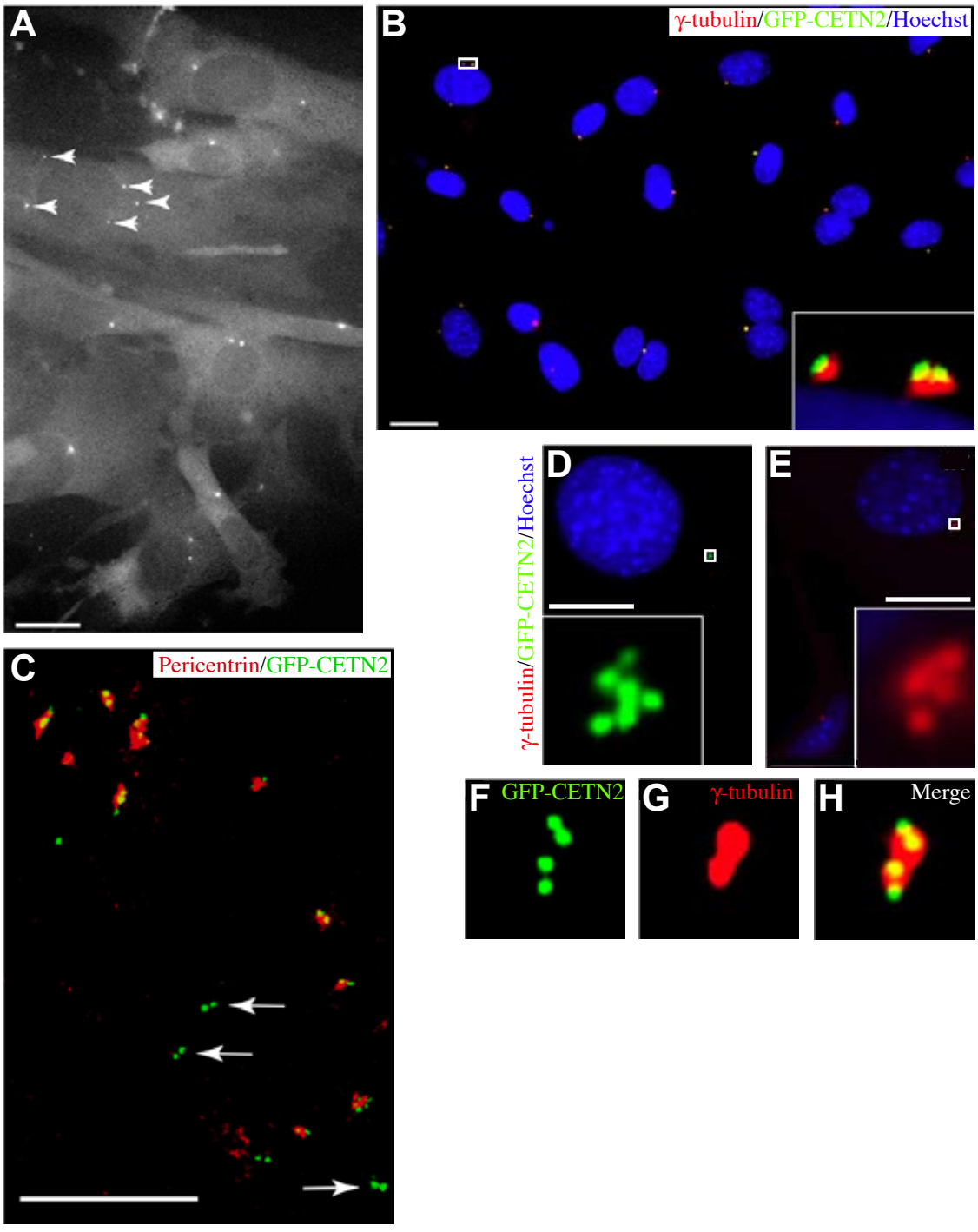
A
B
γ-tubulin/GFP-CETN2/Hoechst
C
Pericentrin/GFP-CETN2
D
E
γ-tubulin/GFP-CETN2/Hoechst
F GFP-CETN2
G γ-tubulin
H Merge

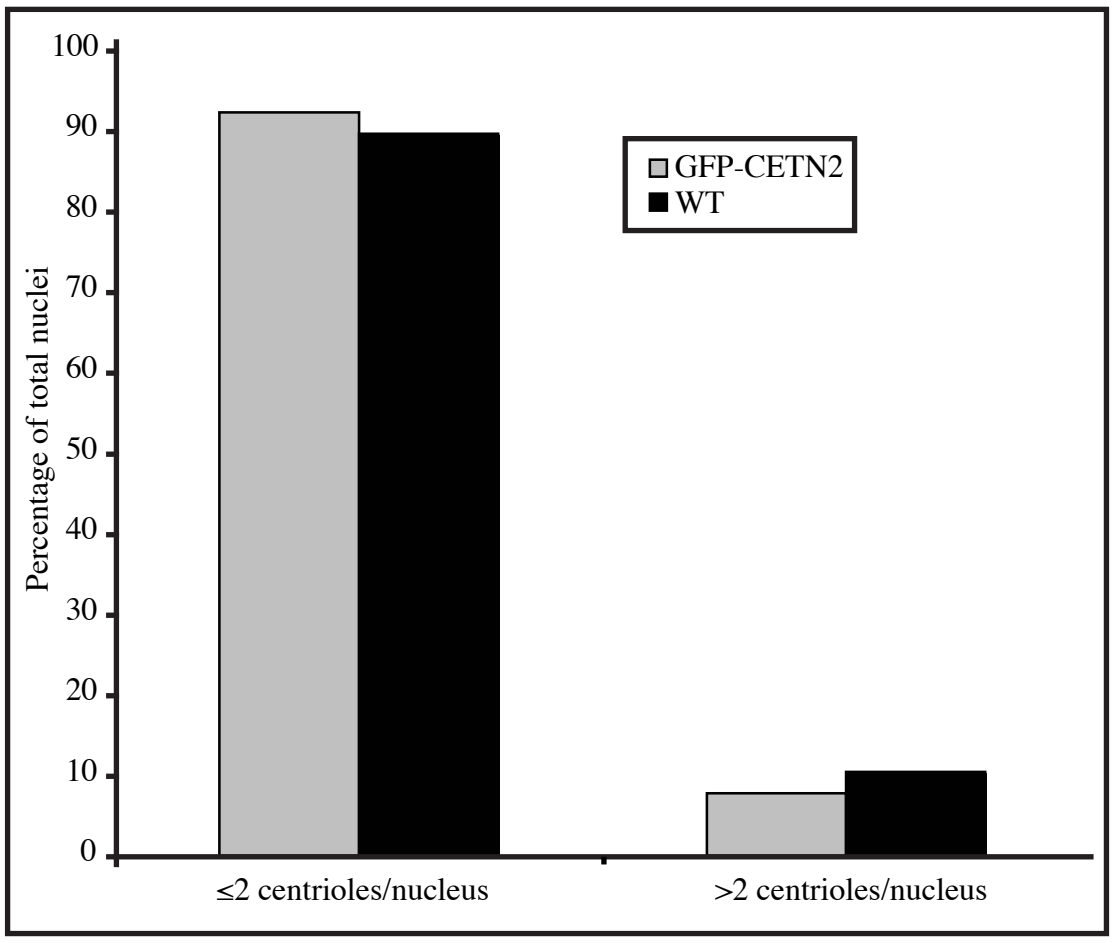

Figure II.3: Number of centrioles per nucleus in GFP-CETN2 and wild-type embryonic fibroblasts. Percentage of nuclei associated with £2 centrioles to nuclei associated with >2 centrioles does not significantly differ between transgenic and wild-type ($p>0.05$, Chi-squared test). n=297 (GFP-CETN2); n=365 (WT).

Figure II.4: Identification of GFP-CETN2-labeled centrosomes in E14.5, P0 and adult transgenic mice. (A-D) Transgenic tissue labeled with γ-tubulin from E14.5 (A-B) and P0 (C-D). (A) VZ of neocortex in E14.5 tissue showing centrosome localization to the apical border of the VZ. VZ lumen border is outlined with a white line. (B) Osteocytes from E14.5 animal. (C) Pulmonary epithelia and (D) renal cortex from P0 animal. Arrows in (C) show GFP signal without a corresponding γ-tubulin signal, suggesting some non-uniformity in immunostaining. Arrowheads in (C) and (D) indicate γ-tubulin signal without a corresponding GFP-CETN2 signal. (E-H) Tissue from WT animals corresponding to (A-D), labeled with anti-centrin2, showing similar patterns of centrosomal number and localization. (I-K) GFP-CENT2 expression in adult tissue. (I) GFP-CETN2 expression in connecting cilia of photoreceptors. Outline indicates boundary between outer nuclear layer (ON) and photoreceptor cell layer (PC). PE= pigment epithelium. (J) GFP-CETN2 signal in adult skeletal muscle. PI=propidium iodide (C) Aggregates of GFP-CETN2 in pyramidal cell layer of hippocampus. Insert shows normal GFP-CETN2 localization at a centrosome. Scale bar in (A-J)=5 microns; in (K), scale bar=15 microns.

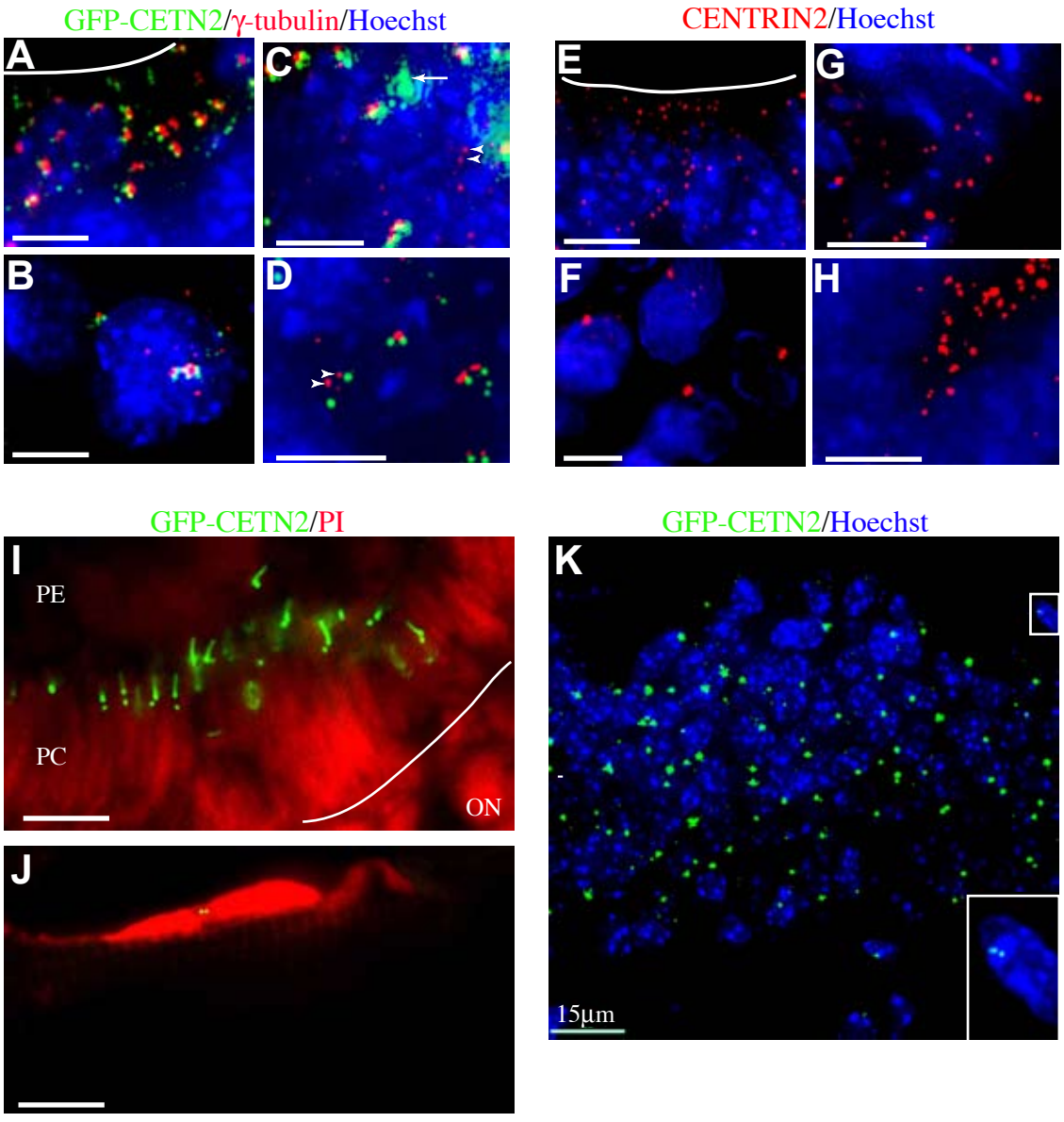
GFP-CETN2/γ-tubulin/Hoechst
CENTRIN2/Hoechst
A
B
C
D
E
F
G
H
GFP-CETN2/PI
GFP-CETN2/Hoechst
I
PE
PC
ON
J
K
15μm

III. NEURONAL POLARIZATION IN RESPONSE TO GUIDANCE CUES: CENTROSOME POSITIONING AND PROCESS OUTGROWTH DURING MIGRATION AND DIFFERENTIATION

ABSTRACT

A key requirement of normal brain development is that during their proliferation, migration and differentiation individual neurons and their precursors establish and maintain a specific cell polarity. Importantly, secreted guidance cues confer directionality to neurons and their precursors during these processes, but the specific mechanisms by which they do this are not well understood. Here we find that in migrating olfactory bulb neuronal precursors, Slit-mediated repolarization consists of growth of a new process from the previous trailing edge, then reorientation of the centrosome followed by nuclear translocation in the reverse direction. Inhibition of cell polarity factors GSK3β or PKCζ results in impaired centrosome reorientation and process stabilization. In migrating projection neurons in the embryonic cortex, the centrosome is positioned at the base of the forming axon during the multipolar stage of migration and then is repositioned to within the leading process, which becomes the apical dendrite. We also report on the role of polarity factors GSK-3β, PKCζ, IQGAP1, APC, and CLIP-170 in axon orientation in the cortex. Lastly, we test for a new role for Wnt signaling in axon guidance in the cortex. Our findings suggest that these signaling pathways modulate the positioning of the centrosome and neuronal process stability, which are important steps in polarization in response to guidance cues.

INTRODUCTION

Neuronal migration and differentiation are under the control of chemoattractant and chemorepellent molecules that determine process orientation, guidance and polarity. Slit-1 and Slit-2 are strongly expressed in the embryonic septum (Li et al., 1999; Nguyen-Ba-Charvet et al., 2004; Wang et al., 1999) and they repel olfactory bulb (OB) precursors migrating tangentially from the anterior subventricular zone (SVZa) en route to the bulb along the rostral migratory stream (RMS) (Hu, 1999; Wu et al., 1999). Importantly, Slit is capable of reversing the direction and not simply inhibiting the migration of neurons through interactions with its cognate receptor, Robo (Brose et al., 1999; Kidd et al., 1999; Li et al., 1999). Migrating neurons that encounter Slit reverse direction by extending a new leading process on the side opposite the source of Slit while retracting the former leading process (Ward et al., 2003; Ward et al., 2005). In cultured slices, neurons in the SVZa have been observed to reverse their migration direction multiple times en route to the OB (Murase and Horwitz, 2004) suggesting that dynamic restructuring of the neuronal cytoskeleton is often required during normal migration.

In a similar manner, radially migrating projection neurons are directed to the cortical plate (CP) by guidance cues and they undergo repeated shifts in polarity during their navigation. Inferences made from electron micrograph studies suggest that most projection neurons in the neocortex shift from a bipolar to a multipolar morphology as they move through the subventricular zone (SVZ). It's in this multipolar phase of migration that the neurons extend an axon before readopting a bipolar morphology and resuming movement to the CP (Noctor et al., 2004; Shoukimas and Hinds, 1978).

Recent data suggests that migrating neurons undergo a repeating of three distinct movements accompanied by cytoskeletal alterations. First, there is extension of the leading process in the direction of migration. This event is followed by repositioning of the centrosome into the leading process (Solecki et al., 2004). Third, there is translocation of the nucleus through a cytoplasmic constriction that requires the activity of myosin II at the rear of the cell, possibly mediating a "pushing" of the nucleus from the rear (Bellion et al., 2005; Schaar and McConnell, 2005). This model suggests positioning of the centrosome in front of the nucleus is an important step in neuronal migration, where it is hypothesized to mediate nuclear-centrosome coupling or leading process stabilization.

Evolutionarily conserved pathways involved in determining body axis formation have been strongly implicated in the determination of cellular polarity. The genetic analysis of asymmetric cell division in *C. elegans* development led to the identification of several PAR (partition-defective) proteins and atypical protein kinase C (aPKC) as key components of the molecular machinery required to generate embryonic polarity (Ohno, 2001). Glycogen synthase kinase 3β (GSK3β) was also identified as a critical factor in determining dorsoventral axis formation in *Xenopus* embryos (Dominguez et al., 1995; He et al., 1995) and was subsequently identified as a direct kinase target of atypical PKCζ (aPKCζ) (Etienne-Manneville and Hall, 2003a). Specifically, Par6 was identified as a direct target of activated Cdc42 and Rac (Joberty et al., 2000), suggesting a model in which a baseline inactive Par-aPKCζ complex is activated by Cdc42, leading to phosphorylation (and thus inactivation) of GSK3β. Localized inactivation of GSK3β, through unknown mechanisms, appears to be critical for proper centrosome localization during establishment of cellular polarity (Etienne-Manneville and Hall, 2003a). In glial-

guided migration of cerebellar granule neurons, Par6 is also required, as knockdown resulted in failure of neuronal migration, a poorly organized microtubule (MT) cytoskeleton and failure of PKCζ localization to the centrosome (Solecki et al., 2004). A role of GSK3β and PKCζ function in centrosome positioning in migrating neurons has not been established.

Intriguingly, many of these same factors play key roles in determining the highly polarized morphology of differentiating neurons. In primary hippocampal neurons, formation of a single axon per neuron depends on the localized regulation of GSK3β, PKCζ, and the recruitment of the Par3/Par6 complex to the tip of the nascent axon (Jiang et al., 2005; Shi et al., 2004; Yoshimura et al., 2005). GSK3β and PKCζ activity is critical for the establishment of a single axon per cell, as inhibition of enzymatic activity resulted in multiple short axon-like processes as well as failure to establish neuronal polarity. In maturing cerebellar granule neurons, which form two axons, the centrosome is sequentially localized to the base of each axon as it extends (Zmuda and Rivas, 1998), but whether this process occurs in cortical neurons is not known. The connection between centrosome position, axon orientation and cell polarity factors in cortical projection neurons is not well understood.

Additionally, members of the IQGAP family of proteins have recently been shown to regulate neurite extension (Li et al., 2005; Wang et al., 2007). IQGAP1 is an effector of the RhoGTPases Rac1 and Cdc42 that functions in MT capture with the MT-plus end protein CLIP-170 at the leading edge of migrating cells and acts as a link between actin filaments and MT-associated APC (Noritake et al., 2005). The role of IQGAP in axon outgrowth in the cortex is not known.

Wnt genes encode for secreted morphogenic molecules that play diverse roles in development including patterning, fate determination, cell proliferation and migration. They are also responsible for various aspects on CNS development including axon guidance (Endo and Rubin, 2007). In the spinal cord, aPKCζ activity is required for Wnt-mediated attraction of commissural axons (Wolf et al., 2008). Several Wnts are expressed during cortical development, but their roles in axon guidance there have not been investigated.

Here we show a role for GSK3β and PKCζ in centrosome positioning and process stabilization during polarity reversal in response to Slit. Utilizing primary olfactory bulb precursor neurons derived from postnatal transgenic mice expressing a GFP-tagged centrosomal protein (Higginbotham et al., 2004), we found that during migration, positioning of the centrosome ahead of the nucleus is a dynamic process, linking the leading process outgrowth phase and the nuclear translocation phase of migration. The centrosome advanced within the leading process and stabilized tens of microns ahead of the nucleus. This event was uniformly followed by rapid translocation of the nucleus towards the centrosome. We found that application of Slit resulted in repolarization and migration in the opposite direction through a stereotypical sequence of events: Stage 1 consisting of new process extending from the previous trailing edge, Stage 2 consisting of centrosome starting reorientation, with concurrent retraction of the old leading process and continued extension of a new process, Stage 3 consisting of completion of centrosome reorientation to the base of the new process and completion of retraction of the old leading process. Stage 4 consisted of initiation of nuclear translocation and cell movement in the new direction. We found that GSK3β or PKCζ inhibition blocked the

transition from Stage 2 to 3. Disruption of the actin but not MT cytoskeleton led to failure of centrosome movement within the cell body. These observations suggest that Slit signaling leads to a stereotypical series of morphological events that require GSK3β and PKCζ signaling and dynamic cytoskeletal reorganization.

Additionally, we analyzed centrosomal positioning during radial migration in the embryonic cortex and found that the centrosome is repositioned from the base of the emerging axon to the leading process during the transition from a multipolar to a bipolar morphology. We also show a possible role for aPKCζ, APC and IQGAP1 in axon orientation using a slice overlay assay.

RESULTS

The centrosome is positioned ahead of the nucleus in migrating SVZa neurons

We ascertained whether SVZa neurons undergoing tangential migration en route to the olfactory bulb show the centrosome positioned in front of the nucleus. We first visualized migrating neurons using an acute brain slice from P5 transgenic mice labeled with a crystal of DiI, a lipophilic dye that integrates into the membrane in a fraction of cells that migrate in close proximity to the crystal (Anton et al., 2004; Doetsch and Alvarez-Buylla, 1996). Twelve hours after labeling, DiI-positive cells that had migrated at least 100 μM from the crystal were identified. In essentially 100% of the labeled neurons the centrosome was positioned ahead of the nucleus and was typically located within the leading process (Fig. I.1A and data not shown). In order to perform quantification, we visualized neurons in the RMS stained for Doublecortin, a marker for migrating neurons, in sections from a GFP-CETN2 transgenic mouse at postnatal day 30

(P30) (Higginbotham et al., 2004; White et al., 2000). In approximately 56% of immunopositive cells, the centrosome was within 20º of the axis of migration, and in 80% it was within 120º of the axis (Fig. III.1B). Therefore, we conclude that the position of the centrosome in front of the nucleus is strongly correlated with the direction of movement in the RMS.

To test if centrosome position also correlates with the direction of movement in isolated neurons, we analyzed primary SVZa neurons migrating through a collagen/Matrigel gel matrix after exiting RMS explants (Ward et al., 2003). These cells display pronounced monopolar morphology in culture during migration. The position of the centrosome was determined at single timepoints in cells that showed polarity oriented away from the explant. In approximately 71% of isolated neurons where the centrosome position could be clearly distinguished, it was located within 20° of the line defined by the long axis of the cell. Most often, the centrosome was positioned within the leading process of the cell (Fig. III.1C-D). Only in a small minority of cells was the position of the centrosome in other locations, such as the trailing process or adjacent to the lateral aspect of the nucleus. This suggests that the position of the centrosome ahead of the nucleus, often within the leading process, is a consistent feature in neurons during migration, as has been recently reported in other cell types (Bellion et al., 2005; Solecki et al., 2004).

Nuclear translocation is coupled to centrosome dynamics

Saltatory neuronal migration is characterized by first, extension of the leading process into the surrounding matrix, which has the effect of lengthening the axis of the

cell. This is followed by an abrupt translocation of the nucleus (Nuclear Translocation, NT) into the leading process concurrent with retraction of the trailing process, which has the effect of shortening the axis of the cell. We confirmed that similar events occur in SVZa cells using time-lapse DIC microscopy (Fig. III.2A).

Concurrent imaging of the centrosome from the *GFP-CETN2* transgenic line indicated a dynamic range of movement within the leading process that appeared to couple the leading process extension phase to the NT phase. Time-lapse analysis revealed that the centrosome moved into the leading process and subsequently stabilized tens of microns ahead of the nucleus (Fig. III.2A, Supplemental Movie III.1). The location of the centrosome was strongly correlated with a bulge in the cytoplasmic membrane of the leading process, suggesting that some cytoplasmic contents move together with the centrosome (Schaar and McConnell, 2005). This event was typically followed by NT towards the centrosome with concurrent retraction of the trailing process. The nucleus typically moved to a position adjacent to the centrosome, but occasionally moved only a variable distance towards the centrosome, or even past the centrosome. The cell then remained relatively stationary while the leading process further extended and the centrosome moved to a new position in the leading process. Occasionally the centrosome would also retract toward the nucleus and the two would meet at some intermediate point. During nuclear movement into the leading process, the cell membrane often was constricted near the rear of the nucleus, segmenting the nucleus into two compartments. Frame-by-frame analysis suggested that the nucleus moves through a membrane-anchored constriction (Fig. III.2A, black arrow), reminiscent of the actin-myosin contractile ring in telophase in other cell types (Feierbach and Chang, 2001).

To quantify centrosomal and nuclear movement, measurements were made of the nuclear-centrosomal (N-C) distance and cumulative NT distance as a function of time in a series of actively migrating cells. We found that nearly all cells showed a stereotypical series of events during the transition from stationary to migratory phases. While the nucleus remained stationary, the N-C distance gradually increased from an average of 10μm to about 15-20 μm. This was followed by a rapid decrease in the N-C distance that coincided with NT. The variability in N-C distance implied there was not a threshold N-C distance above which NT would occur. However, N-C distance typically did not extend beyond ~20 μm without a subsequent NT event. We found that during the course of migration in a population of several hundred cells, the N-C distance did not exceed about 26μm, averaging 4.5μm. NT most often occurred just after a sharp increase in N-C distance (Fig. III.2B). This data suggests that the movement of the centrosome into the leading process is a critical phase in nuclear translocation and neuronal movement. Positioning of the centrosome in the leading process has been proposed to mediate both the N-C coupling during the NT phase, as well as leading process stabilization during the neurite outgrowth phase through its effects on MTs. In order to determine whether process length correlated with N-C distance, we measured these two parameters in single cells as a function of time. As expected, we found that a change N-C distance correlated positively with a change in the length of the leading process (Fig. III.2C).

The neuronal centrosome reorients in response to Slit exposure

To determine whether centrosome position is a critical factor in neuronal migration, we acutely reversed cell polarity and the direction of migration with the

chemorepellent Slit. RMS cells respond to Slit *in vivo* where it is presumed that Slit secreted from the septum drives neurons rostrally towards the OB (Wu et al., 1999). Bath-application of Slit-conditioned media to SVZa neurons (migrating from RMS explants embedded in collagen/Matrigel) causes a reversal of polarity and of migration direction (Ward et al., 2003). Following application, the majority of neurons repolarize and migrate in the opposite direction back into the explant (Supplemental Movie III.2). This allowed us to test the cellular events surrounding repolarization and reversal of migration direction.

To test whether Slit application led to repositioning of the centrosome in the new direction of migration, we monitored centrosome position at hourly intervals. Just before Slit application, the centrosome was nearly uniformly positioned ahead of the nucleus. Following Slit application, there was gradual reversal in centrosome positioning, and by the end of 4 hrs, approximately 53% of cells displayed reorientation of the centrosome (Fig. III.3). Response to Slit was not synchronized among neurons, as evident by the increasing percentage of cells with reorienting centrosomes at hourly intervals, and at further timepoints centrosome reorientation was complete in nearly all cells (data not shown). As centrosome reorientation occurs in the same time frame as reversal of polarity, we tested the sequence of events surrounding Slit-mediated repolarization.

Centrosome reorientation follows new leading process outgrowth but precedes neuronal movement

We hypothesized that following Slit application, centrosome reorientation towards the explant would occur prior to onset of migration in the new direction (back

towards the explant). Therefore, we analyzed the sequence of events as cells undergo reversal of migration direction by monitoring morphology, position of the centrosome and direction of migration following the application of Slit at 5 min intervals in sixty-one cells. We observed four distinct stages during reversal of migration direction in response to Slit (Fig. III.4A-B). In Stage 1, there is emergence of a new leading process in what will be the new direction of migration. This process typically emerges close to 180° from the former leading process, extending directly back towards the explant. In Stage 2, the centrosome begins to reorient to the base of the new leading process, with concurrent retraction of the old leading process and lengthening of the new leading process. In Stage 3, the centrosome reaches the base of the new leading process (i.e. reorients to a position in front of the nucleus in the new direction of migration), and there is continued extension of the new leading process. In Stage 4, the centrosome moves into the new leading process and the nucleus translocates forward (Supplemental Movies III.3-4).

To determine if these four events occur sequentially or randomly, the time interval between each event was determined following the application of Slit. The average interval between Stage 1 and Stage 2 was 38 min (median = 37.5 min). In 98% of neurons scored, the new process was clearly evident before the centrosome began reorientation, as defined by the time point when the centrosome moved past the previous leading edge of the nucleus. The average time interval between Stage 2 and Stage 3 was 22 min (median = 20 min). In 85% of cells, the previous leading process began to retract before the centrosome reoriented to the base of the new process. The average time interval between Stage 3 and Stage 4 was 21 min (median = 10 min). In 78% of the neurons that reversed migration direction during the time interval analyzed, the arrival of

the centrosome at the base of the new process preceded cell movement. After reversal of morphology and reorientation of the centrosome, neurons resumed saltatory motion with the centrosome extending into the leading process followed by NT. Box-and-whisker plots indicate that the median time interval between these stages is consistently above zero, indicating that these stages, on average, occur in sequence (Fig. III.4C). Together, this data suggests that centrosome positioning ahead of the nucleus occurs after leading process initiation, but before stabilization/elongation of the new leading process or NT in the new direction.

GSK3βactivity required for centrosome reorientation and reversal of neuronal polarity.

We next sought to determine which factors participate in reorientation of the centrosome in migrating neurons in response to Slit chemorepulsion. Pharmacological inhibition of either GSK3β or PKCζ causes failure of centrosome reorientation in the direction of a scratched wound in migrating astrocytes, and as a result there is impaired migration towards the wound (Etienne-Manneville and Hall, 2003a). We therefore tested the effects of acute pharmacological inhibition of these factors on the Stage 2 to 3 transition in migrating neurons, encompassing centrosome reorientation in primary SVZa neurons.

We first blocked GSK3β activity by application of the BIO Inhibitor IX, (6-bromoindirubin-3'-oxime) (Leclerc et al., 2001; Meijer et al., 2003), which has an IC50 for GSK3α/β of 5nM, and less affinity for CDKs (80-100 nM) and other kinases (>10 mM). Explants were first cultured for 12 hr before application of BIO, then 5.5 hrs later

Slit-conditioned media was added and time-lapse imaging at 10-minute intervals was initiated. We observed a significant reduction in cells displaying centrosome reorientation, from 67% in vehicle control to 34% after treatment (Fig. III.5A). Similarly, LiCl, a well-established GSK3α/β inhibitor, which has an IC50 in the 10–20 mM range (Davies et al., 2000; Klein and Melton, 1996) and less potent effects on other non-overlapping pathways (Patel et al., 2002) was tested. Even more striking failure of centrosome reorientation was observed, with over 75% failing to show centrosome reorientation in the time course of the experiment. In most cells, after Slit application the centrosome either remained immobile or moved from the base of the previous leading process to a site adjacent to the nucleus without completing reorientation. We conclude that inhibition of GSK3β leads to failure of centrosome reorientation during repolarization.

Because GSK3β has potent effects on MT stability and neurite outgrowth (Goold et al., 1999; Zhou et al., 2004) we evaluated for alterations in the length of the new process relative to control at the Stage 2 to 3 transition following treatment with BIO. As GSK3β-mediated phosphorylation of MT-associated proteins generally leads to inactivation (Sanchez et al., 2000), we anticipated that inhibition would lead to longer or less dynamic processes. Surprisingly, we found that this treatment had a negative effect on new process length following Slit application, with a 60% reduction versus control length at the completion of the experiment (Fig. III.5B). These data suggest that GSK3β also functions in stabilization/elongation of the new process during repolarization.

We tested for a disruption in the establishment of polarity following application of BIO as measured by formation of a single new process following Slit application. We

found that there was a 50% increase in the number of transient new processes formed per cell during the timelapse interval (Fig. III.5C). These processes extended from the cell body and typically fully retracted during the time interval analyzed. These new processes generally extended towards the explant, but also occasionally grew from other regions of the cell body. This data suggests that GSK3β activity is required for the stabilization, but not the initiation of a single process, a critical stage in cell repolarization following exposure to Slit.

Because of the failure of multiple aspects of repolarization, we hypothesized that cell migration in the new direction following Slit exposure would be defective. Therefore, we measured migration distance towards the explant following inhibition of GSK3β with BIO or LiCl, and found over a 50% reduction in the average migration distance relative to control (data not shown). However, GSK3β inhibitors similarly affected overall migration in the absence of Slit (data not shown). Therefore it was not possible to determine a specific role for GSK-3β in the Stage 3 to 4 transition.

Centrosome reorientation correlated with repolarization and migration in the new direction

In the presence of GSK3β inhibitors, we noted a small fraction of cells that appeared to show correct centrosome reorientation as well as some that showed migration rates similar to controls. We therefore tested if the cells that reoriented the centrosome correctly were the same that showed faster migration velocity. We repeated the analysis and divided the recorded cells into two groups based on whether the transition from Stage 2 to 3 was observed (i.e. whether centrosome reorientation was observed during the

recording). Cells that showed proper centrosome reorientation to the base of the new leading process typically displayed longer leading processes in the new direction, followed by rapid migration in the new direction. On the other hand, cells that did not show reorientation of the centrosome showed shorter leading processes and also failed to migrate in the new direction. Typically, such cells often showed multiple transient processes that emerged from various positions around the cell body (Fig. III.6A-B).

The length of neurites and migration distance were then quantitated in neighboring cells that were exposed to the same concentration of BIO but that either displayed or did not display centrosome reorientation during the recording. We found that cells that showed centrosome reorientation had leading processes that were on average over twice as long as cells that failed to show centrosome reorientation (Fig. III.6C). We conclude that even in cells exposed to the same concentration of drug, the occurrence of centrosome reorientation is a major determinant of the length of the new leading process.

We next compared the migration distance among these cell groups in the presence of BIO, LiCl or DMSO vehicle control at the previous concentrations. We found a striking difference in migration distance after Slit exposure, where cells that failed to display centrosome reorientation on average migrated only about one-third to one-fourth the distance back towards the explant compared to neighboring cells, irrespective of the treatment group (Fig. III.6D). We noted a slight negative effect of BIO or LiCl on migration even in cells that showed centrosome reorientation, but this was not as striking as the difference between neighboring cells exposed to the same concentration of drug that were separated based upon centrosome reorientation. We conclude that centrosome reorientation is a major determinant of cell migration distance following exposure to Slit.

PKCζactivity required for centrosome reorientation and reversal of neuronal polarity

The atypical protein kinase family shows an evolutionarily conserved function in establishing cell polarity. There are two aPKC isoforms in mammals, PKCζ and PKCλ/ι, and these kinases are part of the PAR complex that additionally contains PAR-3 and PAR-6 (Ohno, 2001). We therefore further tested whether PKCζ activity is required for centrosome reorientation in response to Slit in migrating SVZa neurons using one nonselective PKC inhibitor, Gö6983 (2-[1-(3-Dimethylaminopropyl)-5-methoxyindol-3-yl]-3-(1H-indol-3-yl) maleimide), IC 50 = 6-60 nM for PKCα, PKCβ, PKCγ, PKCδ and PKCζ) and one specific PKCζ inhibitor, named Pseudo, a membrane-permeable myristoylated pseudosubstrate (IC50 = 10-20 μM, negligible discernable activity for other PKCs) (Gschwendt et al., 1996; Standaert et al., 1999; Standaert et al., 1997). Experiments were performed identically as for GSK3β inhibitors.

Application of Gö6983 or Pseudo resulted in a disruption of centrosome reorientation following Slit application (Fig. III.7A). In both experiments, approximately 35% showed reorientation versus 68% for vehicle control, suggesting that PKCζ activity is required for the transition between Stage 2 and 3. We also examined the average length of new neurites extending towards the explant following the addition of Slit, and found a modest effect that was only statistically significant for the nonselective PKC inhibitor Gö6983 (Fig. III.7B). There was no statistical difference in new process length extending towards the explant following the application of Pseudo. This data suggests that the other PKCs may play a role in neurite stabilization/elongation following Slit application. However, there was a striking effect on the average number of transient new

processes relative to control with both Gö6983 and Pseudo, showing a 3-4 fold increase (Fig. III.7C). Similar to what was observed following GSK3β inhibition, these processes extended both towards the explant and in random directions and did not survive more than 30 minutes.

We similarly tested whether the effect of PKCζ inhibition on migration depended on centrosome positioning, by repeating the experiment using timelapse recordings. We again noted that cells failing to reorient the centrosome also failed to migrate in the new direction (Fig. III.7D). These differences were highly statistically significant in the case of the DMSO control and Gö6983, whereas treatment with Pseudo showed similar results without having statistical significance. A small fraction of cells that showed centrosome reorientation in the presence of PKCζ inhibition typically displayed a long stable process that extended in the new direction, which was rapidly followed by migration back towards the explant. Strikingly, many of the cells that failed to show centrosome reorientation continued to migrate in the previous direction, away from the explant as if Slit were not present (DMSO NR and Pseudo NR). As seen with GSK3β inhibitors, PKCζ inhibitors also had an effect on migration as shown by the reduced migration distance of Pseudo and Gö6983-treated cells as compared with the DMSO control, even in cells where the centrosome reorients. Taken together, we conclude that PKCζ plays a critical role in repolarization and centrosome reorientation in response to Slit, and that defects in centrosome positioning contribute to the migration defect.

Centrosomal reorientation fails to occur following disruption of the actin or MT cytoskeleton

In order to determine if repolarization or centrosome movement of migrating neurons in response to Slit has specific cytoskeletal requirements, we tested the effects of nocodazole, a MT-depolymerizing agent, and latrunculin B, an inhibitor of actin filament polymerization, added one hour after Slit application. Nocodazole applied 1 hr after Slit conditioned media caused dramatic changes in cell morphology. Immunostaining with an anti-tubulin antibody showed an overall decrease in signal intensity throughout the cell (data not shown). Neuronal polarization was altered, with shortening and retraction of cellular processes. However, the rounded neurons continued to extend transiently short budding processes or lamellar sheets from all sides of the cell, possibly reflecting actin/myosin modulation (Schaar and McConnell, 2005). In contrast to controls without nocodazole where the centrosome robustly reoriented to the opposite pole, the centrosome in nocodazole-treated cells initially retracted to the center of the cell body (Fig. III.8A-B). However, it subsequently became mobile within the cell body and was consistently associated with areas of the cell membrane ruffling from which small protrusions or lamellar sheets randomly extended (Fig. III.8C). We did not observe these small processes or lamellar sheets persist or mature into stable leading processes and consequently, the centrosome did not maintain a stable position. Washout of nocodazole with Slit-conditioned media resulted in the recovery of cell polarity and migration back towards the explant (data not shown). The direction of the new leading process was independent of the position of the centrosome at the time of nocodazole washout, but instead predominantly extended back towards the explant (data not shown). The data

suggest that disruption of the MT cytoskeleton leads to failure of centrosome reorientation towards the explant but that some movement of the centrosome into transient processes may be possible.

Pretreatment of cells with latrunculin B led to little change in cell morphology in response to Slit. Actin staining showed a dramatic loss of signal within the leading processes and a corresponding increase of signal near the cell body, indicating a loss of actin networks (data not shown). Cells retained their polarized morphology, but the filopodial branches at the tip of the leading process were no longer visible. No new processes were observed in any region of the cell and the centrosome remained stationary within the leading process or drifted slightly toward the cell body (Fig. III.8D-F). Addition of nocodazole concomitantly with latrunculin B resulted in a similar response to latrunculin B alone, where the leading process remained fixed, as did the centrosome, despite the loss of smaller filipodia (not shown). These data suggest that repolarization and centrosome reorientation in response to Slit fails to occur following disruption of the actin cytoskeleton.

Centrosome position during radial migration

We next turned to an analysis of radially migrating projection neurons in the embryonic brain. Inferences made from electron micrograph studies suggest that most projection neurons in the neocortex shift from a bipolar to a multipolar morphology as they move through the subventricular zone (SVZ). It is in this multipolar phase of migration that the neurons extend an axon before readopting a bipolar morphology and resuming movement to the CP (Noctor et al., 2004; Shoukimas and Hinds, 1978; Tabata

and Nakajima, 2003). We tested whether centrosomal positioning correlated with axon extension in the SVZ, as has been shown in cerebellar granule neurons and suggested in hippocampal neurons *in vitro* (de Anda et al., 2005; Zmuda and Rivas, 1998).

Using DiI labeling of individual neurons in cortical slices from transgenic mice expressing GFP-CENTRIN2 (Higginbotham et al., 2004), we analyzed centrosomal positioning in cells within the SVZ, intermediate zone (IZ) at embryonic day 14.5 (E14.5) and in the CP at postnatal day 13 (P13). Individual neurons were labeled with DiI-coated microparticles propelled from a Bio-Rad gene gun (Fig. III.9A). Analysis of the SVZ region showed that many of cells displayed a multipolar phenotype (defined as having more than one process extending from the cell body) with either a short, thickened or long, thin process oriented towards the ventricle (Fig. III.9B,C). This process was presumed to be the emerging axon. In some cells with a longer axon, another pial-directed process was often observed (Fig. III.9C), suggesting the formation of a migratory leading process. In the IZ, where most cells are migrating, a long, thin axon extended towards the ventricle, and then turned to course through the axon tract, parallel to the ventricle (Fig. III.9D) and (not shown). These cells also displayed a prominent leading process, with other minor processes (Fig. III.9D).

Analysis of centrosome position in cells in the SVZ and IZ showed an interesting phenomenon: by plotting the position of the centrosome relative to the emerging axon and the nucleus, we found that in 75% of cells the centrosome is located at either the base of the axon or within the growing leading process (Fig. III.9E). This suggests in projection neurons in the multipolar phase of migration, the centrosome moves consecutively to the base of the emerging axon and then to the base of the migratory

process. We also examined fully differentiated projection neurons in the CP and found that in all cells analyzed, the centrosome is found at the base of the apical dendrite (Fig. III.9F), which has been suggested to be the derivative of the migratory leading process (Barnes et al., 2008).

The previous analysis was conducted in fixed tissue where the identity of the axon could not be ascertained unambiguously. Therefore we analyzed centrosomal positioning in live cells using the slice overlay assay (Polleux and Ghosh, 2002). In this assay dissociated cortical neurons from E14.5 GFP-CENTRIN2+ embryos are labeled with DiI and overlayed onto a P2 rat cortical slice (Fig. III.10A) After plating, a process begins to emerge which has been shown to be the axon (Polleux and Ghosh, 2002; Polleux et al., 1998; Polleux et al., 2000). In the majority of overlayed cells the axon extends towards the ventricle as a result of Sema3 repulsion (Fig. III.10B,C) (Polleux et al., 1998). Upon plotting the centrosome's position relative to the axon and the nucleus, we found that in 53% of cells, the centrosome was located at the base of the axon, regardless of the orientation of the axon (Fig. III.10D).

Polarity factors and axon orientation

We next asked whether the polarity factors involved in Slit-mediated repolarization of SVZa neurons were also involved in axon orientation in cortical projection neurons. To answer this, we combined the slice overlay assay with shRNA-mediated knockdown or pharmacological inhibition of five factors known to be involved in polarity: aPKCζ, APC, IQGAP1, CLIP-170 and GSK-3β. We electroporated shRNA constructs (OpenBiosystems) together with hrGFPII (Stratagene) or dsRedII (Clontech)

in utero into E14.5 wild-type embryos (Fig. III.11A). After 48 hours we excised form the E16.5 cortex the electroporated regions displaying red or green fluorescence. The cortical explants were dissociated and the cells were overlayed onto early postnatal rat cortical slices for two hours, after which axon orientation was scored. In cells electroporated with dsRedII only, 69% of cells had axons oriented towards the ventricle (Fig. III.11B). However, knockdown of aPKCζ, APC, IQGAP1 and CLIP-170 showed variations in axon orientation, from almost complete randomization of axon orientation in the case of IQGAP1 shRNA #1 (Fig. III.11E) to a strong bias towards the ventricle, as in the case of IQGAP shRNA #2 and CLIP-170 shRNA #2 (Fig. III.11F,H). We further tested the role of aPKCζ and GSK3β using pharmacological inhibitors and found no difference in axon orientation between control and inhibition conditions (not shown). In sum, these results were inconclusive and can only suggest a possible role for aPKCζ, APC, IQGAP1 and CLIP-170 in axon orientation in the cortex. Replication of these experiments will be necessary.

Wnt signaling and axon orientation

Wnt proteins are known to function as positional cues and direct cell polarity (Goldstein et al., 2006). Because of the distinct expression patterns of some Wnts in the embryonic cortex (Grove et al., 1998; Lee et al., 2000), we decided to test whether Wnt signaling might play a role in axon orientation. To do this we inhibited Wnt signaling with secreted frizzled-related proteins (SFRP) in the slice overlay assay (Fig. III.12A). SFRPs constitute a large family of proteins whose members are expressed in complex patterns during brain development. In addition to their roles in axon guidance, they are

also endogenous inhibitors of Wnt signaling (Drescher, 2005). We applied SFRP2 at two different concentrations to embryonic cortical neurons 1 hour prior to being overlayed onto postnatal rat slices. After 2 hours we analyzed axon orientation. We found that although the bias of axon orientation towards the ventricle was less prominent in these experiments than in the shRNA experiments, there was no significant difference between control and SFRP-treated conditions at two different concentrations (Fig. III.12B-D). Further work is needed to further address the role of Wnt signaling in axon orientation in the cortex.

DISCUSSION

The unique morphology and molecular requirements of migrating neurons (Bielas and Gleeson, 2004; Hatten, 2002) suggests that specific signaling and cytoskeletal mechanisms exist to allow for efficient movement through the complex environment of the developing brain. We find that neuronal migration is characterized by a repeating of three basic events: 1. Leading process extension, 2. Centrosome positioning within the leading process, and 3. Nuclear translocation. In response to Slit, repolarization occurs in four stereotypical steps. 1. New process extension from the previous trailing edge, 2. Start of centrosome reorientation, 3. Completion of centrosome reorientation, 4. Initiation of movement in the new direction. Our data do not exclude the possibility that there were other stage orders, but in observing large populations of cells, we rarely found exceptions. Inhibition of GSK3β activity led to a failure of the Stage 2 to 3 transition, and an increase in transient neuronal processes. Cells failing to repolarize in response to GSK3β also failed to migrate in the new direction, likely a result of this repolarization

failure, because cells that repolarize properly in the presence of GSK3β inhibition showed higher migration rates. Similar effects were observed following inhibition of PKCζ function, and although the effect on new process elongation was not as striking, there was a more potent effect on migration. We found that an intact MT cytoskeleton is necessary for maintenance and growth of a leading process, but not for centrosomal movement within the cell body, whereas an intact actin cytoskeleton is necessary for repolarization and centrosome reorientation. Together these results suggest that cell polarity factors are required for reversal of polarity in response to Slit-mediated chemorepulsion.

Centrosome positioning during directed migration

In several cell types, the centrosome is positioned between the leading edge of the cell and the nucleus, where it is thought to play a critical role in stabilizing MTs or in transport of organelles. In newt eosinophils, the centrosome is positioned in front of the nucleus and laser irradiation of the centrosome results in randomly directed movement, suggesting a requirement for the centrosome in determining the direction of motility (Koonce et al., 1984). During migration in *Dictyostelium discoideum*, only chemotactically migrating cells display positioning of the centrosome ahead of the nucleus (Sameshima et al., 1988). In these cells, pseudopods emerge from several different sites, but the one that attracts the centrosome determines which direction the cell will migrate. If the centrosome fails to reorient, the pseudopodium is soon retracted (Ueda et al., 1997).

Most studies have determined that centrosome repositioning follows the protrusion of the leading edge in response to external stimuli and, in doing so, stabilizes cell movement through unknown mechanisms (Schliwa et al., 1999). Therefore, it appears that positioning of the centrosome ahead of the nucleus is a common feature of directed migration in many cell types from diverse organisms. These studies suggest that centrosome position is important for stabilizing the cytoskeleton in the new direction of migration, but probably does not act as a steering mechanism to determine the new direction of migration. As the major MT organizing center of the cell, the position of the centrosome is likely essential for efficient delivery of newly generated MTs and membranous vesicles into the leading process during migration (Abal et al., 2002; Ahmad and Baas, 1995; Gregory et al., 1988; Hatten, 1993; Yu et al., 1993).

We found that SVZa cells show a repeating of centrosome positioning followed by NT, similar to the "two-stroke" model of NT that has been proposed in migrating cerebellar granule neurons (Solecki et al., 2004). Furthermore, in cells undergoing reversal of direction in response to Slit, movement in the new direction uniformly followed centrosome reversal. Therefore, positioning of the centrosome ahead of the nucleus appears to be a prerequisite for neuronal migration.

Nuclear-centrosome coupling

Interestingly, a connection between the nucleus and basal body/centrosome is conserved in many organisms and is crucial for cell polarity and must be preserved during centrosome reproduction (Bornens and Azimzadeh, 2007). The forces that generate centrosomal movement within the leading process in migrating cells are

unknown, but may require dynamic interplay between centrosome-directed forces at the leading edge of the process and at the nucleus. In wound-edge NIH3T3 fibroblasts, a dynein/dynactin/Lis1 complex localizes to the leading edge during migration (Dujardin et al., 2003). Dynein was also found at the cortex in dividing epithelial cells, and its activity was required for proper movement of the mitotic asters during cell division (Busson et al., 1998). This proposed model, in which dynein anchored at the cell membrane acts to pull the centrosome, assumes that a significant proportion of MTs remain tethered to the centrosome during migration. Ninein, a minus-end MT-associated protein, localizes to the centrosome in cultured neurons (Baird et al., 2004), where it may serve to anchor MTs (Mogensen et al., 2000). These centrosomally-anchored MTs may become captured in the leading process through interactions between the Rac1/Cdc42 effector IQGAP and the plus-end MT tip protein CLIP-170 (Fukata et al., 2002), which has been shown to associate with dynein at cortical sites (Vaughan et al., 1999). Dynein anchored at the cortex may generate the force that moves the centrosome into the leading process.

The forces that generate nuclear movement towards the centrosome are also unknown, but previous work suggests that these may also be dynein/MT dependent. Recent studies have suggested that a MT link between the nucleus, centrosome and cell cortex is important for proper migration. A cage-like distribution of MTs around the nucleus of migrating neurons has been described (Gregory et al., 1988; Rivas and Hatten, 1995) and shown to converge at the centrosome (Tanaka et al., 2004). A defect in N-C coupling has been identified in neurons with reductions in the migration genes LIS1 or NUDEL (Shu et al., 2004; Tanaka et al., 2004), two dynein-associated factors localized to the N-C region (Faulkner et al., 2000; Yan et al., 2003). The results presented here

support a model in which the nucleus is dynamically coupled to the centrosome during migration.

Cell polarity factors determine centrosome position

What are the cell biological and genetic factors that contribute to centrosome positioning and process outgrowth during neuronal repolarization in response to guidance cues? Stimulation by Slit leads to an increased association between its receptor, Robo, and Slit-Robo GTPase-activating proteins (srGAPs), which leads to localized inactivation of Cdc42 (Wong et al., 2001). Thus, changes in small GTPase activity may mediate the cytoskeletal changes that underlie cellular repolarization. Similarly, in wounded monolayer cultures, centrosome reorientation in front of the nucleus appears to critically depend on Cdc42 (Palazzo et al., 2001). Integrin-mediated activation leads to polarized recruitment of Cdc42, which in turn leads to polarized recruitment and activation of a cytoplasmic mPar6/PKCζ complex (Etienne-Manneville and Hall, 2001). This complex directly phosphorylates GSK3β, locally inhibits its activity, and promotes polarization of the centrosome in the direction of cell protrusion. This occurs through unknown mechanisms involving spatially-restricted association of adenomatous polyposis coli (APC) to MT ends, where it likely functions to stabilize MTs in the newly-growing leading process (Etienne-Manneville and Hall, 2003b; Zumbrunn et al., 2001).

Our data suggest specific cytoskeletal requirements for reversal of polarity in neurons. MT depolymerization prevented the formation of a stable leading process, but not the dynamic movement of the centrosome within the cell body. Actin disruption may have prevented centrosomal movement either because the cells failed to establish new

processes, or because of disrupted cortical actin-myosin interactions (Rosenblatt et al., 2004). This suggests that MT dynamics play a dominant role in maintaining centrosome positioning within the leading process, but actin dynamics are necessary for the initiation of polarity reversal.

In differentiating neurons, GSK3β, PKCζ and centrosome positioning have been implicated in the establishment and maintenance of the nascent axon. Inhibition of PKCζ in cultured hippocampal neurons prevented the formation of axons (Shi et al., 2003). In dorsal root ganglion (DRG) neurons, nerve growth factor (NGF) induced rapid axonal growth through localized phosphatidylinositol 3-kinase (PI3K) activation and GSK3β inactivation in the neurite destined to become the axon, leading to a strengthened interaction of APC with the plus-ends of the growing axonal MTs (Zhou et al., 2004). Interestingly, GSK3β inhibition in differentiating hippocampal neurons results in the formation of multiple axon-like processes and converts existing dendrites into axons (Jiang et al., 2005; Yoshimura et al., 2005). These observations parallel those seen in repolarizing astrocytes where inhibition of GSK3β or PKCζ results in random cell protrusions (Etienne-Manneville and Hall, 2001; Etienne-Manneville and Hall, 2003a), and agrees with our observations. Although we found that new process stabilization fails to occur in the absence of centrosome reorientation, there remains the possibility that centrosome reorientation is blocked as a result of impaired process stabilization rather than process stabilization being blocked as a result of impaired centrosome reorientation. To differentiate between the two possibilities, further experiments including centrosome ablation and process severing will be informative. Considering that GSK3β and PKCζ inhibition impairs process stabilization and centrosome reorientation, these proteins also

likely play significant roles in the three phases of migration: process outgrowth, centrosome movement into the leading process, and nuclear translocation. Indeed, we found that the inhibitors used here reduced migration even in the absence of Slit.

Centrosome position and axon outgrowth

Recent data suggests that the position of the centrosome is critical in determining where the nascent axon will eventually protrude (de Anda et al., 2005). In radially-migrating cortical projection neurons, we found that the centrosome consistently localizes to the base of the emerging axon during the multipolar stage of migration in the SVZ. The centrosome then reorients to the base of the leading process as cells move into the cortical plate.

Why does the centrosome localize to the base of the axon? Growing axons require a steady delivery of membrane and MTs to the migrating growth cone, along with proteins like guidance cue receptors to enable the axon migrate in the correct direction. In differentiating neurons, the centrosome is the primary source for MTs destined for axons and dendrites (Baas and Yu, 1996) and the Golgi co-localizes with the centrosome (Zmuda and Rivas, 1998). This suggests that centrosome position is important as a center for membrane trafficking and polarized MT delivery to the axon.

Real-time experiments in hippocampal neurons have suggested that the first process to extend from an unpolarized cell becomes the axon and that the Golgi/centrosome is located at its base, but these findings were not replicated *in vivo* (de Anda et al., 2005). In maturing cerebellar granule neurons, which form two axons, the centrosome is sequentially localized to the base of each axon as it extends (Zmuda and

Rivas, 1998). Initiation of the secondary axon can be prevented by depolymerization of actin, which results in randomization of centrosome position (Zmuda and Rivas, 2000). However, if the second axon has initiated growth prior to addition of the actin-depolymerizing drug, actin disruption does not prevent continued extension of the second axon (Zmuda and Rivas, 2000). Therefore, the centrosome's position at the base of the axon might be required only for the initiation of axon growth. The coordination between actin and centrosome-dependent MT growth is likely to be a key component of axon extension. Axotomized neurons could provide a model to analyze the requirement for centrosome positioning during axon extension and specification because these neurons form a new axon from a preexisting dendrite. The position of the centrosome during this process has not been tested (Dotti and Banker, 1987).

Guidance cues and axon orientation

The guidance cues that direct cell migration and centrosome position in fibroblasts and astrocytes also direct the outgrowth of axons and dendrites in primary neurons using many of the same molecules (Etienne-Manneville and Hall, 2001; Etienne-Manneville and Hall, 2003a). Netrin-1 from the floor plate or ganglionic eminence can act as a chemoattractant for axons, while semaphorin3 (Sema3) and Slit1 in the cortical plate or marginal zone act as repellants (Metin et al., 1997; Polleux et al., 1998; Polleux et al., 2000; Richards et al., 1997; Whitford et al., 2002). Sema3 secreted from the marginal zone repels growing axons towards the white matter and its deletion results in randomization of axon orientation (Polleux et al., 1998). Sema3 can also act as an attractant for apical dendrites and its disruption leads to randomization of apical dendrite

orientation (Polleux et al., 2000). Sema3 is a guidance cue secreted from the marginal zone that plays an important role both in the guidance of the migrating neurons and the orientation of the nascent axon (Chen et al., 2008; Polleux et al., 1998; Polleux et al., 2000). Sema3 secreted from the marginal zone repels growing axons towards the white matter while simultaneously acting as an attractant for the migratory leading process. It is tempting to speculate that the multipolar morphology of cells in the SVZ is a result a mixed cytoskeletal response to factors that are both attractive and repellant.

One molecule in the Sema3 pathway, collapsin response mediator protein (CRMP-2), has received recent attention for its role in polarity maintenance in hippocampal neurons. Repulsion by Sema3 depends on the localized inactivation of GSK-3β and accumulation of active CRMP-2 in the nascent axon tip (Uchida et al., 2005; Yoshimura et al., 2005). This allows targeting of the Par3/Par6/aPKC complex to the tip by APC, MT capture through IQGAP1 and CLIP-170 (Fukata et al., 2002) and subsequent axon specification (Shi et al., 2004; Shi et al., 2003; Zhou et al., 2004). It remains to be seen whether axon specification by these molecules occurs through modulation of centrosome position.

We found a possible role for IQGAP1, CLIP-170, aPKCζ, and APC in axon orientation in cortical neurons, suggesting that their activity might be required during polarization in response to guidance cues like Sema. The varying effects on axon orientation that we found can be explained in several ways. Most importantly, the shRNAs were not rigorously tested for knockdown effect. In addition, the slice overlay assays were conducted only 48 hours after electroporation, which may not have been sufficient time for complete depletion of the targeted proteins. The lack of effect using

pharmacological inhibitors might be a result of using concentrations that were too low for a protocol using postnatal cortical slices. Further experiments are needed.

From experiments using SFRP to inhibit Wnt, we found that Wnt signaling apparently has no effect on axon orientation. This is somewhat surprising, considering the role for Wnts in axon guidance in other systems. Further manipulation of Wnt signaling through alternative means such as genetic knockdown will be required to explore this issue more fully. Together these studies suggest interplay between polarity factors and centrosome positioning in multiple neuronal cell types in determining polarity during migration and differentiation.

METHODS

Immunohistochemistry of rostral migratory stream

A 30-day-old mouse transgenic for the GFP-CETN2 transgene was perfused-fixed (PFA 4%). The brain was drop-fixed in additional PFA and frozen sections made for IHC. Goat anti-doublecortin (Santa-Cruz) used at 1:300. Hoechst (Molecular Probes) used to stain nuclei. Images were taken with an inverted microscope (IX-70, Olympus) and deconvolved using Softworks (Applied Precision).

DiI labeling of sagittal slices

Sagittal slices of postnatal day 5 GFP-CENT2 transgenic mice were made with the MX-TS tissue slicer (SD Instruments). A small DiI crystal (Molecular Probes) was placed on the RMS and the slices were cultured for 8-12 hours on a nitrocellulose filter in DMEM + 10% FCS.

Dissection and culture of SVZa explants

The SVZa explant assay has been described previously (Ward et al., 2003; Wu et al., 1999). Coronal sections (~400μm) of the olfactory bulb from postnatal day 5 GFP-CETN2 transgenic mice were made with the McIlwain Tissue Chopper (Mickle Laboratories Engineering Co. Ltd.). The translucent RMS was dissected from the middle of the slices and cut into small explants (200-400 μm diameter) and embedded in a 2:2:1 collagen (Vitrogen): Matrigel (BD Biosciences): DMEM mixture. Explants were incubated overnight in DMEM + 10% FCS, 37°C, 5%CO_2. Bath-application of Slit-conditioned media to RMS explants induces turning through an unknown mechanism (Ward et al., 2003).

Measurement of centrosome angles in RMS and SVZa

Doublecortin (Dcx) labeling identified cells migrating through the RMS. Using low magnification, the axis and direction of the RMS was determined. Images acquired at higher magnification were used for individual cell measurements (n = 110 cells). Reference lines were drawn parallel to the axis of the RMS through the middle of the nuclei of Dcx-positive neurons.

Time lapse imaging of migrating SVZa neurons

DIC and fluorescent images were taken every 5 minutes after ~20-24 hours of culture at a time when many of the neurons had exited the explant and were actively migrating. Images were captured on a DeltaVision inverted Olympus microscope with a 60X objective and a custom 37°C CO_2-controlled incubator. Time lapse images were acquired at five 1.0 μm steps to ensure identification of the centrosome at each timepoint. Experiments were performed using the multipoint revisiting feature in order to image several neurons concurrently. Measurements of nuclear-centrosomal distance and migration distance were made with Softworks software (Applied Precision).

Conditioned media

Slit-expressing HEK cells were kindly provided by Yi Rao (Washington University, St. Louis, MO). These were cultured overnight in DMEM + 10% FCS and the unconcentrated media was collected for use on the SVZa explants.

Measurement of centrosome reorientation in response to Slit

Slit-conditioned media was added to cultures of SVZa explants and fluorescent images were taken every hour. A reference line was drawn perpendicular to the explant, bisecting the nucleus of each cell. The location of the centrosome was categorized into

three different regions. Those centrosomes in the region bound by a 30° angle above and below the reference line on the far side of the nucleus were considered "away" from the explant. Those centrosomes in the region between the nucleus and explant bound by a 30° angle above and below the reference line were considered oriented "toward" and all other intermediate locations were categorized "intermediate". The proportion of cells from the three regions was averaged at each time point.

Cell turning analysis

For studies analyzing the distinct events in cell turning, Slit-conditioned media was added to SVZa explant cultures. Images were taken every five minutes using DIC and fluorescence for GFP-CETN2. New process outgrowth was defined by the first appearance of a leading process that eventually became the new leading process. If this occurred before the time-lapse imaging began, the event was scored as if it had occurred at t=0. Commencement of centrosome reorientation was defined as the point when the centrosome crossed the old leading edge of the nucleus, and its termination was defined as the arrival of the centrosomes at the base of the new leading process. Cell movement in the new direction was defined as the movement of the trailing edge at least one nuclear length (~10μm).

GSK3β and PKCζ inhibitors

All inhibitors were used at concentrations that minimized toxicity and resulted in a phenotype. GSK3β inhibitor IX (i.e. BIO, Calbiochem) (1μM) and LiCl (EM Science) (50mM), PKC inhibitor Gö6983 (832nM) and PKCζ myristoylated pseudosubstrate inhibitor (i.e. Pseudo 539624) (1μM) (Calbiochem) were added to SVZa culture ~5 hours before time lapse studies. Slit-conditioned media with additional drugs was added just

before imaging began. Measurements of centrosome angles were measured as described above. Centrosome reorientation was defined as movement from either an "away" or "intermediate" position to a "toward" position during the time lapse.

Percent reorientation was measured by scoring cells that reoriented the centrosome to a "towards" position sometime during the course of the timelapse. Relatively few cells underwent more than one reorientation event. Process length measurements were obtained by averaging the length of the new processes that extended towards the explant over the course of the timelapse. Transient new processes were defined as any protrusion that extended from the cell body after Slit addition that extended and fully retracted during the time course analyzed.

Disruption of Actin and MT cytoskeletons and immunostaining

Latrunculin B (Calbiochem) (1μg/ml) and nocodazole (Sigma) (50 ng/ml) were added to SVZa cultures 1 hour after the addition of Slit-conditioned media. For immunostaining, cells were fixed with 0.5% glutaraldehyde and stained with anti-β-tubulin (Sigma) and AlexaFluor 568 phalloidin (Molecular Probes).

DiI labeling of cortical slices

Coronal slices (0.5 to 1mm) of E14.5 cortex from GFP-CENTRIN2+ embryos were fixed and labeled with DiI-coated gold particles (0.5μm) using the Bio-Rad gene gun, as has been described (O'Brien and Lummis, 2004). Briefly, 0.125 mg of DiI is dissolved in 100 μl methylene chloride and is added to gold microparticles (Bio-Rad) spread on a glass slide. Coated microparticles are sonicated and loaded into Tefzel tubing, which is cut and inserted into the Bio-Rad gene gun. Thick coronal slices (0.5 to 1mm) from embryonic or postnatal cortex are fixed in 4%PFA and the labeled

microparticles are fired into them at a pressure determined empirically. Slices are then incubated overnight to allow complete diffusion of the dye into the neuronal processes.

Plotting of centrosomal position

In both slice overlay assay and DiI labeling, the centrosome was plotted relative to the nucleus and axon. First, the axon and centrosome were identified. In the slice overlay assay, the longest process was considered the axon. In the DiI experiments, the longest process projecting from the basal half of the cell (the half nearest the VZ) was scored as the axon. Centrosome position fell within one of four quadrants that converged at the center of the nucleus.

Plotting of axon orientation in DiI labeled slices

The location of the SVZ was determined anatomically whose lower boundary was the cell dense VZ and upper boundary was the upper limit of the corticofugal axon tract. Only cells with a process oriented towards the VZ were scored and the longest process was considered the axon. The axon's orientation was scored relative to the pial surface and the VZ.

shRNA-mediated knockdown in cortex

ShRNA constructs for aPKCζ, APC, CLIP-170, and IQGAP1 were purchased from Open Biosystems and electroporated into cortex of ICR embryos *in utero* at E14.5, as described previously (Tabata and Nakajima, 2001). After 48 hours, embryos were removed and GFP or dsRed+ neurons were removed and dissociated using the papain dissociation method. Dissociated cells were then overlayed onto slices taken from P2-P6 rat cortical slices cultured on Millicell organotypic membrane inserts at 1 X 10^6 cells/well.

SFRP and Inhibitors

SFRP was kindly provided by Yimin Zhou and Jean Lu. SFRP was purified using the baculovirus expression system as described: (Lyuksyutova et al., 2003). SFRP at 0.5 μg/μl was diluted in culture medium and applied to cells 15 minutes prior to overlaying the cells onto the cortical slices. SFRP was also added to the culture medium. Inhibitors to PKCζ and GSk-3β were identical to those used for migration experiments. Dissociated cells were exposed to the drugs 45 minutes prior to overlaying onto cortical slices.

ACKNOWLEDGEMENTS

The authors wish to thank K. Oegema, J. Isaacson, D. Cleveland, D. O'Leary, B.A. Hamilton and members of the Gleeson lab for helpful discussions. M. Ward and Y. Rao provided Slit reagents and SVZa protocols. Y. Zou provided SFRP. This work was supported by the NINDS (NS41357 to J.G.G.), the UCSD Neuroscience Microscopy Shared Facility (NS047101) and the Neuroplasticity of Aging Training Grant (to H.H).

Some of this work was published as: Higginbotham, Holden; Tanaka, Teruyuki; Brinkman, Brendan; Gleeson, Joseph G. GSK3beta and PKCzeta function in centrosome localization and process stabilization during Slit-mediated neuronal repolarization. Mol Cell Neurosci. **32**(1-2): 118-32, 2006.

Supplemental Movie Legends

Supplemental Movie III.1: Migration of SVZa neuron in collagen/Matrigel showing movement of the centrosome (green, arrow) into the leading process followed by translocation of the nucleus (Frames 10-11, 34). Nucleus moves up to and past centrosome in frames 15-19. Frames captured every 5 minutes.

Supplemental Movie III.2: Application of Slit-conditioned media reverses SVZa neuron migration. SVZa explants from RMS were embedded in Matrigel/collagen matrix and cultured for 24 hours. Slit-conditioned media was added just after timepoint 0:00 and time lapse images were taken every hour. Slit-conditioned media caused a dramatic reversal of direction where most neurons migrated back into the explant over the four-hour period.

Supplemental Movie III.3: SVZa neuron reversing direction in response to Slit with centrosome (white arrow) reorientation. Corresponds to Fig. III.4A. Slit-conditioned media added before initiation of recording. Centrosome begins reorientation at frame 9. Previous leading process is retracted at frame 12 as the nucleus translocates forwards. Centrosome arrives at base of new process at frame 11 before NT.

Supplemental Movie III.4: Reorientation of the centrosome (white arrow), followed by centrosome extension into the leading process (T=01:10:15.000) and then nuclear translocation (T=01:25:18.000). Slit-conditioned media added before initiation of recording. Nucleus is outlined in the first five frames. An * indicates old leading process. The ^ indicates new leading process.

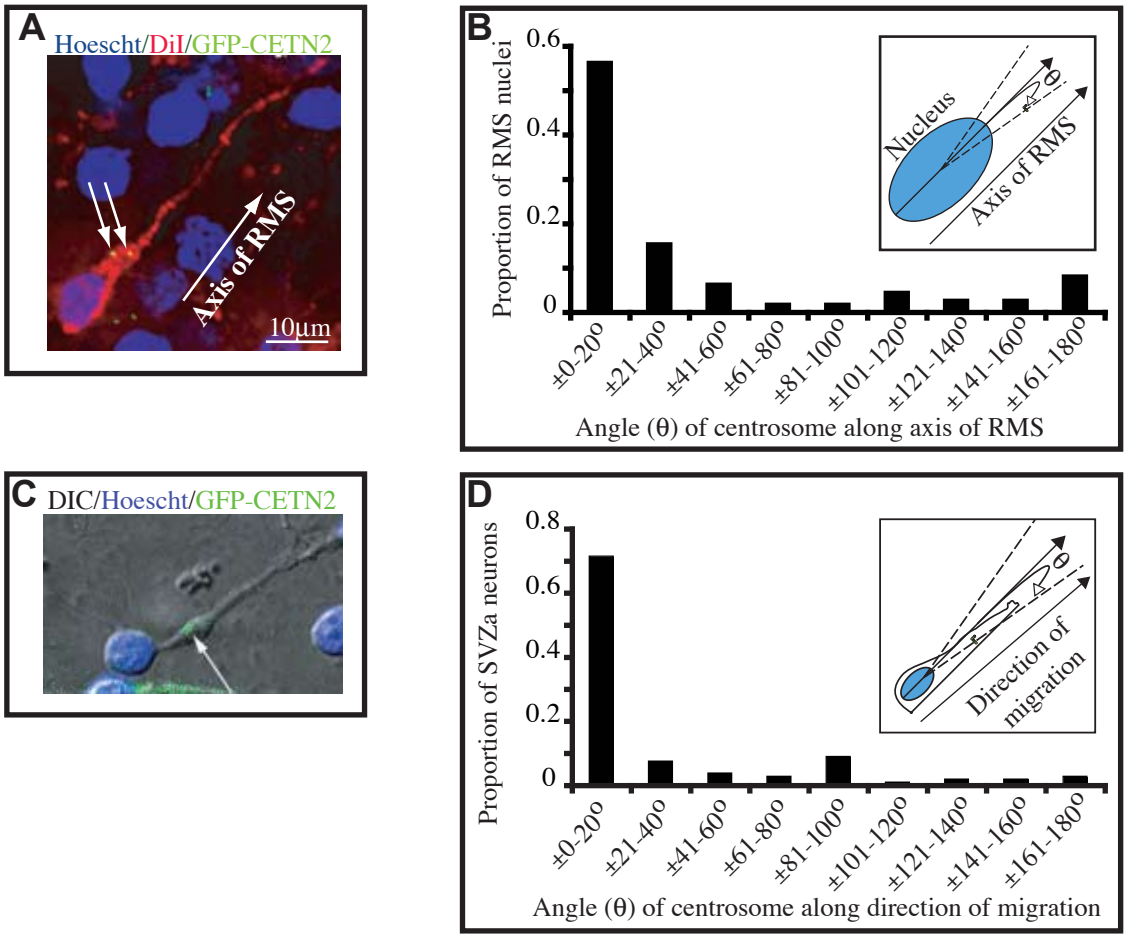

Figure III.1: The centrosome is positioned ahead of the nucleus in migrating SVZa neurons. (A) DiI-labeled neuron (red) from P5 GFP-CETN2 (green) transgenic mouse migrating in the RMS of a sagittal slice. Arrow indicates the direction of migration along the caudal-rostral axis of the RMS. Hoechst (blue) marks the nuclei, double arrows mark the two centrioles of the cell. (B) Measurement of the angle of centrosome position relative to the axis of the RMS and the nucleus. Insert shows the method of angle measurement (n = 110). (C) GFP-CETN2-positive SVZa neuron migrating from an RMS explant showing the position of the centrosome within the leading process (green, arrow). (D) Measurement of the angle of centrosome position relative to the axis of migration. Line drawn through the long axis of the neuron, as shown in the insert. (n = 213).

Figure III.2: Centrosome movement into the leading process is coupled to nuclear translocation. (A) Time lapse images of a migrating SVZa neuron. Arrow indicates centrosome (green). Star marks secondary branch that retracts before nuclear translocation. The black arrow at 2:00 indicates transient concentric nuclear constriction. Scale bar = 20 μm. (B) Dynamic relationship between centrosomal movement and nuclear translocation. Cumulative migration graphs from two representative cells, with nuclear-centrosome (N-C) distance (black line) and cumulative distance traveled by the nucleus (grey line) as a function of time. Green vertical lines indicate peaks of N-C distance that are uniformly followed by rapid nuclear movement. (C) Scatter plot showing positive correlation between change in N-C distance and change in leading process length during 5-minute intervals. (n = 1141 intervals from 33 cells).

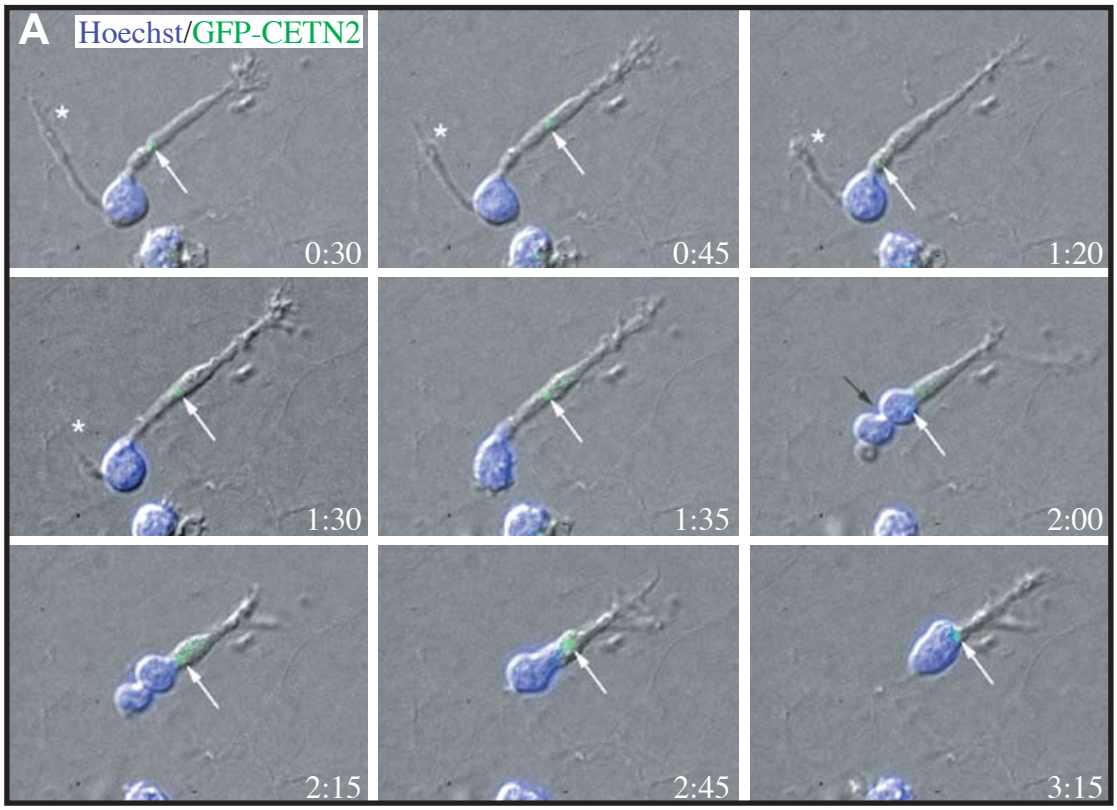
A
Hoechst/GFP-CETN2
0:30
0:45
1:20
1:30
1:35
2:00
2:15
2:45
3:15

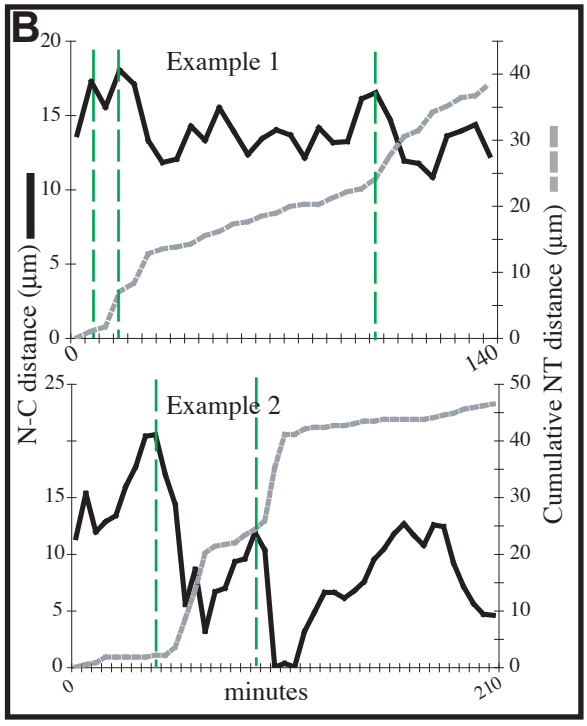
B
Example 1
Example 2
N-C distance (µm)
Cumulative NT distance (µm)
minutes
0
140
210

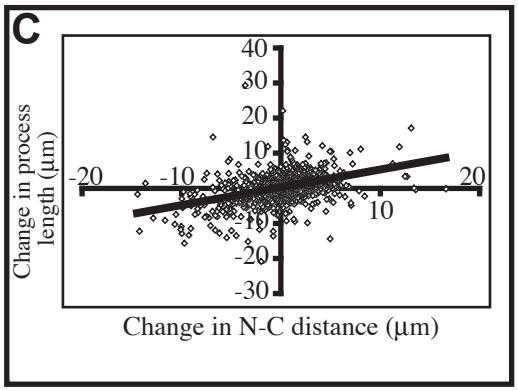
C
Change in process length (µm)
Change in N-C distance (µm)

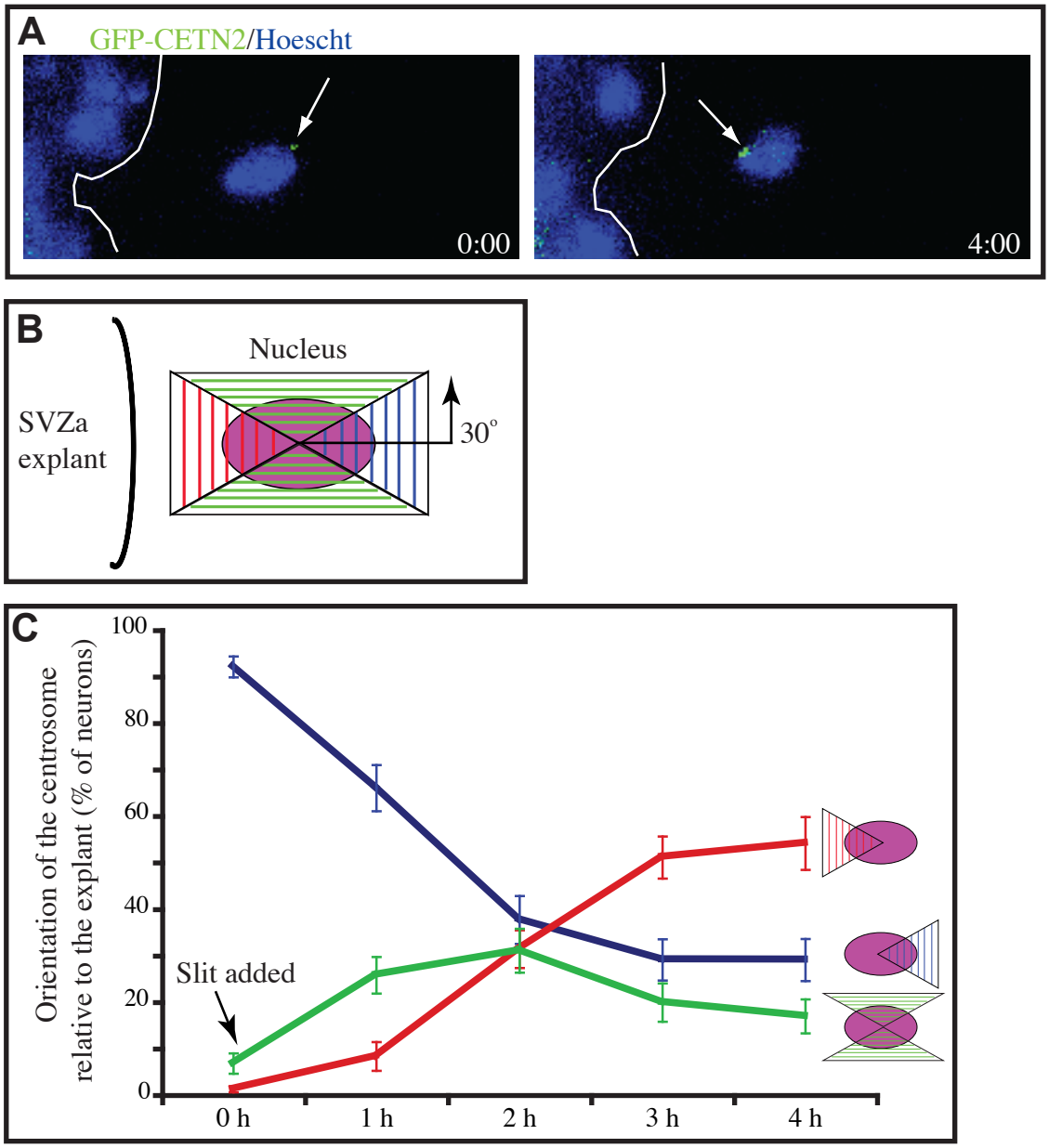

Figure III.3: Centrosome reorientation during repolarization in SVZa neurons in response to the chemorepellent Slit. (A) Nucleus and centrosome position during migration from explant (white outline). The centrosome reorients from a position away from the explant to a position toward the explant within 4 hours of exposure to Slit-conditioned media. (B) Method of quantification for (C). The striped regions define possible locations of the centrosome. The centrosome was considered "away" if found within the blue-striped region, "toward" if in the red-striped region, and "intermediate" if found in the green region. (C) Quantification of 37 explants (872 neurons) exposed to Slit at time 0h shows a gradual increase in the percentage of centrosomes oriented toward the explant.

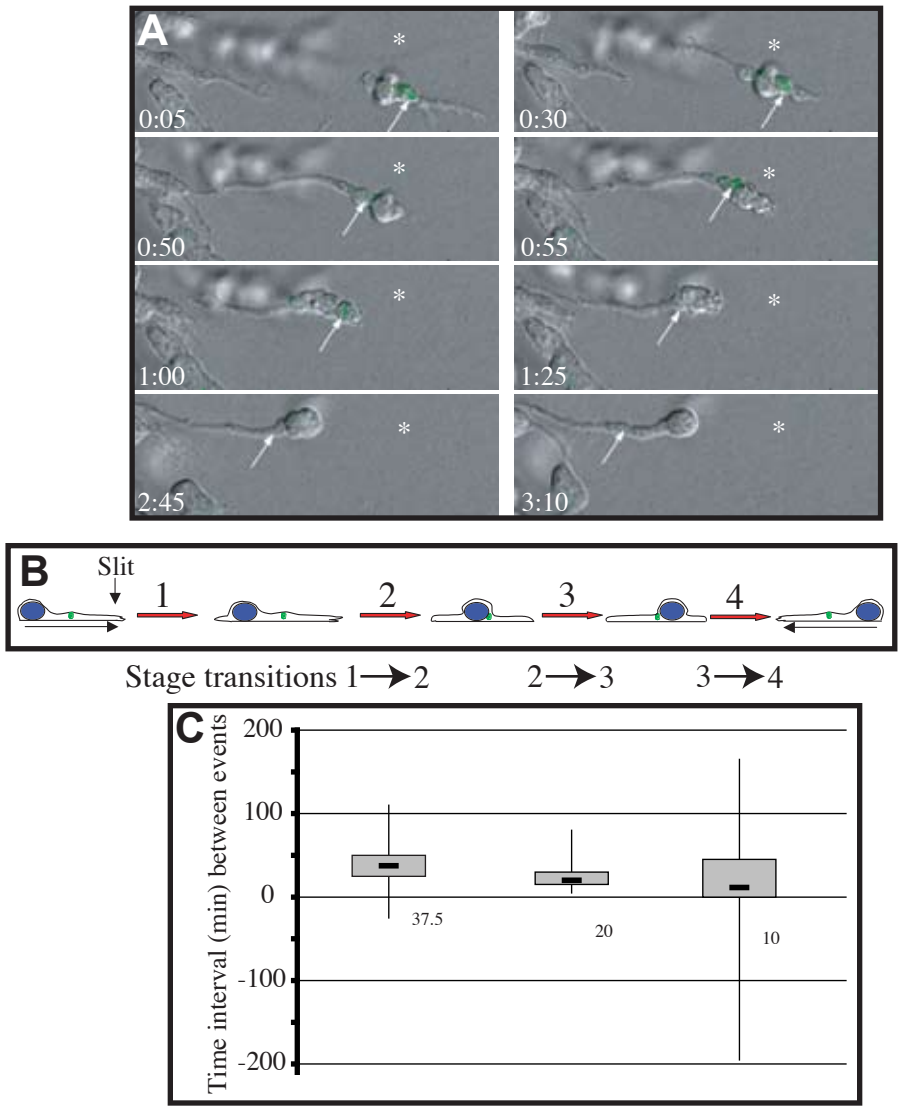

Figure III.4: Centrosome reorientation follows new leading process outgrowth but precedes nuclear translocation. (A) Time lapse images showing neuronal repolarization followed by reversal of migration direction towards the explant (left) in response to Slit. Cell body outlined in first frame, arrow = centrosome, arrowhead = leading process, * = point of reference. Time intervals h:mm. (B) Following Slit application, Stages occur in the following order: 1. A new process extends from the previous trailing edge. 2. The centrosome begins reorientation, with concurrent retraction of the old leading process and continued extension of the new process. 3. The centrosome finishes reorientation, arriving at the base of the new process and retraction of the old leading process, and 4. The cell initiates movement in the new direction. (C) Box-and-whisker plots showing the time interval range between Stages 2, 3 and 4. Grey-filled box shows middle 50% of measurements, black line shows median, vertical lines show upper and lower 25% of measurements. An average of 38 minutes elapses between Stages 1 & 2, 22 min between 2 & 3 and 21 min between 3 & 4. N = 61 cells from 14 explants.

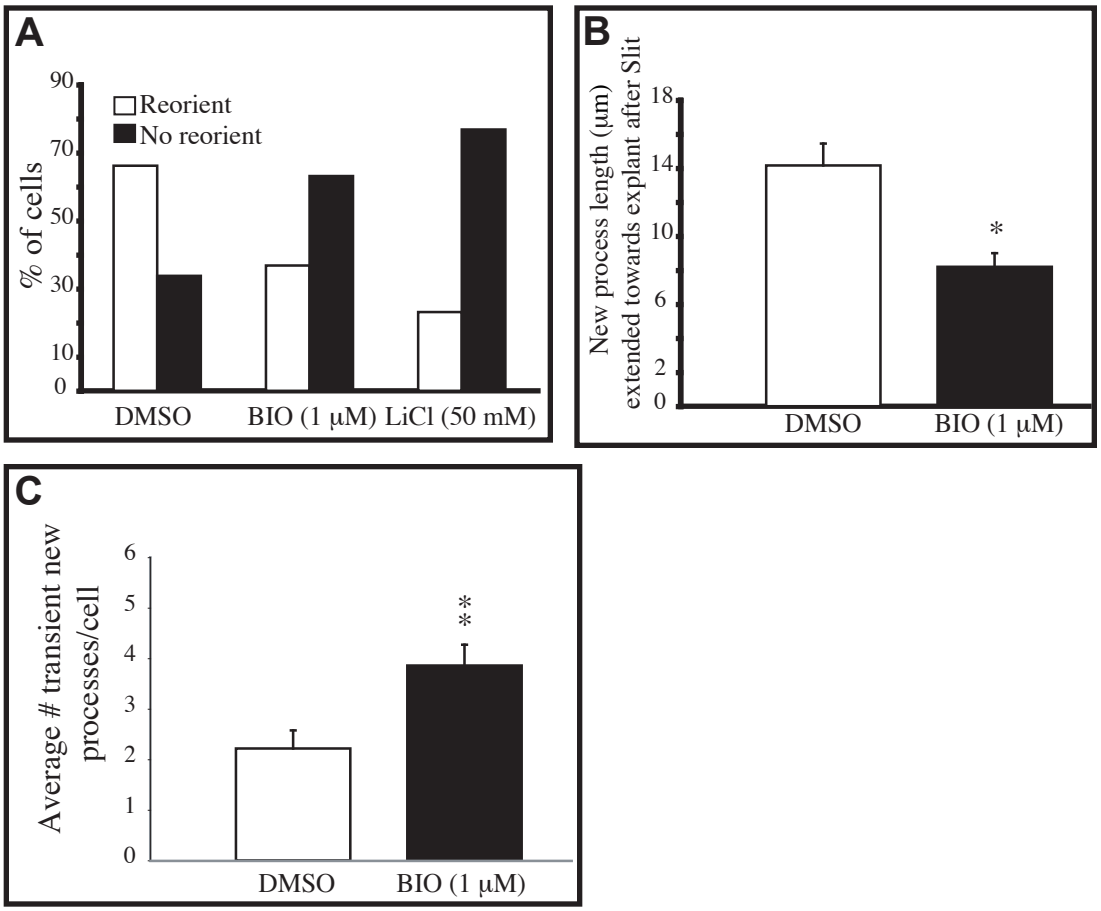

Figure III.5: Inhibition of GSK3β prevents centrosome reorientation and new process elongation/stabilization in response to Slit. Inhibitor was added 5.5 hrs before Slit and onset of time-lapse recording (acquired every 10 min for 6 h). (A) Percentage of cells where centrosome reorientation occurred by the completion of the experiment. Both BIO and LiCl application led to impairment of centrosome reorientation (n = 170 cells). (B) Average length of the new process extending towards the explant following Slit. BIO application led to impairment in process length (* = $p < 0.05$). (C) Average number of transient new processes per cell following Slit. Data points were acquired every 10 minutes for 6 hours. BIO application led to an increase in the number of these transient processes. (* = $p < 0.05$, ** = $p < 0.01$, Student t-test).

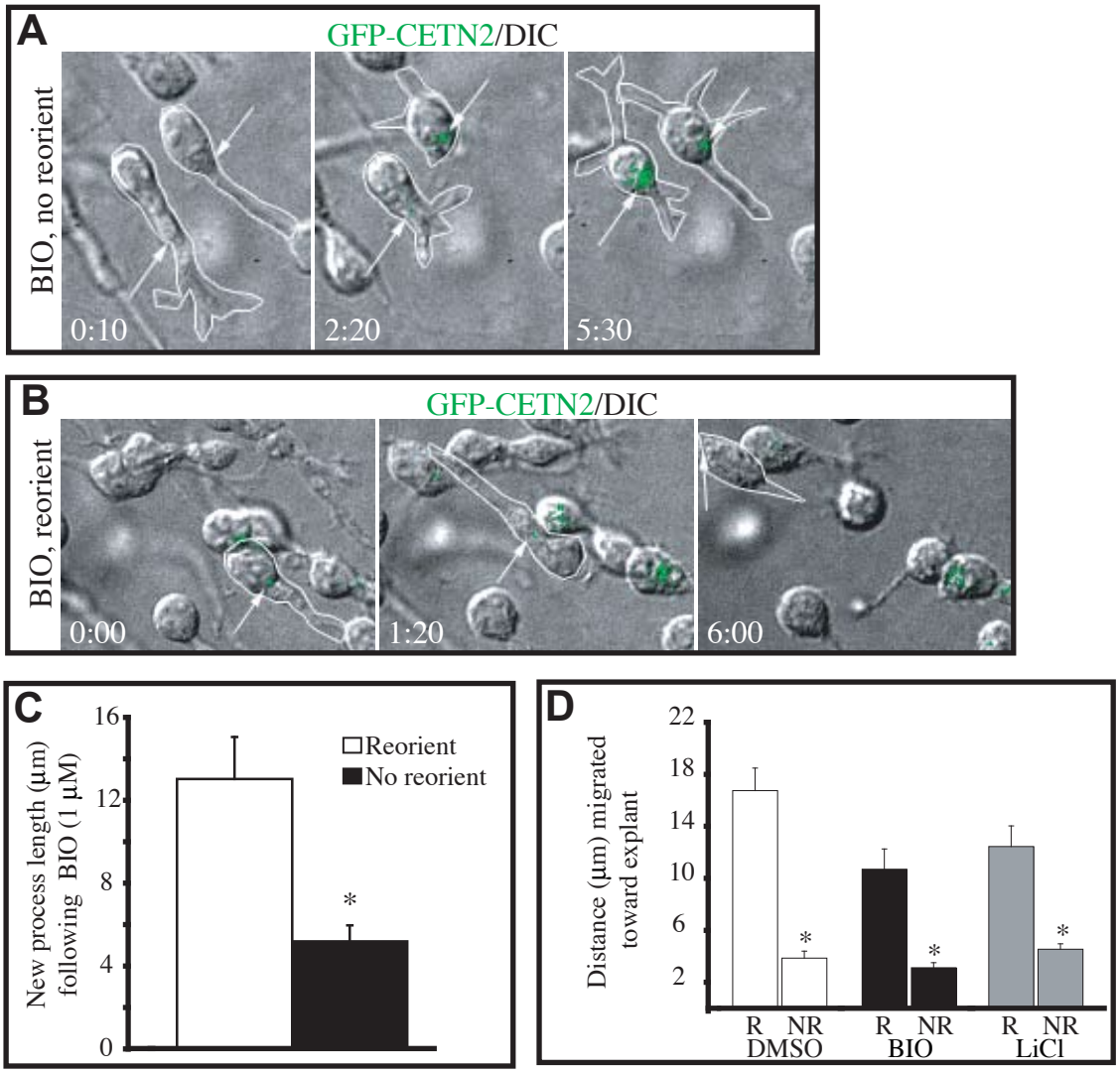

Figure III.6: Neurite outgrowth and migration in the new direction fails to occur in the absence of centrosome reorientation. (A-B) Timelapse images showing neurons exposed to the same concentration of BIO with initial polarity oriented to bottom right. (A) In these two cells centrosome reorientation fails and subsequently there is failure of migration in the new direction. Arrow = centrosome, outline = cell morphology. (B) In this cell both centrosome reorientation and migration in the new direction are successful. (C) New process length is significantly greater in reorienting cells (R) than in non-reorienting cells (NR) in the presence of the same BIO concentration. (D) Average distance of migration towards the explant following Slit in cells exposed to DMSO (control), BIO or LiCl. Application of the drugs themselves had a modest effect on migration in R cells (compare DMSO R, BIO R and LiCl R, approximately 20-30% decrease). A more striking defect was noted in NR cells, where migration distance decreased to 1/3 of control. DMSO: n = 156, BIO: n = 168, LiCl; n = 129, Error bar = SEM, * = $p < 0.05$, Student t-test.

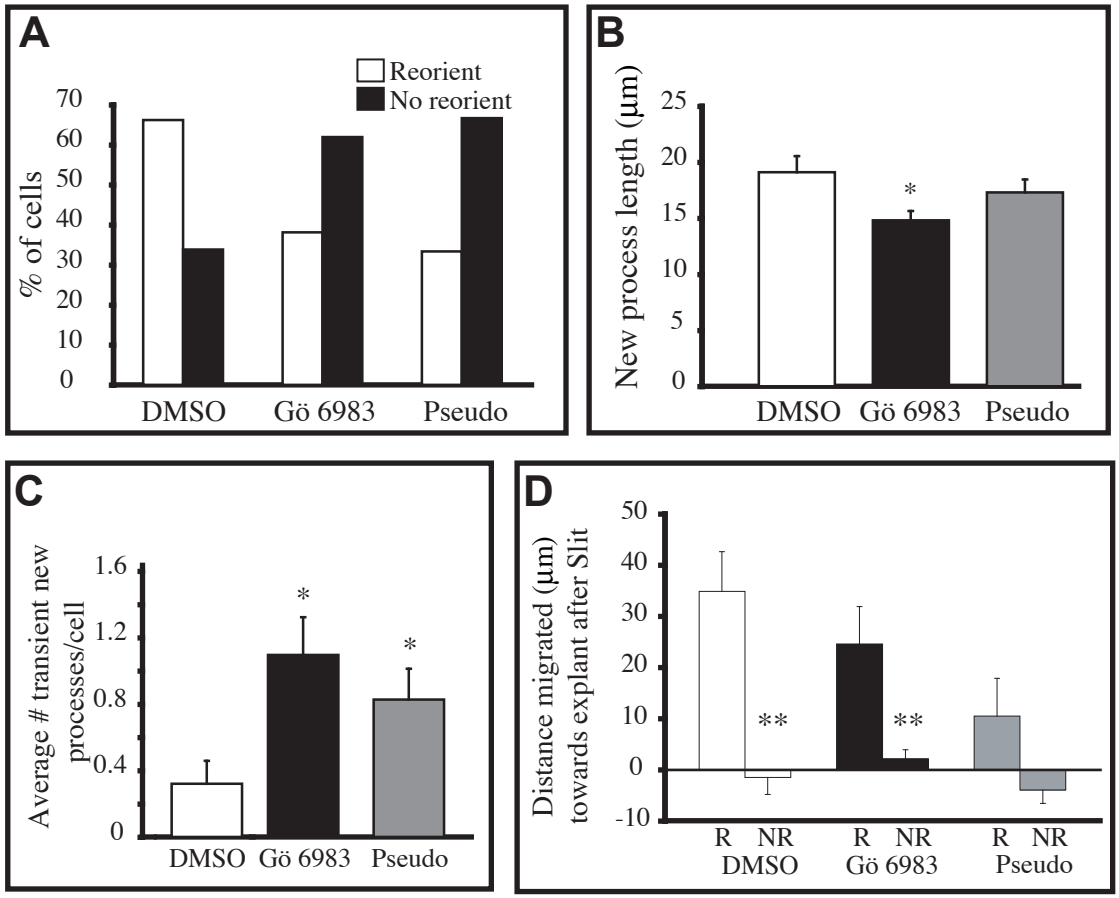

Figure III.7: Inhibition of PKCζ prevents centrosome reorientation, repolarization and migration of neurons in response to Slit. (A) Percentage of cells where centrosome reorientation occurred by the completion of the experiment. Both Gö6983 (non-selective PKC inhibitor) and Pseudo (myristoylated PKCζ-specific pseudosubstrate) led to impairment of centrosome reorientation (n = 162 cells). (B) Average length of the new process extending towards the explant following Slit. Application of either Gö6983 or Pseudo led to a mild decrease, but a significant difference was detected only for Gö6983. (C) Average number of transient new processes per cell following Slit. Both Gö6983 and Pseudo led to an increase in the number of these transient processes. Data points were acquired every 40 minutes for 6 hours. (D) Average distance of migration towards the explant following Slit in cells exposed to DMSO (control), Gö6983 or Pseudo. Application of the drugs themselves had a modest effect on migration cells where centrosome reorientation was successful (DMSO R vs. Gö6983 R vs. Pseudo R, approximately 20-30% decrease, no statistical difference). A more striking defect was noted in cells that failed to reorient the centrosome, where migration decreased to negligible levels (following Gö6983) or proceeded in the previous direction (for DMSO and Pseudo, indicated by a negative mean). DMSO: n = 172, Gö6983: n = 123, Pseudo: n = 131. Error bar=SEM, * = $p < 0.05$, ** = $p < 0.01$, Student t-test.

Figure III.8: (A-B) MT depolymerization prevents process outgrowth and stabilization, but not centrosome movement within cell body. Nocodazole was added (double arrows) to migrating SVZa neurons that were bathed in Slit-conditioned media 1 hour earlier (single arrow). Nocodazole caused a rounding of the cell, bringing the majority of the centrosomes to an "intermediate", random position (green line in B). (C) The centrosome continued to move within the cell after nocodazole treatment to areas near the cortex where filopodial or lamellar sheets transiently extended (2:30, 5:30). (D-E) Prevention of actin polymerization inhibits centrosome movement. Application of latrunculin B to neurons exposed to Slit almost completely prevented centrosome reorientation. (F) The neuron retained its polarized morphology with the leading process extended away from the explant (left). No new leading processes were seen to sprout from any part of the cortex. In some cells, the centrosome (white arrow) occasionally would fall slightly towards the cell body. Latrunculin B: $n = 76$ from 16 explants, Nocodazole: $n = 167$ from 14 explants.

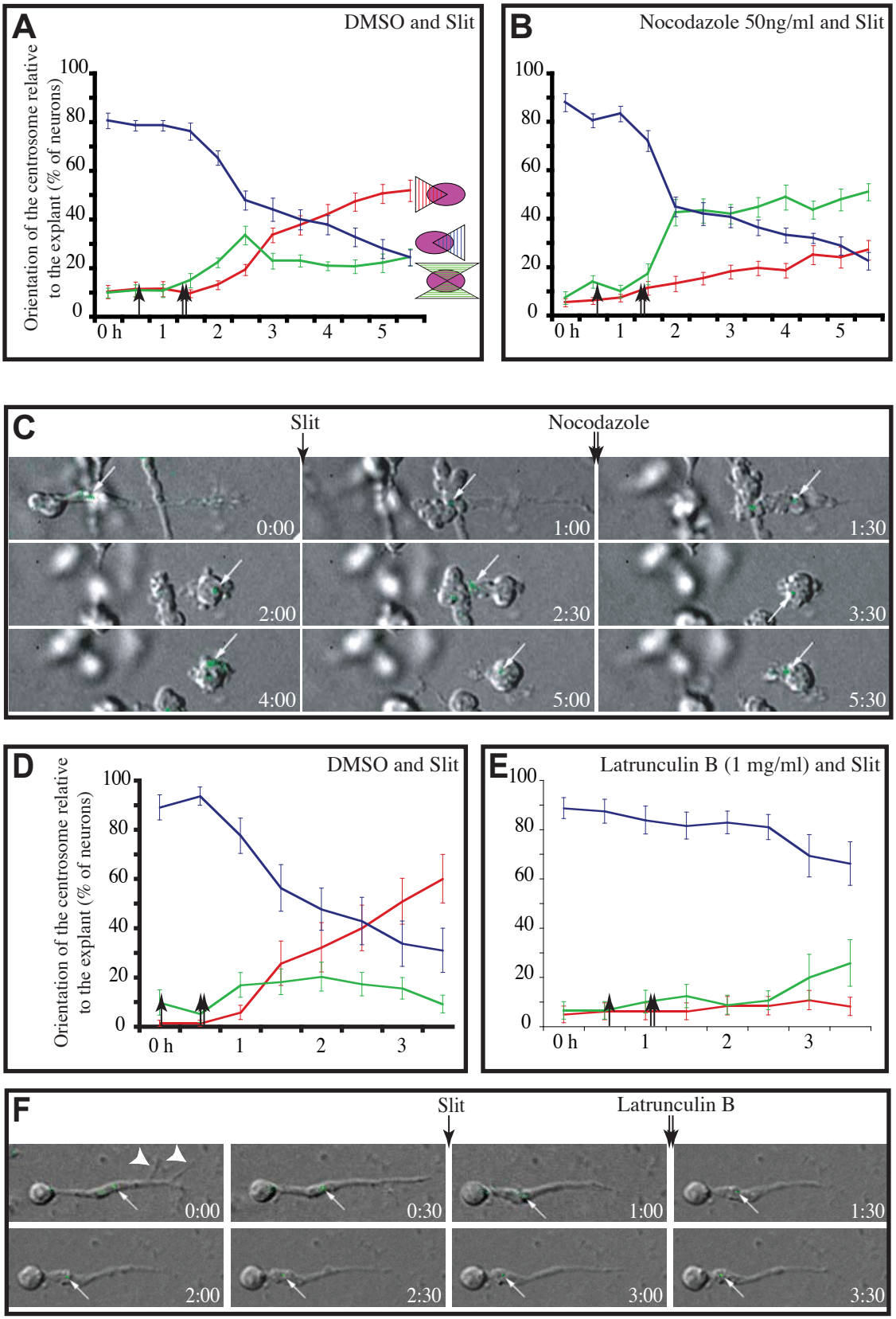
A
DMSO and Slit
Orientation of the centrosome relative to the explant (% of neurons)
100
80
60
40
20
0
0 h
1
2
3
4
5
B
Nocodazole 50ng/ml and Slit
C
Slit
Nocodazole
0:00
1:00
1:30
2:00
2:30
3:30
4:00
5:00
5:30
D
DMSO and Slit
E
Latrunculin B (1 mg/ml) and Slit
F
Slit
Latrunculin B
0:00
0:30
1:00
1:30
2:00
2:30
3:00
3:30

Figure III.9: Centrosome position during pyramidal neuron migration and differentiation. (A) Schematic of experimental protocol. E14.5 cortex from GFP-CETN2 transgenic animals was Vibratome sliced, fixed, and loaded with DiI-coated microparticles using the Bio-Rad gene gun. After 24 hours, DiI-labeled cells were visible throughout the cortical wall and their axons could be traced to the corticofugal and callosal axon track that courses through the SVZ. Centrosome position was analyzed in cells from three locations, corresponding to B, C, and D. (B) Confocal multi-plane projection image of a representative DiI-labeled multipolar cell in the SVZ displaying a short, presumptive axonal process extended towards the VZ (filled arrowhead). Intersecting yellow lines indicate the position of the centrosome at the base of the process. Insets show a cross section of the cell at the plane of the centrosome verifying that the GFP-CETN2 signal corresponds to the cell. (C) Representative cell located just above the SVZ displaying a longer axon that extends to the VZ and merges into the axon track (filled arrowhead). The centrosome is located within the cell soma. A short presumptive leading process extends towards the pia (hollow arrowhead). (D) Representative cell within the IZ displaying a pia-directed leading process (hollow arrowhead)) and an axon extending towards the VZ. The centrosome is located within the leading process. (E) Plot of centrosome position (green dots) relative to the nucleus (blue circle) and the axon (hollow arrow) in DiI-labeled cells within the SVZ and IZ. The plot was divided into 4 quadrants representing the apical/basal and lateral domains of the cell. In most cells in both SVZ and VZ, the centrosome is located within the apical-basal axis of the cell, suggesting a correlation with its position and that of the axon or leading process. n=85 cells. (F) Mature pyramidal neuron labeled with DiI from CP of postnatal day 13 GFP-CETN2 transgenic mouse. The centrosome was located at the base of the apical dendrite (open arrowhead) in all cells analyzed (n=15). Filled arrowhead indicates the descending axon. Scale bar=50 microns.

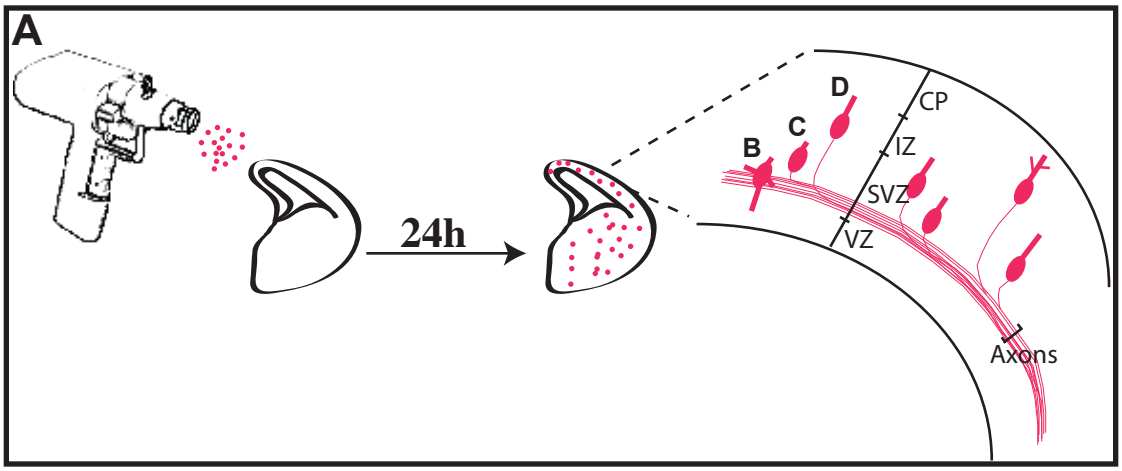

DiI/GFP-CETN2/Hoechst

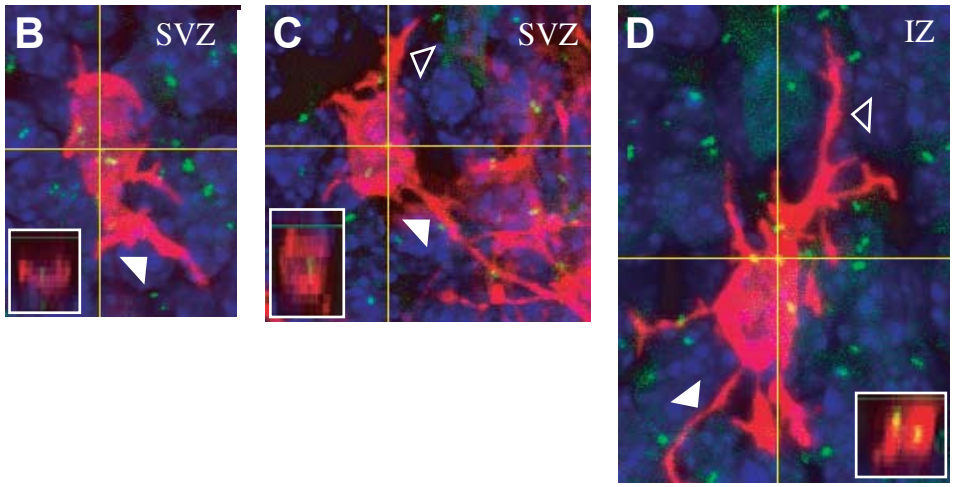

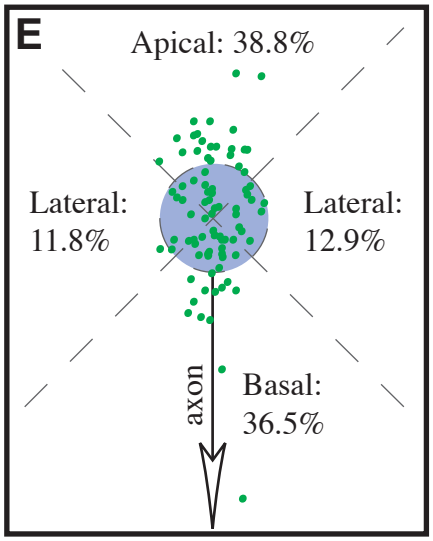

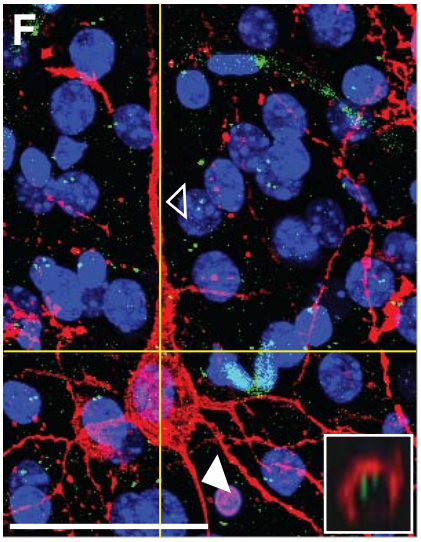

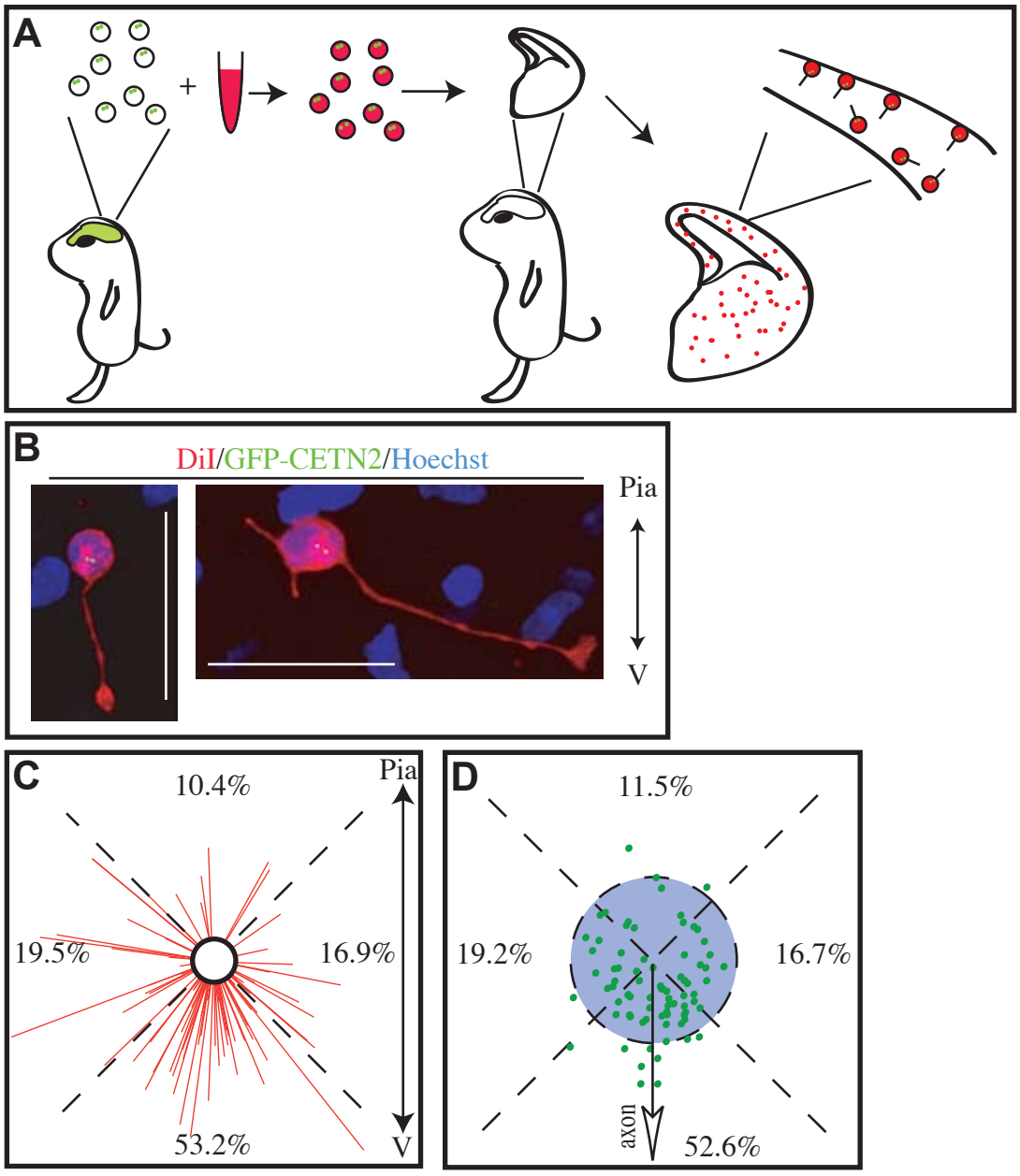

Figure III.10: The centrosome is located at the base of the axon in cortical neurons in slice overlay assay. (A) Schematic of slice overlay assay. Dissociated cortical neurons from E14 GFP-CETN2 transgenic mice are labeled with DiI and overlayed onto cortical slices from P2 rats. Axon outgrowth and centrosomal position is evaluated after 2 hours. (B) Representative DiI-labeled cells overlayed on cortical slice. The orientation of the pia and ventricle (V) is indicated. (C) Plot of axon orientation and length for overlayed neurons. Percentages of cells with axons in each quadrant is indicated. The hollow circle represents the nucleus. (D) Plot of centrosome position (green dots) relative to the nucleus (blue circle) and the axon (hollow arrow). Percentage of cells with centrosome located in each quadrant is shown. n=78 cells. Scale bar=30 microns.

Figure III.11: Plots of axon orientation in slice overlay assay after shRNA-mediated knockdown of aPKCζ, APC, IQGAP1, and CLIP-170. (A) Schematic of experimental procedure. shRNA and either dsRedII or hrGFPII is co-eletroporated into E14.5 embryos *in utero*. At E16.5 dsRedII or hrGFPII-expressing portions of cortex are dissected, dissociated, and overlayed onto slices of P5-6 rat cortex. After 2 hours slices are fixed and scored for axon orientation. (B) Plot of axon orientation of cells electroporated with dsRedII only. Panel inset shows a representative overlayed cell. Percentage of cells with an axon extending within one of four quadrants is shown. Pia-->Ventricle (V) axis is indicated. (C) Co-electroporation of dsRedII and aPKCζ shRNA. (D-H) Co-electroporation of hrGFP and shRNAs to APC (D), IQGAP1 (E-F), or CLIP-170 (G-H). n=16 (B); 20 (C); 53 (D); 63 (E); 58 (F); 20 (G); 29 (H).

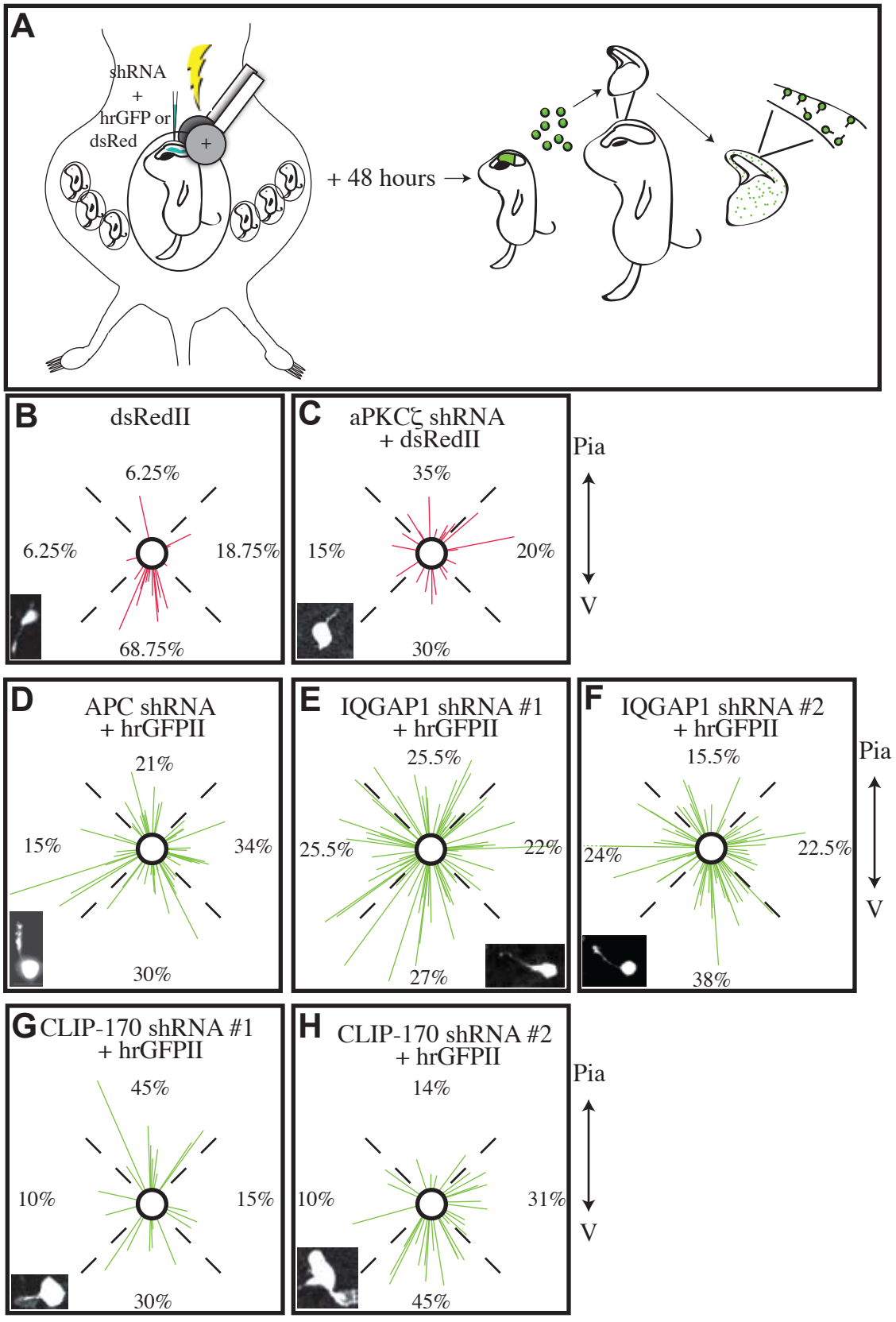
A
shRNA
+
hrGFP or
dsRed
+ 48 hours
B
dsRedII
6.25%
6.25%
18.75%
68.75%
C
aPKCζ shRNA
+ dsRedII
35%
15%
20%
30%
Pia
V
D
APC shRNA
+ hrGFPII
21%
15%
34%
30%
E
IQGAP1 shRNA #1
+ hrGFPII
25.5%
25.5%
22%
27%
F
IQGAP1 shRNA #2
+ hrGFPII
15.5%
24%
22.5%
38%
Pia
V
G
CLIP-170 shRNA #1
+ hrGFPII
45%
10%
15%
30%
H
CLIP-170 shRNA #2
+ hrGFPII
14%
10%
31%
45%
Pia
V

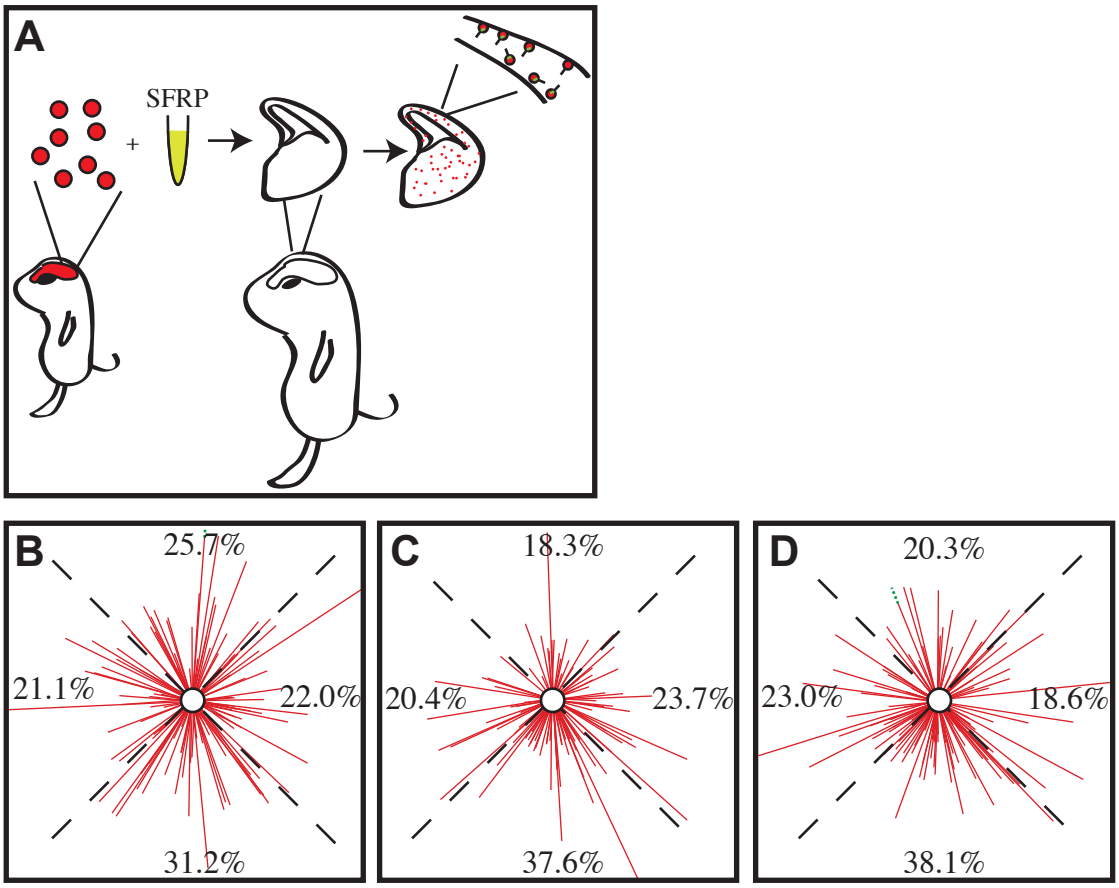

Figure III.12: Wnt inbition by SFRP in a slice overlay assay has no effect on axon orientation. (A) Schematic of experimental protocol. Dissociated cortical neurons from E14.5 DCX:dsRed+ embryo are incubated with SFRP or control media for 15 minutes before being overlayed onto a cortical slice from P2 rat. Slices were incubated in culture medium with SFRP for 2 hours after which axon orientation was scored. (B-D) Plots of axon orientation for control (B), SFRP @ 0.5µg/ml (C), and @ SFRP @ 3.3µg/ml (D). n=109 cells (B); 93 cells (C); 113 cells (D).

IV. DOUBLECORTIN IS REQUIRED FOR CONSOLIDATION OF THE LEADING PROCESS DURING TANGENTIAL AND RADIAL MIGRATION

ABSTRACT

Hemizygous mutations of the microtubule-associated protein *Doublecortin* (*DCX*) result in classical lissencephally in human males. However, in the mouse, deletion of *DCX* shows no observable lamination defect in the cortex. In addition to the compensatory role played by the DCX family member DCK1 in radial migration, the phenotypic difference between the mouse and human genetic deletion might also be explained by the longer migratory route taken by projection neurons in humans. Here we show that doublecortin (DCX) deletion in mice results in a severe morphological defect in the rostral migratory stream, where cells migrate up to ten times farther than in the neocortex. The delayed migration in the RMS is independent of direction or responsiveness to Slit chemorepulsion. DCX is required for nuclear translocation and maintenance of a bipolar morphology during migration. Additionally, using live-cell imaging analysis we show a role for DCX and DCK1 in the transition from a multipolar to a bipolar morphology during radial migration in the neocortex. These studies reinforce a role for DCX family members in the consolidation of a leading process during migration in both embryonic and adult cortex.

INTRODUCTION

Classical lissencephally is one of the most severe human disorders of neuronal migration. Children born with it present clinically with developmental delay, intractable epilepsy and low muscle tone (Kerjan and Gleeson, 2007). Brain magnetic resonance imaging shows that the spacing between the gyri and sulci of the brain are either wider than normal or completely absent. The cortical grey matter is considerably thickened and is composed of only four layers as opposed to the normal six layers. In addition, the cells are morphologically defective. Because most of the projection neurons are mispositioned within the lower part of the cortical plate, lissencephaly is considered a migration disorder.

Mutations in three genes have been identified to date as responsible for lissencephally: platelet-activating factor acetylhydrolase 1B α subunit (PAFAH1B1, encoding the LIS1 protein), doublecortin (DCX) or tubulin α 1A (TUBA1A) (des Portes et al., 1998; Gleeson et al., 1998; Keays et al., 2007). The products of all three genes are cytoskeletal factors.

LIS1 is a highly-conserved protein that is consistently complexed with the microtubule (MT) minus-end motor dynein and is involved in nuclear movement. In migrating neurons, it localizes to the centrosome its partial loss causes an increase in nuclear-centrosomal distance in cultured cerebellar granule neurons (Feng et al., 2000; Tanaka et al., 2004a). Although mice normally have a smooth brain, partial loss-of-function of Lis1 in mice does cause disordered cortical layering of projection neurons (Gambello et al., 2003). Lis1 has also been shown to be required for tangential migration of interneurons from the MGE (McManus et al., 2004).

Mutations in the X-linked gene doublecortin (DCX) in humans result in either classical lissencephally or double cortex syndrome. The presumptive migration defect is likely to be cell-autonomous, because in females with a heterozygous mutation, approximately half of the neurons are misplaced within the cerebral cortex, forming a subcortical band heterotopia. This would be expected if only half of the cells were DCX-deficient as a result of random X-chromosome inactivation. In contrast, males who lack any functional DCX allele show a four-layered agyric cortex.

Like LIS1, DCX is a MT-associated protein (MAP) that has potent MT-bundling and stabilizing activity (Gleeson et al., 1999). DCX patient mutations cluster primarily in the MT-binding domains, emphasizing the importance of MT regulation for migration (des Portes et al., 1998; Gleeson et al., 1998). DCX staining labels the MT-cage that surrounds the nucleus of migrating neurons (Tanaka et al., 2004a), suggesting a possible role with LIS1 in nuclear translocation. The interaction between LIS1 and DCX is not clear, but in migrating cerebellar granule neurons, overexpression of DCX can rescue both the nuclear-centrosomal coupling defect and slow migration seen in LIS1 +/- neurons (Tanaka et al., 2004a).

Phosphorylation of both LIS1 and DCX regulates their activity. DCX is serine/threonine phosphorylated at several sites by kinases that include MARK, JNK, and CDK5 (Gdalyahu et al., 2004; Graham et al., 2004; Schaar et al., 2004; Tanaka et al., 2004b). Phosphorylation by these kinases reduces DCX's affinity for MTs together with its stabilizing and bundling properties, suggesting that its regulation by kinases/phosphatases may play an important role in establishing cell polarity during migration. In fact, recent work has shown that dephosphorylation of DCX by its

phosphatase PP1 is required for MT bundling within the axon shaft of differentiating cortical neurons and suppression of collateral branches on the axon (Bielas et al., 2007) and the DCX kinase CDK5 is required for neurons to exit the multipolar stage during radial migration (Ohshima et al., 2007).

In contrast to LIS1 mouse mutants, loss of DCX in the mouse cortex showed a surprisingly mild phenotype, with no discernible lamination defects in the cortex and only a moderate delamination in the CA3 region of the hippocampus (Corbo et al., 2002). RNAi-mediated knockdown of DCX in both rat and mouse cortex resulted in laminar displacement, but in the adult subcortical band heterotopia was observed only in rat (Bai et al., 2003; Ramos et al., 2006). These results suggest that genetic deletion of DCX differs from acute knockdown, but that DCX plays a role in radial migration in rodent as it does in humans.

One possible explanation for the phenotypic differences between humans and mice after genetic deletion of DCX is the order-of-magnitude greater distance (approximately 2–3 cm in humans versus 2–3 mm in rodents) required for neurons to traverse the cortical width in humans. A shorter travel distance to the appropriate neuronal layer might compensate for slower migration in rodents but not humans.

Another possible explanation for the phenotypic differences is that compensatory mechanisms may be functional during mouse development that are either not present in humans or are inefficient. This could also explain why knockdown of DCX results in a phenotype; the compensatory mechanisms aren't activated after acute knockdown. The most probable mechanism for gene compensation is the activity of additional DCX gene family members.

Doublecortin-like kinase 1 and *2* (*DCK1* and *DCK2*) are two genes that have been identified from the DCX family (Edelman et al., 2005; Lin et al., 2000). They both contain an N-terminal DCX-like domain and a C-terminal Ca^{2+}/calmodulin-dependent serine-threonine kinase domain. DCK1 expression overlaps with DCX in the cortex and also associates with and polymerizes MTs (Lin et al., 2000).

Genetic deletion of DCK1 alone has negligible effects on neuronal migration, but RNAi-mediated knockdown in mice results in laminar deficiencies similar to DCX knockdown and disruption of mitosis in neuronal precursors (Koizumi et al., 2006b; Shu et al., 2006). Mutual compensation between DCX and DCK1 was confirmed with the double knockout mice, which showed a severe defect in radial migration and axon outgrowth (Deuel et al., 2006; Koizumi et al., 2006b). The defects were dosage-dependent so that double heterozygous mice had an intermediate migration defect. The specific cellular defects during migration in the DCX/DCK1 double knockout are not known. RNAi knockdown studies suggest that the multipolar stage of radial migration may be a transition point during migration where DCX and DCK1 function together to establish a bipolar migratory morphology because knockdown of either gene arrests cells in the multipolar stage (Bai et al., 2003; Koizumi et al., 2006b). This hypothesis has not been tested *in vivo*.

Here, we tested for disrupted neuronal migration in the RMS of adult DCX knockout mice, where neurons migrate greater distances (up to 5 mm) than in cortex throughout the life of the mouse. We also analyzed radial migration in the DCX/DCK1 double knockout and tested for their role in establishing a bipolar morphology during the shift from the multipolar phase in the SVZ.

RESULTS (PART 1)

DCX expression in the RMS

We determined that DCX is expressed at high levels in a population of cells within the SVZa, along the RMS, and remains detectable in these cells as they migrate into the olfactory bulb (Brown et al., 2003; Nacher et al., 2001) (Supplementary Fig. IV.1). DCX expression was downregulated in postmigratory neurons within the granule cell layer and glomerular layer of the olfactory bulb (data not shown). The only other location of appreciable DCX expression in the adult brain was in a small number of hippocampal subgranular layer cells (data not shown). The polysialyated form of neural cell adhesion molecule (PSA-NCAM) marks early committed neurons that are located within the RMS. We found codistribution of DCX with PSA-NCAM in these regions. We concluded that DCX is selectively expressed by migratory populations of cells within the SVZa, RMS and proximal olfactory bulb.

DCX deletion results in RMS morphological defects

Because DCX-/y males do not mate well, we focused our analysis on male DCX-/y and DCX+/y littermates, which result in equal numbers from intercrossing DCX+/y males and DCX+/- females. Parasagittal sections from adult mice through the SVZa, RMS and olfactory bulb were stained using cresyl violet to delineate the cell-dense RMS (Chazal et al., 2000). Notably, we were surprised to find a substantial alteration in the morphology of the RMS: the structure was approximately doubled in thickness along much of its length (Fig. IV.1a). This increased thickness was noted along the length of the RMS through the rostral flexure in the region of the septum, where it appeared to

revert to a normal thickness. Approximately 10 mice from each genotype were analyzed using this method, and all DCX-/y mice had a similar appearance. In order to be certain that this morphological defect was not dependent on the lateral-medial plane of sampling, we sectioned in the coronal plane and again observed that the width of the RMS was increased along its entire length (Fig. IV.1b and Supplementary Fig. IV.1). We concluded that the RMS is enlarged in the absence of DCX. To determine if this phenotype was present in female mutants, we additionally analyzed both DCX+/- and DCX-/- mice. We found that none of the four DCX+/- mice examined had a thickened RMS (Supplementary Fig. IV.1). As expected, however, the DCX-/- female mice had a phenotype that was indistinguishable from DCX-/y males, as both are complete-null for DCX in all cells (Supplementary Fig. IV.1). We concluded that the RMS phenotype is fully expressive in both the complete-null male and female mice.

We next performed an immunohistochemical study to determine if the increased size of the RMS in mutant mice was due to an increase in the number of neurons, glia or other cell types. We noted that the increase in size of the RMS corresponded to an increase in the width of the GFAP (glia) and PSA-NCAM or beta3-tubulin (TuJ1) (early committed neuron) cell stream (Fig. IV.1c,d). We estimated cell numbers by measuring total pixel number of GFAP versus PSA-NCAM signal, and found no differences (data not shown), suggesting that there is no alteration in the proportion of cell types in the expanded RMS. We noted the same close approximation of the GFAP- and TuJ1-positive cells in both DCX+/y and DCX-/y brains. In DCX+/y mice, the orientation of glia and neurons was uniformly in the direction of migration, with glial and neuronal processes extending in the ventral and rostral direction (Fig. IV.1d, arrow); however, in DCX-/y

mice, this was not always evident and the orientation of glial and neuronal processes appeared not as well ordered as in the wild type (Fig. IV.1d, arrowheads). We reasoned that these stalled migratory cells may have one of several fates, so we tested for alterations in NeuN-positive cells (a marker for differentiated neurons) and activated caspase-3–positive neurons (CAS3, a marker for programmed cell death). The RMS in DCX-/y mice contained many more NeuN-positive and CAS3-positive cells along its entire length compared with the RMS in the wild type (Fig. IV.1e,f), suggesting that these cells that failed to migrate may have differentiated into postmigratory neurons by default and/or died.

DCX deletion causes migration defects in adult forebrain

The previous data suggested a delay or block in the ability of newly generated neurons to migrate into the olfactory bulb, which was tested with 5-bromodeoxyuridine (BrdU) birth date labeling. Mice were injected with BrdU injections at postnatal day (P) 28 and then killed 7 d later. In both DCX-/y and DCX+/y mice, approximately the same numbers of labeled neurons were present in the SVZa (Fig. IV.2a), suggesting that mitotic generation of neuroblasts is not affected by the loss of DCX. Analysis of the RMS, though, revealed a striking paucity of BrdU-positive neurons in more rostral regions (Fig. IV.2b). In DCX+/y littermates, BrdU labeled a thin stream of neurons within the descending and rostral branch of the RMS; most of these labeled cells were within the fanned-out region of the RMS and in the granule cell layer of the olfactory bulb, suggesting that many of these neurons had migrated into this structure. In matched sections through the RMS in DCX-/y mice, most of the labeled cells were present within

the descending branch of the RMS in a thick collection that was reminiscent of PSA-NCAM/GFAP staining in mutants (Fig. IV.1c). There were very few labeled cells within the fanned-out region of the RMS and within the limits of the olfactory bulb. We concluded that DCX is required for the migration of neurons within the RMS into the olfactory bulb.

Many of these adult-born neurons eventually position themselves within the glomerular layer of the olfactory bulb and differentiate into GABAergic periglomerular interneurons, express unique marker subsets (Kosaka et al., 1995) and survive for an extended period of time (over a year) (Winner et al., 2002). To determine if the migration of newly generated neurons to the final position in the olfactory bulb is disrupted in DCX knockout mice, we repeated the BrdU injections at P28 and then killed the mice 4 weeks later. We counted BrdU-positive cells in the glomerular layer and found only about half the number in DCX-/y mice (Fig. IV.2c,d). To determine if specific populations of neurons are depleted in the absence of DCX, we stained sections from both mutant and wild-type mice for calbindin, calretinin, parvalbumin and tyrosine hydroxylase, some of the most widely used markers for these populations, which stain largely distinct neuronal classes (Brinon et al., 1992; Kosaka et al., 1995). When compared with wild-type controls, DCX-/y mice had significantly fewer calbindin-positive neurons in the glomerular layer (Fig. IV.2e,f; $P < 0.01$) and somewhat reduced but borderline statistically significant differences in the number of calretinin-, parvalbumin- and tyrosine hydroxylase–positive neurons ($P < 0.05$ for calretin-positive, $P > 0.05$ for parvalbumin- and tyrosine hydroxylase–positive; Supplementary Fig. IV.2). There were no statistical differences in the numbers of BrdU- or marker-positive cells in the external

plexiform layer or granule cell layer ($P > 0.05$), possibly because these neurons migrate over shorter distances (data not shown). We concluded that defective migration leads to a reduction in the number of specific subsets of interneurons within the olfactory bulb.

New method for measuring migration within the RMS

The in vivo data suggested possible slowed or otherwise impaired migration. To test this, we used an RMS slice culture system to collect time-lapse images of labeled neurons from postnatal DCX+/y and DCX-/y littermates. We labeled the RMS with a crystal of DiI in P5 slices and performed time-lapse imaging of labeled migrating neurons. In DCX+/y slices, we observed many DiI-labeled neurons that were migrating, whereas in DCX-/y slices, very few of the neurons showed similar movements (Fig. IV.3a). However, the number of migrating labeled cells that could be identified in each microscopic field was low, and there was substantial interexperiment variability in migration speeds. These negative factors may have been a result of phototoxicity or damage to the RMS induced by manipulating the DiI crystal. An alternative method is transgenic labeling of cells with a fluorescent reporter. We tested transgenic mice that expressed green fluorescent protein (GFP) under the control of the DCX promoter [DCX::EGFP; (Gong et al., 2003)], because this model should allow visualization of the whole population of migrating RMS neurons. A strong GFP signal was found exclusively in the SVZ, RMS and olfactory bulb in both adult (data not shown) and P5 (Fig. IV.3b) slices, and overlapped precisely with DCX expression. Using multiphoton microscopy, which minimizes photobleaching and phototoxicity and has intrinsic z-axis resolution, recordings of neuronal migration were captured for as long as 24 h in P5 slices without an

apparent decrease in migration rate or viability of the slice. This transgenic line was next crossed with DCX+/- to generate DCX-/y;DCX::EGFP mice. Acute brain sections through the RMS showed no alteration in GFP intensity within individual cells in wild-type and mutant sections. We concluded that this model can allow the long-term visualization of migrating neurons.

Impaired average velocity reflects 'stutter' in DCX-/y

In the DCX-/y; DCX::EGFP mice, as expected, we noted a substantial increase in the number of GFP-positive cells within the RMS (Fig. IV.1e). Comparison of movies from five separate experiments from each genotype showed overall slowed migration in DCX-/y slices. In these experiments, neurons in wild-type slices typically showed bipolar or monopolar morphology and migrated at saltatory rates throughout the recording, whereas neurons in mutant slices showed frequent multipolar morphology that tended to correlate with a long pause in migration. The multipolar phenotype and delayed migration rates appeared to be the same as those in DiI-labeled migrating neurons (Fig. IV.3a). Assessment of merged datasets (by tracking the position of individual neurons in the x-y-t dimensions) showed that some mutant neurons were capable of rapid migration for brief periods, but this was frequently interrupted by long stuttering-like pauses in which cell bodies oscillated slightly (Fig. IV.3c). We found that average velocity was decreased from 0.54 μm/min to 0.22 μm/min in mutant slices (Fig. IV.3d). Because the movement of neurons is stochastic and may not follow a normal distribution, we also ranked the average velocity per neuron. We noted that mutant neurons were capable of migrating at speeds approaching those of wild-type neurons, but showed rates that were,

on average, significantly slower (Fig. IV.3e; $P < 0.01$). There was no notable difference in the direction of migration or maximum velocity achieved by each neuron during the recording (Fig. IV.3f,g). We concluded that average velocity is primarily affected in the DCX-/y, which is probably a reflection of an increase in migration stutter as evidenced by the long migration pauses.

Migration defects but normal response to Slit in DCX-/y

These migration defects suggest a cell-intrinsic block in the ability of SVZa-derived neurons to migrate properly. To test this, we monitored the migration of neurons exiting P5 DCX+/y and DCX-/y SVZa explants in vitro. In the wild type, there was robust migration away from the explant over the 12-h time course of the experiment (Ward et al., 2003; Wu et al., 1999). Parallel experiments performed with mutant explants showed a severe reduction in neuronal migration, without an apparent effect on cell exit from the explant (Fig. IV.4a). In both genotypes, approximately the same number of neurons extended neurites away from the explant and appeared to have initiated migration, but mutant cells did not achieve similar migration distances. Quantification of this effect showed that mean migration distance from the edge of the explant was significantly reduced—by over 50% (Fig. IV.4b; $P < 0.01$). In separate experiments, we used time-lapse imaging to analyze migration velocity of over 100 neurons from each genotype, and found a significant reduction in this parameter (Fig. IV.4c; $P < 0.01$). We concluded that DCX is required for the migration of SVZa-derived neurons in vitro.

We considered that the migration defect might be the result of an inability to transduce extracellular guidance cues such as Slit to the neuronal cytoskeleton, as this is a

major extracellular guidance cue of SVZa migration (Wu et al., 1999) and evidence suggests that specific cytoskeletal proteins may transduce extracellular guidance cues (Del Rio et al., 2004). Slit application to explants resulted in the vast majority of neurons reversing polarization within 2 h and subsequently migrating back into the explant over the next 2–4 h (schematic in Supplementary Fig. IV.3a). During neuronal repolarization, we observed the withdrawal of the previous leading process and extension of a new process in the new direction of migration that was dependent on an intact neuronal cytoskeleton (data not shown). In response to Slit, approximately 70–75% of cells from both DCX+/y and DCX-/y explants underwent repolarization, and there was no statistical difference between the datasets (Supplementary Fig. IV.3; $P > 0.05$). We concluded that DCX-/y neurons do not show a defect in response to Slit stimulation.

Defects in nuclear translocation in DCX-/y

Neuronal migration consists of a repetition of three basic events: (i) leading process extension (event 1), (ii) positioning of the centrosome in the leading process (event 2) and (iii) translocation of the nucleus toward the position of the centrosome (event 3)25. As DCX localizes to the microtubules of the perinuclear cage, the leading process and the growth cones (Francis et al., 1999; Friocourt et al., 2003; Tanaka et al., 2004a), we examined for defects in each of these. We first tested for a defect in the last two events. The N-C distance (distance between the centrosome and the leading edge of the nucleus) is thought to reflect a dynamic interplay between movement of these two organelles, and altered N-C distance has been proposed to underlie the migration defect in some cell models (Shu et al., 2004; Solecki et al., 2004; Tanaka et al., 2004a). A

decrease in N-C distance should reflect a defect in centrosome positioning (event 2), whereas an increase should reflect a defect in nuclear translocation (event 3). We therefore measured N-C distance by first mating DCX+/- mice with beta-actin::Cetn2-EGFP mice, which express a centrin2-GFP fusion protein under the control of the chick beta-actin promoter (Higginbotham et al., 2004). Neurons from this transgenic mouse display a single pair of fluorescent centrioles and intact centrosome behavior. SVZa explants from the resultant DCX-/y; beta-actin::Cetn2-EGFP and DCX+/y; beta-actin::Cetn2-EGFP littermates were similarly cultured and subjected to time-lapse fluorescent imaging to visualize the nuclear outline and the centrosome (Supplementary Videos IV.1 and 2). We detected no significant ($P > 0.05$) difference in average N-C distance between wild-type and mutant neurons (Fig. IV.4d). However, it was clear that the mutant cells had a defect in nucleokinesis, as the nuclei did not translocate at the proper rate (Fig. IV.4c).

To test for a specific defect in the coupling of centrosome positioning to nucleokinesis, we compared kymographs of N-C dynamics. In DCX+/y neurons, we found that following a peak in the N-C distance, the nucleus immediately translocated toward the centrosome about one-third of the time, whereas in DCX-/y neurons, nuclear translocation (NT) occurred much less frequently (Fig. IV.4e). In these DCX-/y neurons, we typically observed the centrosome falling back toward the nucleus following an N-C peak rather than the nucleus translocating toward the centrosome. This effect was quantitated by measuring the number of nuclear NT events (defined as nuclear movements over a distance of 3 μm) per number of N-C peaks (defined as maximum N-C distance at two consecutive time points) in DCX+/y and DCX-/y neurons. NT events

occurred half as frequently in DCX-/y neurons as in DCX+/y neurons following an N-C peak (Fig. IV.4f). We concluded that in DCX-/y neurons, there is a defect in nuclear translocation toward the centrosome, but not in centrosome positioning.

Branching defects of the primary neurite in DCX-/y

We next tested for a defect in the first phase of neuronal migration: leading process extension. We found a notable defect in the length of the leading process and an increase in the percentage of cells with secondary neurite branches, suggesting a defect in neurite stabilization or organization in the absence of DCX. The average length of the leading process of DCX-/y neurons was 30% shorter than that in DCX+/y neurons (Fig. IV.5a,b).

We tested whether there was a difference in the number of cells with a simple bipolar shape and those with branched leading processes, because this has been identified as a possible defect following siRNA knockdown of DCX (Bai et al., 2003) and we observed this frequently in RMS slices from knockouts (Fig. IV.3a). A secondary branch was defined as a protrusion from either the primary neurite or the cell body that was at least 1 somal length and more than 1 somal length removed from the tip of the growth cone (to differentiate these from branched growth cones). There was a marked increase in the average number of secondary branches per cell: DCX-/y neurons had twice as many secondary branches, on average, over the course of the analysis (Fig. IV.5c). These secondary branches either extended from the cell body adjacent to the primary neurite or from the base of the primary neurite (Fig. IV.5a). We questioned whether these secondary branches might relate to the migration defect, so we compared the average number of

secondary branches per cell per frame with average migration velocity in a cohort of DCX-/y neurons. There was a clear negative correlation: cells with fewer secondary neurite branches showed more rapid rates of migration (Fig. IV.5d). We concluded that DCX is required for the maintenance of the bipolar shape during migration.

NT defects are probably secondary to branching phenotype

We questioned whether the defect in nuclear translocation might be secondary to the defect in neuronal morphology, as it is possible that slowed migration could lead to excessive branching. To address this issue, we tested the frequency of nuclear NT events per N-C peak in both wild-type and mutant cells, and grouped them based on whether the cells had a single process or multiple processes. In wild-type cells with a single leading process, an NT event occurred at approximately 50% of the N-C peaks (Fig. IV.5e). In rare wild-type cells with more than one branch (defined as a branched process greater than 1 somal length), NT events occurred at approximately 20% of the N-C peaks. These data indicated that branched neurons are less likely to show NT events following N-C peaks and suggested that the nuclear translocation defect we observed in DCX-/y neurons may be secondary to the increased number of branched neurons. To test this, we performed the same analysis in DCX-/y neurons. We found that there were fewer NT events per N-C peak in cells with single processes from DCX-/y neurons compared with DCX+/y neurons (Fig. IV.5e). Even more notable, however, was that DCX-/y neurons with multiple processes showed many fewer NT events per N-C peak than those with single processes. These data suggest that DCX is required for suppression of multiple branching and that this branching defect may lead to the NT defect we observed.

RESULTS (PART 2)

Loss of DCX/DCK1 does not affect proliferation

In contrast to the striking defect in the RMS of adult DCX-knockout mice, the cortex shows few abnormalities besides delamination in the hippocampus (Corbo et al., 2002). However, the severe cortical phenotype of the DCX/DCK1 double knockout suggests that DCX does in fact play a role in radial migration in the cortex in conjunction with DCK1 (Deuel et al., 2006; Koizumi et al., 2006a). To determine what specific stages of cortical development were defective, we observed proliferation and migration in slice culture from wild-type and double knockout embryos. Electroporation of GFP was performed in E14.5 embryos from DCX+/-; DCK1+/- females mated to either DCX-/y; DCK1+/- or DCX+/y; DCK1-/- males. With this mating schema, either 12.5% of all offspring or 50% of the males will be DCX-/-; DCK1-/-, respectively. Slice cultures were made at E16.5 and GFP+ live-cell imaging was performed on GFP+ cells with the FV1000 confocal microscope (Olympus).

Initial observation of dividing radial glia in the double knockout (DCX-/-; DCK1/- or DKO) suggested a possible defect in interkinetic nuclear movement (INM), where the nucleus normally moves to the ventricle during M-phase of mitosis and then resumes a position within the upper VZ for the rest of the cell cycle. We found what appeared to be a defect in the ventricle-directed translocation of the nucleus in some cells (not shown). To investigate this further, we analyzed two aspects of INM in fixed cortices electroporated with GFP: the length of ventricular processes in radial glia and PH3 staining. If a defect exists in nuclear translocation to the VZ, the radial glial process that contact the ventricular surface should on average be longer than in wild-type (WT) (Xie

et al., 2007). However, we found no significant difference in process length in four DKO cortices compared to two DCX+/y; DCK1+/- cortices (not shown). Anti-PH3 staining labels the nuclei of cells in all stages of mitosis. A defect in INM and mitosis would show a difference in both the distance of PH3+ nuclei from the ventricle and the number of PH3+ nuclei (Xie et al., 2007). Comparison of two DKO samples to one WT, one DCX+/y;DCK1+/- and one DCX+/+;DCK1-/- showed no significant difference in either aspect (not shown). This data suggests no defect in INM or mitosis in the DKO cortex, in contrast to a study performed previously using RNAi knockdown of DCK1 in progenitors (Shu et al., 2006).

DKO pyramidal neurons show normal orientation and polarity postnatally

We next analyzed several aspects of radial migration in the DKO. Considering the polarity defects in SVZa cells in the RMS, we tested whether radially migrating neurons in the DKO have morphological defects during migration. Analysis of cortical sections of DKO and DCX single knockouts electroporated with GFP at E14.5 and fixed at P0 showed a striking defect in the proportion of cells located in the upper levels of the CP (Figure IV.6A). Bin distribution analysis showed that in the DKO, the positions of projection neurons were distributed evenly across the cortical width, in contrast to accumulation in the upper layers of the DCX single KO. Higher magnification analysis of individual cell morphology could reveal no significant defects in either leading process branching, length, or directionality (Figure IV.6B). All of this suggests that in the DKO, response to guidance cues and establishment of a bipolar morphology in late stages of migration is not defective.

Radial glial scaffold is normal in DKO

Cell polarity and directionality appears to be normal in the DKO in late stages of migration, so an alternative explanation for retarded migration is necessary. One possibility is a disruption in the radial glial scaffold that guides neurons into the CP. This idea is supported by a study that showed that a splice variant of DKC1 was expressed in radial glia and that RNAi knockdown disrupted mitotic spindle integrity and radial process stability (Vreugdenhil et al., 2007). We labeled individual radial glia by injecting a small amount of *GFP*-containing Sindbis virus into the lateral ventricles of E14.5 embryos from a DCX+/-; DCK1+/- pregnant female. After 12.5 hours, the embryos were fixed. Individual radial glia with intact ventricular and pial processes were visualized and imaged with confocal microscopy. Careful analysis of radial glial morphology showed no significant differences between two DKO animals and a DCX+/+;DCK1+/- animal (not shown).

Defect in transition from multipolar to bipolar phase

Because fixed tissue analysis yielded little understanding of the migration defect, we returned to live-cell imaging of electroporated slice cultures. Long-term timelapse imaging of radially migrating neurons in wild-type slices showed robust radial migration, with multipolar cells in the SVZ becoming bipolar and moving rapidly into the cortical plate (Supplementary Movie IV.3). Cells moved with an average net velocity of 0.044μm/min (Fig. IV.7A). In contrast, cells in the DKO slice had an average velocity of 0.018μm/min while cells in a DCX-/-;DCK1+/- slice had an average of 0.032μm/min

(Fig. IV.7A). The maximum velocities reached were 0.225μm/min, 0.183μm/min, and 0.103μm/min for WT, DCX-/-; DCK1+/-, and DKO slices, respectively (Fig. IV.7A) In addition to the slower net velocity, cells in the DKO and DCX-/-; DCK1+/- slices showed a striking accumulation in the SVZ, where most cells displayed a multipolar morphology and moved little during the timelapse interval (Supplementary movie IV.4). In both WT and mutant slices, cell moving into the CP would exhibit one of three behaviors in the SVZ: 1. Adopt a multipolar morphology in the SVZ and remain there for the duration of the timelapse. 2. Become multipolar first and then become bipolar and migrate into the CP. 3. Multipolar migration does no occur, but bipolar migration continues unimpeded throughout the timelapse. Most cells in WT slices exhibited behaviors 2 and 3, with few cells remaining multipolar (Fig. IV.8A). In contrast, in DKO and DCX-/-; DCK1+/- slices significantly more cells exhibited behaviors 1 and 2 (Fig. IV.8B), where most mutant cells in the SVZ underwent a multipolar phase but did not exit it. The multipolar cells in both WT and mutant slices showed slowed migration velocity, as has been described (Tabata and Nakajima, 2003), and the high numbers of multipolar cells in the mutant slices likely accounts for the decrease in average migration velocity.

This assumption was verified by an additional observation: In some cells of the mutant (DKO and DCX-/-;DCK1+/-) slices a transition from a multipolar to bipolar morphology occurred. A subset of those bipolar, mutant cells migrated normally into the cortical plate at velocities comparable to WT cells (Fig. IV. 7A, Fig. IV.8B, Supplementary Movie IV.4). From this data, we hypothesized that the migration deficit seen in the DKO and DCX-/-;DCK1+/- postnatally is an embryonic defect in the transition from a multipolar to a bipolar morphology.

We tested this hypothesis by quantifying the migration arrest in the SVZ by artificially dividing the slices in the timelapse images into an upper and a lower region, consisting of the CP/IZ and VZ/SVZ, respectively. Net migration velocity was measured for cells in both regions, and if cells moved from the lower to the upper part of the slice net velocity was measured for each region separately. In WT slices, migration velocity averaged 0.058μm/min in the VZ/SVZ and 0.033μm/min in the IZ/CP (Fig. IV.7B). The slower velocity in the IZ/CP compared to the VZ/SVZ is due to neurons completing their migration during the timelapse and coming to rest in the CP for the duration of the timelapse.

Interestingly, we found the opposite trend in the DCX-/-;DCK1+/- slice: velocity averaged 0.030μm/min in the VZ/SVZ and 0.045μm/min in the IZ/CP (Fig. IV.7B), suggesting that migration velocity in the VZ/SVZ is significantly impaired. However, in the DKO, velocities averaged 0.021μm/min in the VZ/SVZ and 0.018μm/min in the IZ/CP (Fig. IV.7B). This indicated that in the DKO, migration is defective in both the upper and lower regions of the cortical width, and suggests further defects exist in the DKO beyond a defect in phase transition in the SVZ.

To further test the idea of a defect in a phase transition, we quantified the percentage of cells that entered the IZ from the VZ or SVZ during the timelapse. We found a 51% decrease in the number of cells entering the IZ/CP during the timelapse in the DCX-/-; DCK1+/- slice and a 76% decrease in the DKO slice compared to WT (Fig. IV.7C). Taken together with the fact that DCX-/-; DCK1+/- mice show significant lamination defects similar to the DKO (Koizumi et al., 2006b), these results suggest that reduced dosage of DCK1 in the DCX KO background results in a specific defect in cells

migrating through the VZ/SVZ, where cells are defective in the transition from a multipolar to a bipolar morphology.

DISCUSSION

Loss of DCX in humans results in a severe migration phenotype, but in DCX-deficient mice cortical lamination is normal. One of the possible reasons for the discrepancy is a difference in the migratory distance required of neurons in humans vs. mice. Here we have tested the hypothesis that neurons in DCX-mice that have longer migratory paths than cortical projections neurons will show a migratory defect. Accordingly, we show that the microtubule-associated protein DCX is expressed by tangentially migrating neuroblasts in the RMS. We found that DCX inactivation correlated with a phenotype of disrupted neuronal migration in this location. As a result of the disruption in neuronal migration, we observed a reduction in the number of neurons that achieve correct final positioning. The neurons in this mutant did not achieve proper velocity, but showed no defect in the direction of migration or response to guidance cues. In these neurons, DCX functions in suppressing the secondary branching of the leading neurite and in translocating the nucleus in the direction of migration. We have also explored further the mutually compensating roles of DCK1 and DCX in radial migration. We show a specific defect in the transition from multipolar to bipolar morphology in radially migrating projection neurons after loss of DCX and DCK1.These findings imply that DCX and DCK1 have a critical role in embryonic and adult forebrain in forming a bipolar morphology and in nuclear translocation during migration.

Role of DCX in the RMS and olfactory bulb

The stalled neuroblasts seem to have one of several fates, as we found evidence of an increased number of differentiated neurons and apoptosing cells in the RMS. Other gene defects resulting from defective neuronal migration also show morphological defects in the RMS. Mutations in the transcriptional regulator Arx (aristaless related homeobox), a gene required for neocortical development, and in Ncam, which encodes a cell adhesion molecule, among others lead to disrupted RMS migration and reduced olfactory bulb size (Chazal et al., 2000; Yoshihara et al., 2005). This may be a result of the failure of adult-generated SVZa neurons to deposit within the olfactory bulb or may reflect an earlier requirement for these genes during development. We found only a modest reduction in olfactory bulb size in the DCX mutant, which was not statistically significant (P approx 0.05; data not shown). The results from several studies have indicated that disrupted migration results in reduced numbers of GABAergic neurons in the olfactory bulb, although the functional implication of these alterations has not been thoroughly tested. We performed an electrophysiological assessment of glomerular physiology and were unable to identify a notable difference in GABAergic potentials in DCX+/y and DCX-/y littermates (data not shown). This might relate to the relatively small number of newly generated neurons that survive long term in the olfactory bulb or to a compensatory increase in the amount of GABA released from cells.

Essential role of DCX in translocation of the nucleus

We identified a requirement for DCX in mediating coupling between the nucleus and the centrosome during neuronal migration in SVZa-derived neurons. The centrosome

is an organelle best known for its role in mitosis. It serves as the microtubule-organizing center, and most microtubules emanate from the centrosome. Microtubules are intrinsically polarized and grow exclusively from the 'plus' end. The centrosome serves to anchor the 'minus' end of microtubules, where they are nucleated through a combined effect of pericentrosomal proteins including gamma-tubulin. Notably, we found no defect in centrosome number or morphology in DCX-/y neurons, based on immunofluorescence of pericentrin and centrin (Supplementary Fig. IV.4).

During neuronal migration, the centrosome of the cell is uniformly positioned in front of the nucleus (Gregory et al., 1988; Rakic, 1971; Rivas and Hatten, 1995); this has led to the idea that the nucleus is translocated along microtubules in the minus direction through minus end–directed motors including dynein. Indeed, disruption of dynein function, or alterations in LIS1 or NDEL1, which are dynein components, similarly lead to alterations in this coupling, as measured by an increased distance between the nucleus and centrosome (that is, coupling) (Shu et al., 2004; Tanaka et al., 2004a). The overexpression of DCX leads to an amelioration of the migration defects in Pafah1b1+/- neurons and corrects the nucleus-centrosome coupling defect (Tanaka et al., 2004a). We have now showed that deletion of DCX leads to a defect in nuclear translocation that was not evident by measurement of N-C coupling alone. As DCX is a potent microtubule-associated protein and is localized prominently to perinuclear microtubules (Francis et al., 1999), we hypothesize that it is required for the formation or stabilization of these microtubules or for mediating the transport of the nucleus along these microtubules, possibly in association with the LIS1/NDEL1/dynein complex.

Essential role of DCX in maintaining bipolar morphology

We found that neurites from DCX-/y neurons were shorter and more highly branched. A similar branched phenotype has been reported in migrating neurons in the cortex of the Cdk5r1 mutant (Gupta et al., 2003), where it is thought to contribute to altered cortical lamination. As the p35/CDK5 complex interacts with DCX (Tanaka et al., 2004b), it is possible that this interaction relates to the branched phenotype. What could the role of DCX be in maintaining this bipolar morphology? We excluded a defect in transducing guidance cues, as the reversal of polarity in response to Slit was normal. Altered microtubule dynamics is a possibility, but we excluded an obvious defect in microtubule plus-end dynamics as measured by the rate of movement of EB1-positive punctae (Supplementary Fig. IV.4). We also excluded an obvious defect in the rate of neurite retraction or extension following the application and washout of the microtubule-depolymerizing agent nocodazole in DCX-/y neurons (Supplementary Fig. IV.4). This argues against a major defect in microtubule growth. However, these tests do not evaluate defects in microtubule bundling. Our preliminary data suggest a defect in microtubule cross-linking and bundling in stationary neurons (data not shown), arguing that such a defect may underlie the branched morphology phenotype that results in the mutant.

Our data suggest that the branched phenotype we observed may be at least partly responsible for the difference in NT events in DCX-/y neurons. We found that cells with branched morphology had fewer NT events per N-C peak, irrespective of DCX genotype. The fact that the branched phenotype was more common in DCX-/y neurons may therefore account for the failure in migration. SVZa neurons may use branching as a means of changing migration direction, and cells with branched morphology typically

stabilize a dominant process and withdraw the secondary process before initiating nuclear movement (Ward et al., 2005). Therefore, NT and cell morphology seem to be temporally related; further work into this connection is warranted.

DCX as a regulator of radial and tangential migration

Recently, two groups found that DCX functions redundantly with DCK1 (doublecortin-like kinase) in radial migration (Deuel et al., 2006; Koizumi et al., 2006b). Loss of DCK1 in the DCX null background led to severe defects in radial migration and axon outgrowth. To determine what aspect of migration in affected, we conducted live-cell analysis of migration in slice culture. Preliminary observations of dividing radial glia in the DKO suggested a possible defect in INM. This seemed a reasonable possibility considering that RNAi knockdown of DCK1 resulted in defective spindle formation and mitosis (Shu et al., 2006) and in *C. elegans* the DCK1 homolog associates with the TACC homolog, which controls INM (Bellanger et al., 2007; Xie et al., 2007). However, we failed to find a defect in either the mitotic index or radial glial nuclear positioning in fixed samples. In addition, we found no defect in radial glial process morphology, in contrast to what is seen with DCK1 knockdown (Vreugdenhil et al., 2007). Considering that DCK1 but not DCX is expressed in radial glia and that DCK1 single knockouts don't have a neocortical phenotype, perhaps other unidentified genes are compensating for loss of DCK1 in the knockout but not after knockdown. In fact, DCK2 is expressed with DCK1 in glial progenitors and could play a compensatory role (Tuy et al., 2008).

Analysis of radial migration in postnatal tissue confirmed previous results that showed that loss of both DCX and DCK1 severely impaired radial migration into the

upper layers of the cortex. Surprisingly, we found no obvious defects in polarity or directionality in postnatal cortex, suggesting that DCX and DCK1 together are not required for response to guidance cues. This corresponds to our observations in SVZa cells in response to Slit. However, examination of postnatal tissue doesn't indicate what occurred embryonically with regards to polarity and directionality. It is possible that defects in migration could be corrected late in development, with expression of a compensatory gene or a change in the cellular environment that enables proper polarization. So we performed slice culture analysis of embryonic cortex.

In the DCX/DCK1 DKO slices analyzed, we found a substantial decrease in overall migration velocity in both the DCX-/-; DCK1+/- and DKO, which correlates with the misplaced cells in postnatal cortex. Interestingly, the fastest cell from either mutant genotype had a velocity above that of 75% of the WT cells. Since migrating cells undergo periods of rapid movement followed by long pauses, the defect seen here may reflect an increase in pausing time, and not a defect in nuclear translocation velocity. This phenomenon was also noted in the SVZa cells: When a single leading process was generated, rapid nuclear translocation was more likely to occur.

Closer analysis of the slice culture movies showed an apparent accumulation of migrating neurons in the SVZ in both the DKO and DCX-/-; DCK1+/- slices. Most of these cells were multipolar and moved little during the timelapse. It is not clear whether this multipolar phenotype is equivalent to the normal multipolar phase or is a direct result of loss of DCX and DCK1. Considering that most cells in postnatal cortex have a normal orientation and polarity, it seems likely that the accumulation of multipolar cells we see in the DKO and DCX-/-; DCK1+/- is simply a delay in the normal transition from a

multipolar to a bipolar morphology. This hypothesis is supported by RNAi knockdown of DCX, where the accumulation of multipolar DCX-deficient cells in embryonic stages is absent in the adult, although laminar placement is defective (Ramos et al., 2006).

Not surprisingly, we also found an overall migration defect in the DKO, where cells across the entire cortical width showed multipolar morphology and were stalled in their migration. This suggests further defects exist in the DKO beyond a defect in phase transition in the SVZ. This would suggest that the underlying reason for a defect in transition from the multipolar to bipolar phase is an ineffective consolidation of the leading process. In the DKO, there appears to be an additional defect in the long-term maintenance of the leading process once it forms, resulting in stalled migration even outside the SVZ.

The multipolar stage appears to be a particularly sensitive phase of neuron migration (LoTurco and Bai, 2006). RNAi knockdown or inhibition of several genes including LIS1, DCX, MARK2, CDK5, C3G results in an arrest in the multipolar stage. From this, it seems likely that the transition from a multipolar to bipolar phenotype is a complex process that requires the concurrent action of several genes to repolarize the cytoskeleton. Axon outgrowth also occurs during the multipolar stage and, as discussed in the previous chapter, the centrosome is positioned at the base of the axon in multipolar cells. Defects in resumption of a bipolar morphology might reflect the inability to reorient the centrosome from the base of the axon to within the leading process.

DCX and DCK1 play important roles in MT stability and bundling. Acquisition of a single leading process requires tight bundling of MTs within the process shaft and the repression of collateral branching. In fact, these two processes may be interdependent.

Cortical neurons lacking both DCX and Spinophilin, a regulator of DCX activity, contain splayed MTs in the axon shaft and increased collateral branching (Bielas et al., 2007). In the presence of Spinophilin, DCX directly associates with actin filaments. Cortical actin polymerization is an initial step in leading process protrusion, so DCX acting as a MT-actin cross-linker might stabilize MTs growing into the protrusion. One hypothesis that is currently being tested is that during the early part of the multipolar stage, DCX is not expressed and multiple transient process form in the cell from lack of MT stabilization at sites of cortical actin activity. In the late multipolar stage, DCX expression is activated and functions in cooperation with DCK1 to stabilize MTs in one of the transient processes that will become the leading process. Loss of both DCX and DCK1 causes cells to be stuck in a phase of transient process extension and retraction. Thus consolidation and stabilization of the leading process requires the combined functions of several cytoskeletal proteins to stabilize the process, reorient the centrosome, and transmit forces generated in the leading process to the nucleus to move the cell forward.

MATERIALS AND METHODS

Histochemistry

Antibodies to DCX (C-terminal polyclonal, Santa Cruz), and PSA-NCAM, NeuN, active caspase-3, tyrosine hydroxylase (Chemicon), TuJ1, pericentrin (Covance), calbindin D-28K, parvalbumin (Sigma), calretinin (Swant), centrin2 (gift of J. Salisbury, Mayo Clinic, Rochester, Minnesota) were used as described previously (Gleeson et al., 1999).

Mice

Mice were cared for in accordance with animal protocols approved by the University of California, San Diego. The DCX+/- mice were maintained on a mixed genetic background composed of C57/Bl6 and 129SVJ (Corbo et al., 2002). GFP-CETN2 mice were maintained on a mixed background composed C57/Bl6 and BALBc (Higginbotham et al., 2004). The DCX::EGFP mice originated on a FVB/N; Swiss Webster line. All experiments were performed on experimental and wild-type littermates. BrdU labeling was performed with 0.1 mg BrdU per g body weight and detected with an antibody to BrdU (Becton Dickinson) and Vector ABC detection system (Vector Laboratories).

Acute slice preparation

Mice were genotyped at P5. Uniform parasagittal 300-μm brain sections (MX-TS Tissue Slicer) were mounted in a 1:1 collagen /culture media mixture, stabilized for several hours, then subject to multiphoton microscopy. DiI labeling was performed as reported (Ward et al., 2003), except that after a 12-h incubation, slices were immobilized in collagen gel and subject to multiphoton microscopy.

SVZa explants

This assay was carried out as reported (Wu et al., 1999). Slit2 was applied as conditioned media (Liu and Rao, 2003) to explants. As Slit diffuses through the collagen-Matrigel matrix, neurons respond by repolarizing and reversing migration direction back toward the explant (Ward et al., 2003). Nocodazole was added at 1–3 mug ml-1. Neurite length was determined using the SoftWorx software package from Applied Precision.

Microscopy

Confocal images were acquired using an Olympus FV1000 system. Multiphoton live cell acute slice imaging was performed using an Olympus FV300 upright microscope with a Coherent MaiTai laser and with temperature and CO2 incubation at an excitation of 900 nM. Images were acquired with a z-step of 2 μm and depth of 100 μm through the RMS. Cell tracking was performed with ImageProPlus (Media Cybernetics). Fluorescent and DIC live cell migration imaging of SVZ explants was performed with a DeltaVision deconvolution system and with temperature and CO2 incubation using multipoint revisiting. Images were acquired with a z-step of 2 μm.

Lentivirus production

EB1 (Mimori-Kiyosue et al., 2000) was cloned into pLentiLox 3.7 (Rubinson et al., 2003) by removal of the EGFP of pLentiLox, followed by ligation of the full-length EB1-EGFP. High-titer viral particles were obtained as described (Miyoshi et al., 1998), then incubated with RMS explants for 30 h. Explants were plated for an additional 18 h before imaging.

In utero electroporation

In utero electroporation was conducted as described previously (Tabata and Nakajima, 2001). Pregnant females were anaesthetized and the uterus was removed from the body cavity. Injections of 1-2μl of DNA and Fast Green were injected into the lateral ventricles of the embryos. Electrical current was passed across the uterus at the level of the cortex. The embryos were then reintroduced into the mother.

Sindbis-virus

Sindbis-GFP was kindly provided by Gentry Patrick (UCSD). Injection was performed *in utero*. Timed pregnant females were anaesthetized and the uterus removed from the body cavity. Small amounts (1-2µl) of virus were injected into the lateral ventricle. Embryos were reintroduced into the mother and were then fixed after 12 hours.

Slice culture and time lapse imaging

Electroporated embryos were removed at E16.5 and Vibratome sliced into 250µm coronal sections. Slices were cultured on Millicell inserts in cover glass bottomed Petri dishes. Imaging was performed with a water-immersion lens on the FV1000 system (Olympus).

ACKNOWLEDGEMENTS

H.K. conducted the in vivo experiments. H.K., H.H. and T.P. conducted the in vitro experiments. H.H. prepared the virus and conditioned media. T.T. and B.C.B. provided technical and imaging expertise. All contributed to data analysis and manuscript preparation. We wish to thank A. Wynshaw`-Boris (University of California, San Diego) and C. Walsh (Howard Hughes Medical Institute, Harvard Medical School, Boston) for DCX knockout mice; M. Hatten and N. Heitz (Rockefeller University, New York; http://www.gensat.org; NIH NS02331), and J. Winkler and L. Aigner (University of Regensburg, Regensburg, Germany) for DCX::EGFP mice; M. Ward and Y. Rao (Northwestern University, Chicago) for help with the SVZa explant culture system and for the Slit-producing stable HEK293T cell line; S. Tsukita (Japan Science and Technology Corporation, Kyoto, Japan) for the GFP-EB1 clone; N. Woods and R. Marr

(Salk Institute, La Jolla, California) for lentiviral vectors and assistance; and J. Isaacson for electrophysiological measurements. This work was funded by the National Institute of Neurological Disorders and Stroke (R01 NS04387 and NS47101). We thank the Neurosciences Microscopy Shared Facility at the University of California, San Diego, for imaging support.

Part of this chapter was published as: Koizumi, Hiroyuki; Higginbotham, Holden; Poon, Tiffany; Brinkman, Brendan; Gleeson, Joseph G. Doublecortin maintains bipolar shape and nuclear translocation during migration in the adult forebrain. Nat Neurosci. **9**(6): 779-86. 2006.

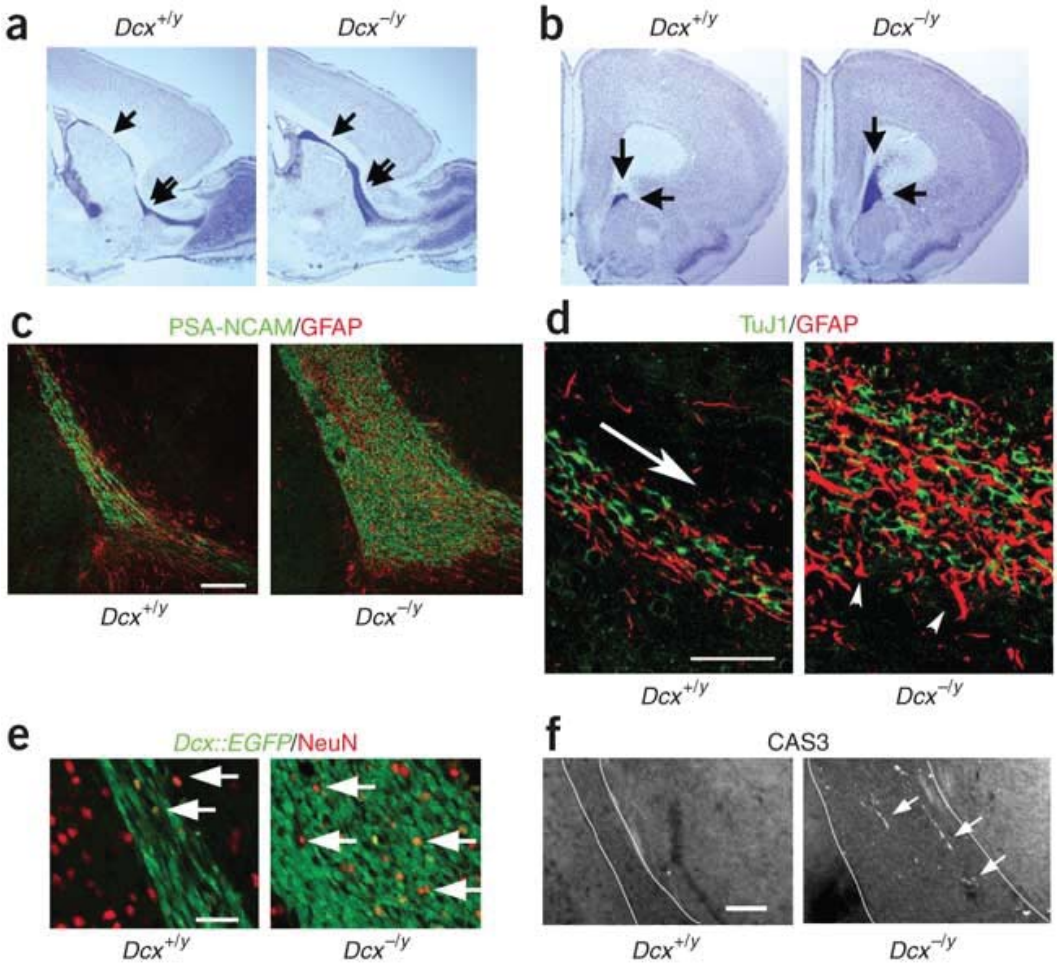

Figure IV.1: Abnormally thickened RMS in Dcx-/y mutant mice. (a) Cresyl violet-stained, matching parasagittal sections from adult Dcx +/y and Dcx -/y littermates. Note the thickened appearance of the RMS, especially in the central region (double arrows). (b) Matching coronal sections from the rostral forebrain of Dcx +/y and Dcx -/y littermates. The RMS is outlined by perpendicular arrows. RMS size was notably greater in mutants. (c) Thickened RMS in mutants consists of PSA-NCAM– and GFAP-positive cells. Scale bar, 100 mum. (d) High-power view of RMS costained for TuJ1 and GFAP. In Dcx +/y mice, there was an orderly appearance of the migratory TuJ1-positive neurons and GFAP-positive glia, with uniform orientation in the direction of migration (indicated by arrow). In Dcx -/y mice, the close juxtaposition of TuJ1- and GFAP-positive cells was maintained, but the cell orientation was less orderly (arrowheads indicate GFAP-positive cells of nonuniform orientation). Scale bar, 100 mum. (e) Increased number of NeuN-positive (red nuclei) differentiated neurons in Dcx -/y RMS. RMS defined by Dcx::EGFP signal. Scale bar, 50 mum. (f) Increased number of activated caspase-3 (CAS3)-positive cells in Dcx -/y RMS. Note cells in Dcx -/y (arrows) within the limits of the RMS (white lines) that are not apparent in Dcx +/y. Scale bar, 100 mum.

Figure IV.2: Newly generated neurons do not migrate properly in DCX-/y mice. (a) BrdU was administered at P28 and brains harvested at P35. Appearance of BrdU-labeled neurons (black signal, highlighted by arrows) in the SVZa in DCX +/y and DCX -/y mice is indistinguishable. Anterior edge of ventricle outlined by dashed line. Scale bar, 200 mum. (b) Failure of BrdU-labeled neurons to transverse the SVZa. In DCX +/y mice, BrdU-labeled cells were visible in the thin stream of the RMS (large arrow), where they fanned out in the proximal olfactory bulb (double arrows) and in the granule cell layer (small arrows). In the mutant, many BrdU-positive neurons were visible in the proximal RMS (large arrow), a smaller number were visible in the rostral RMS (double arrows) and very few were visible in the granule cell layer (*). Scale bar, 600 mum. (c) BrdU was administered at P28 and brains harvested at P56. BrdU-labeled neurons (brown, highlighted by arrows) in the glomerular layer were less numerous in the mutant. (d) Quantitation of the number of BrdU-positive cells in the glomerular layer (e and f, normalized to standard area) showed about a 50% decrease. Three serial matched sections from n = 3 mice for each genotype. * $P < 0.01$, Student's t-test. (e) Decreased number of calbindin-positive cells per glomerulus in 50-mum sections in the DCX -/y mutant. Glomeruli outlined by black circles. Note decreased number of brown cells in mutant (arrows). (f) Quantification from serial sections shows a significant decrease in the number of positive cells. $n > 30$ glomeruli from each of three mice of each genotype from matched sections. Error bars represent s.e.m. * $P < 0.01$, Student's t-test. GL, glomerular layer; EPL, external plexiform layer; GC, granule cell layer.

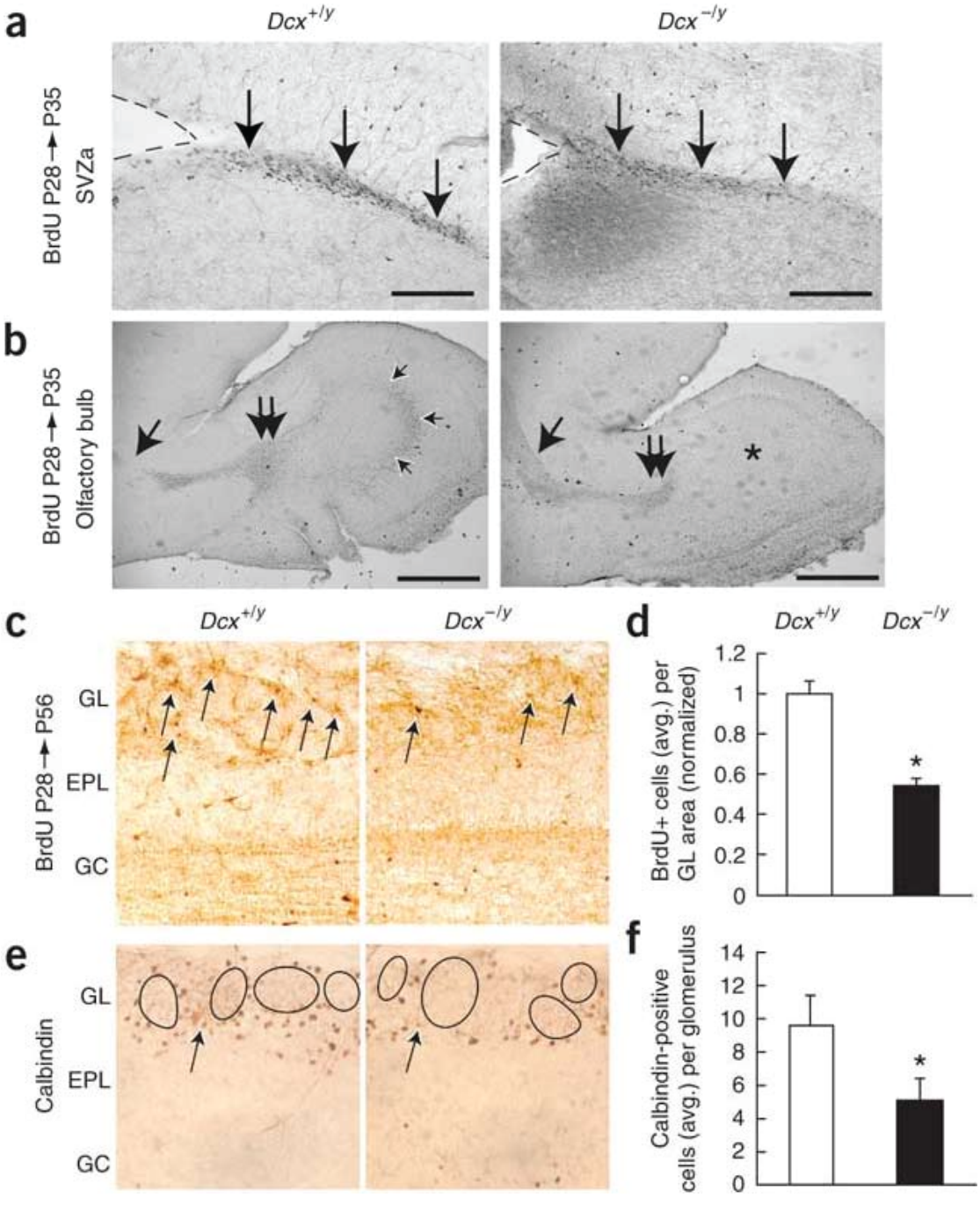
a
Dcx+/y
Dcx−/y
BrdU P28→P35
SVZa
b
BrdU P28→P35
Olfactory bulb
*
c
Dcx+/y
Dcx−/y
BrdU P28→P56
GL
EPL
GC
d
Dcx+/y
Dcx−/y
BrdU+ cells (avg.) per GL area (normalized)
1.2
1
0.8
0.6
0.4
0.2
0
*
e
Calbindin
GL
EPL
GC
f
Calbindin-positive cells (avg.) per glomerulus
14
12
10
8
6
4
2
0
*

Figure IV.3: Defect in average velocity reflects 'stutter' in the initiation of migration in slices from DCX-/y mice. (a) DiI-labeled RMS slices showing multiphoton images from DCX +/y and DCX -/y live brain slices through the RMS. The wild-type cell is shown moving toward the olfactory bulb at a steady rate, with regular advances of the leading process (arrowhead) followed by movement of the soma (arrow). In the mutant, there was excessive branched morphology (arrowheads) and the cell soma did not move well. Olfactory bulb is to the right. Time in min. Scale bar, 50 mum. (b) Fluorescent image of GFP signal from DCX::EGFP transgenic mouse, showing endogenous GFP signal along the RMS (arrowhead). Scale bar, 500 mum. (c) x-y-t maximum-z projection tracing, showing starting point (large colored circle) and migration steps (5-min intervals). Note steady rate of movement in most cells in the wild type, whereas cells in the mutant show frequent and long stuttering (arrows). (d,e) Average and ranked velocity were severely decreased in mutant neurons (Student's t-test and Kruskal-Wallis rank-sum test, respectively; * $P < 0.01$). n = 53 wild-type and 44 mutant neurons traced over 10 h from 300-mum z-axis image stack acquired every 5 min. Error bars represent s.e.m. (f) No alteration in direction of migration in mutant slices. (g) No alteration in the ranked maximum velocity for each cell, showing similarly shaped curves and no statistical differences ($P > 0.05$, Kruskal-Wallis rank-sum test). For c–g, only cells that moved at least one cell-body length during the experiment were tracked.

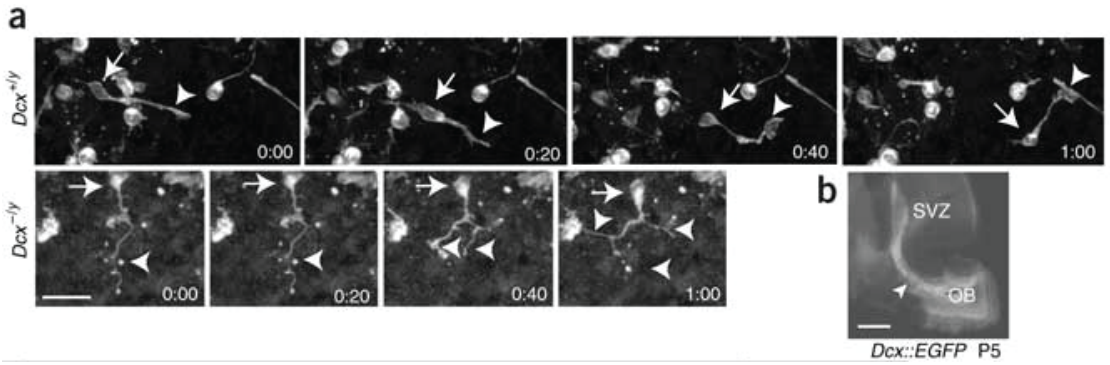

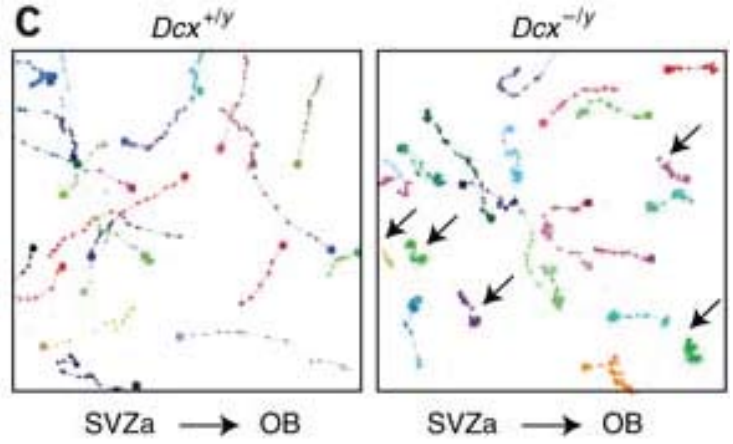

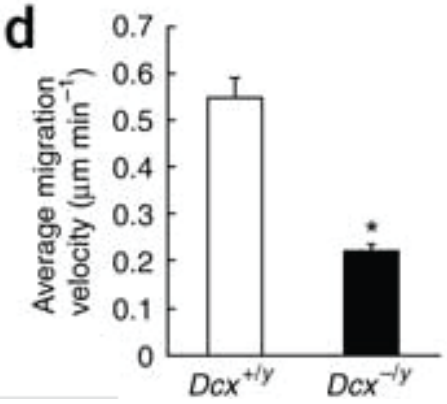

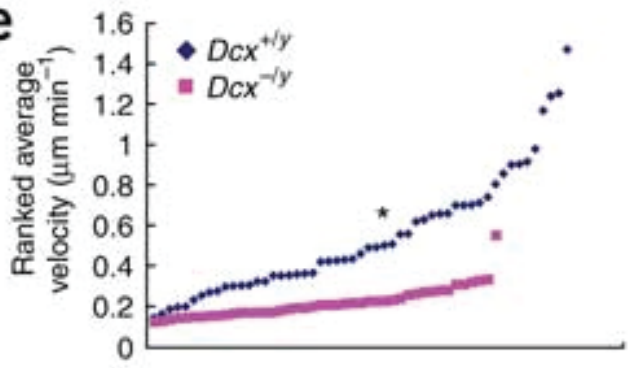

f

Direction	$Dcx^{+/y}$	$Dcx^{-/y}$
SVZ → OB	47.2	44.2
OB → SVZ	47.2	48.8
SVZ ↔ OB	5.6	7.0

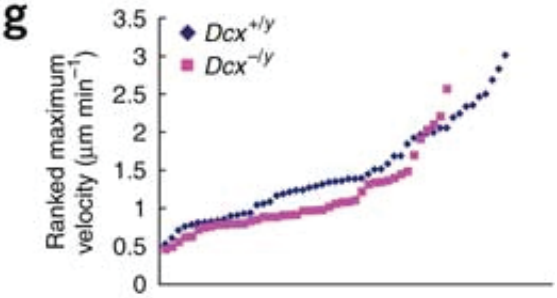

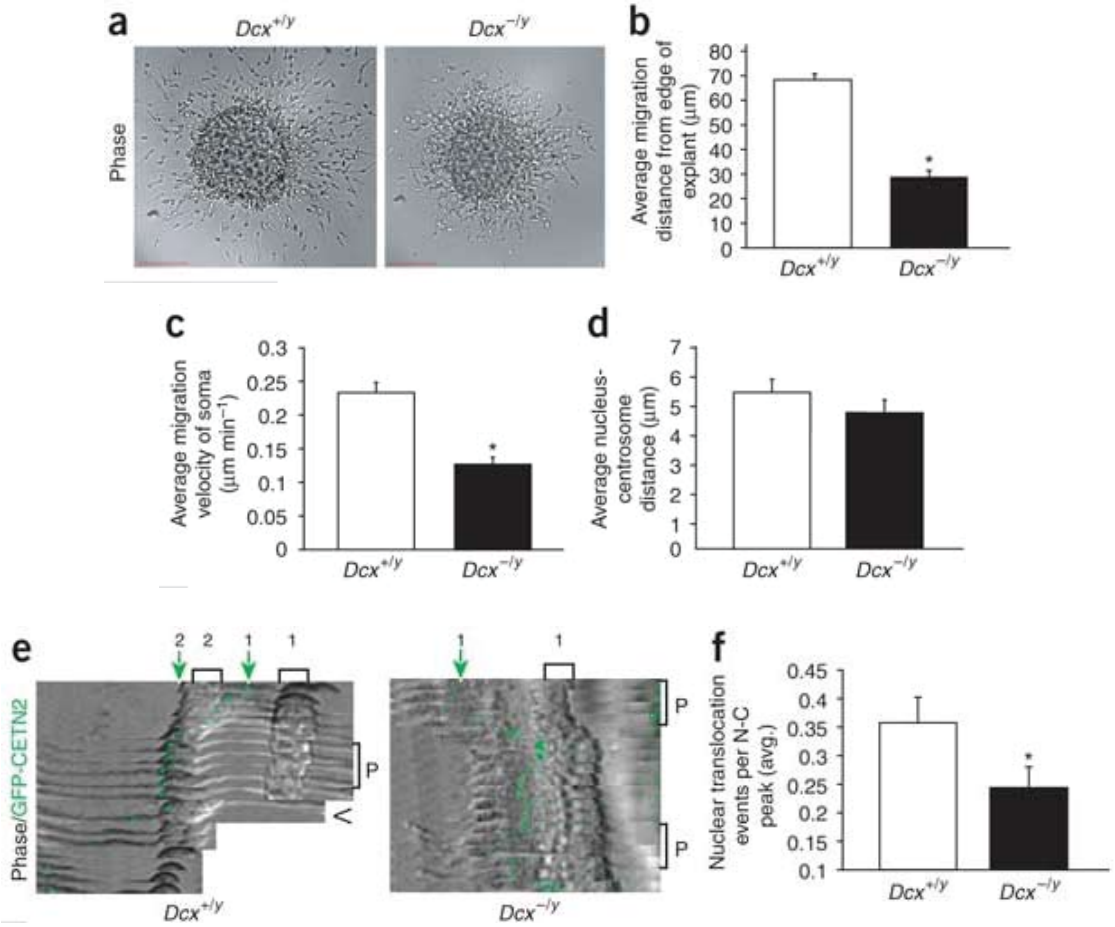

Figure IV.4: Decreased migration of neurons exiting the SVZa, due to a defect in nuclear translocation events. (a) Severely impaired neuronal migration of SVZa cells in Dcx -/y. Scale bar, 100 mum. (b) Decrease in average migration distance from edge of reaggregates in Dcx -/y. n > 22 explants and 1,200 cells for each genotype. * P < 0.01, Student's t-test, summed from three experiments. (c) Decrease in the average migration velocity. n > 100 neurons of each genotype. * P < 0.01, Student's t-test, summed from three experiments. (d) Average nucleus-centrosome distance was not altered in Dcx -/y neurons. n = 111 wild-type and 76 mutant neurons. P > 0.05, Student's t-test. (e) Kymograph of wild-type and mutant N-C dynamics. Initial nuclear position and initial centrosome position, respectively, are indicated by the bracket and green arrow marked '1'. In the wild type, following a peak in the N-C distance ('P' bracket), there was an abrupt NT event ('<') within 10 min. The '2' bracket and arrow represent the new positions. In the mutant, there were two N-C distance peaks ('P' brackets), and neither was followed by NT. Each frame, 3.5 min. (f) Decreased NT events per N-C distance peak in the mutant (see text for definitions). In the wild type, N-C distance peaks led to an NT event approximately 37% of the time, whereas this occurred 25% of the time in the mutant. n = 85 events, total of 15 neurons from each genotype. * P < 0.01, Student's t-test. Error bars represent s.e.m.

Figure IV.5: DCX functions in suppression of branching of the primary neurite. (a) Isolated neuron showing typical bipolar morphology of DCX +/y neuron and typically highly branched morphology of DCX-/y neurons. Excessive branches were evident from both proximal (arrow) and distal (arrowhead) segments of the neurite. GFP-labeled centrosome is evident (white arrows pointing to green spots). (b) Average leading process length (measured as a line from the base to the tip of the process) was decreased by approximately 30% in the mutant (32 mum in wild type versus 22 mum in mutant). n > 100 of each genotype. * $P < 0.01$, Student's t test. (c) In the mutant, there was a marked increase in the average number of secondary branches as a function of time. Each frame, 7.5 min. n = 109 wild-type and 52 mutant cells. * $P < 0.01$, Student's t-test. (d) Strong inverse correlation between average migration velocities (ranked in decreasing order) and average number of secondary branches per cell per frame. Total 16 frames of 15-min interval. (e) NT events per N-C peak was significantly reduced in neurons with multiple processes compared to those with single processes, in both DCX +/y and DCX -/y neurons. * $P < 0.01$, Student's t-test. Error bars represent s.e.m.

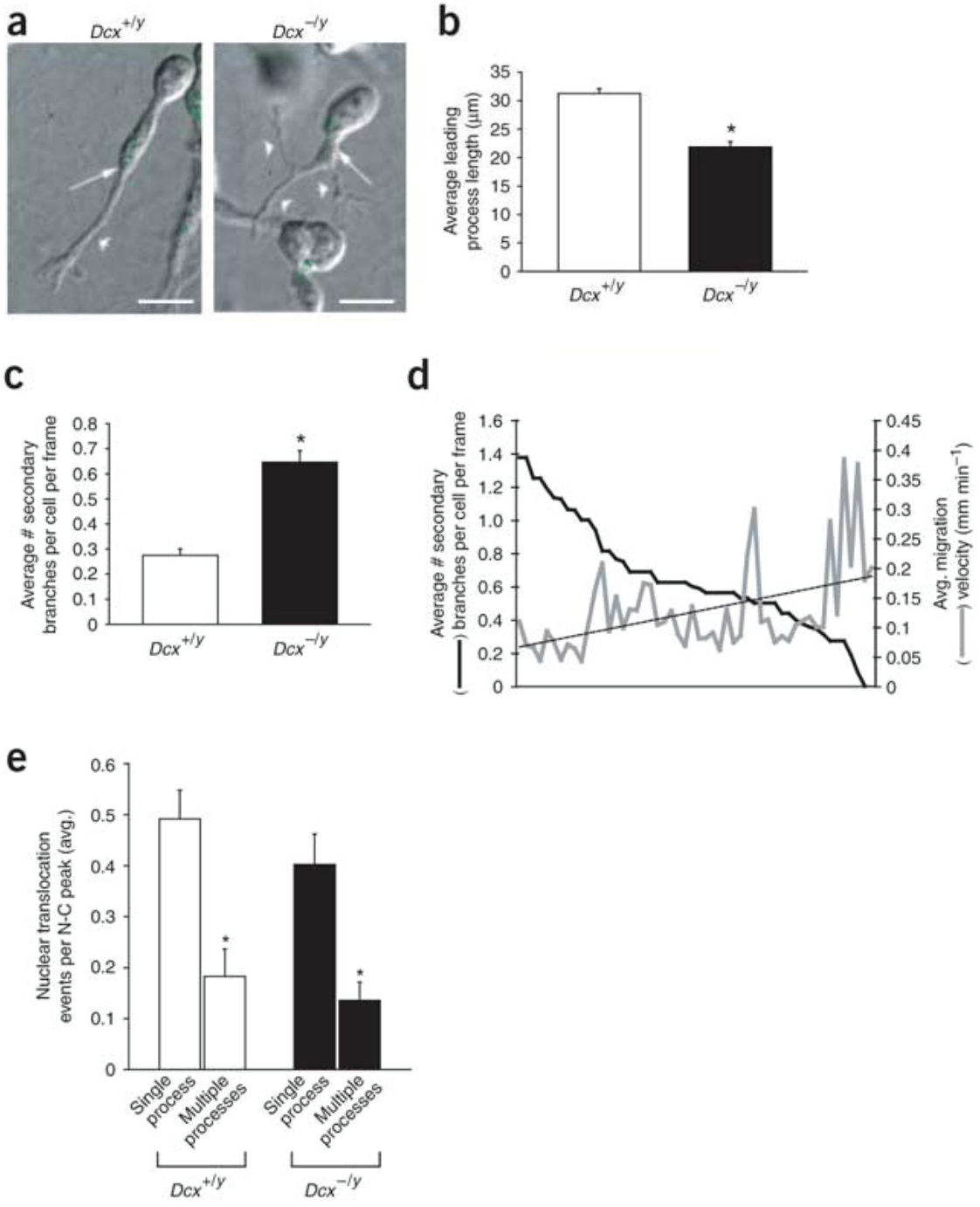
a
Dcx+/y
Dcx−/y
b
Average leading process length (μm)
35
30
25
20
15
10
5
0
*
Dcx+/y
Dcx−/y
c
Average # secondary branches per cell per frame
0.8
0.7
0.6
0.5
0.4
0.3
0.2
0.1
0
*
Dcx+/y
Dcx−/y
d
Average # secondary branches per cell per frame
1.6
1.4
1.2
1.0
0.8
0.6
0.4
0.2
0
0.45
0.4
0.35
0.3
0.25
0.2
0.15
0.1
0.05
0
Avg. migration velocity (mm min−1)
e
Nuclear translocation events per N-C peak (avg.)
0.6
0.5
0.4
0.3
0.2
0.1
0
*
*
Single process
Multiple processes
Single process
Multiple processes
Dcx+/y
Dcx−/y

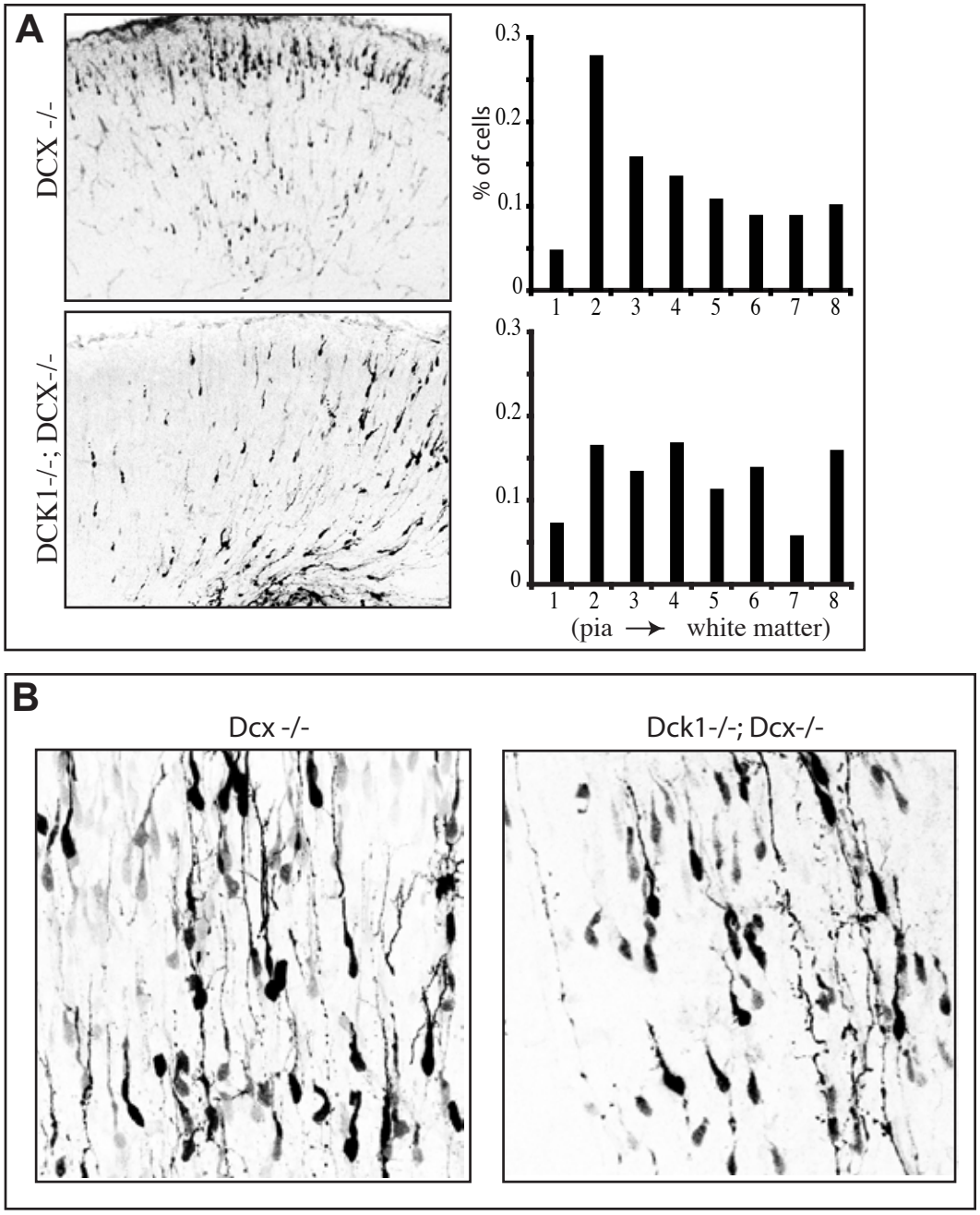

Figure IV.6: Migration defect in DXC-/-;DCK1-/- is not associated with a polarity defect. (A) P0 cortical slices electroporated with hrGFPII at E14.5 show a migration defect but no polarity defects. Graphs show bin distribution of cells along the cortical width. (B) Higher power inages show no obvious morphological differences between DCX single knockout and DCX/DCK1 double knockout.

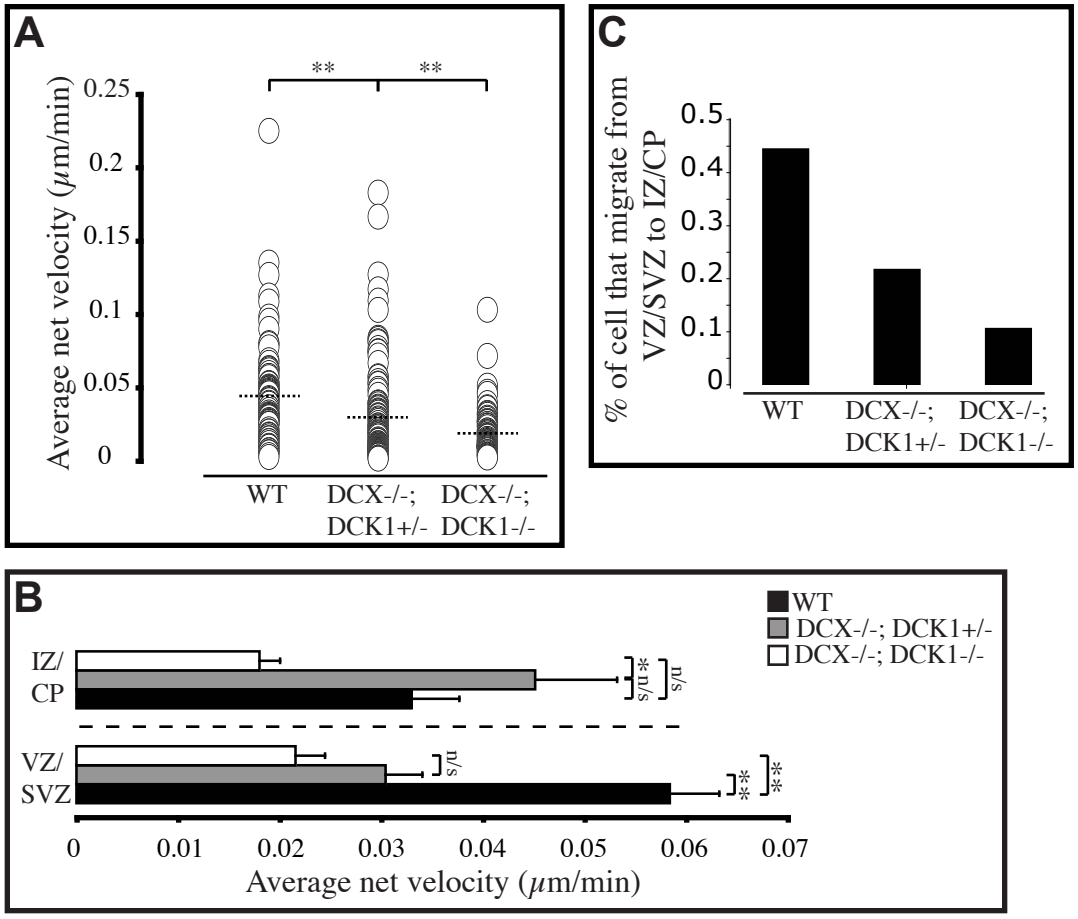

Figure IV.7: Loss of DCX and DCK1 leads to migration arrest in the VZ/SVZ. (A) Average net velocities of cells electroporated with hrGFPII at E14.5 and timelapse imaged in slice cultures at E16.5. Dashed lines indicate mean values. n=85 (WT); 101 (DCX-/-;DCK1+/-); 77 (DCX-/-; DCK1+/-). (B) Average net velocity of cells migrating either in VZ/SVZ region or IZ/CP region. Cells that moved from one region to the other were counted in both categories. (C) Percentage of cells that resided in the VZ/SVZ region when timelapse imaging began and moved into the IZ/CP region during the course of the timelapse. *p<.05; **p<.01, Tukey HSD Test. Error bars are SEM.

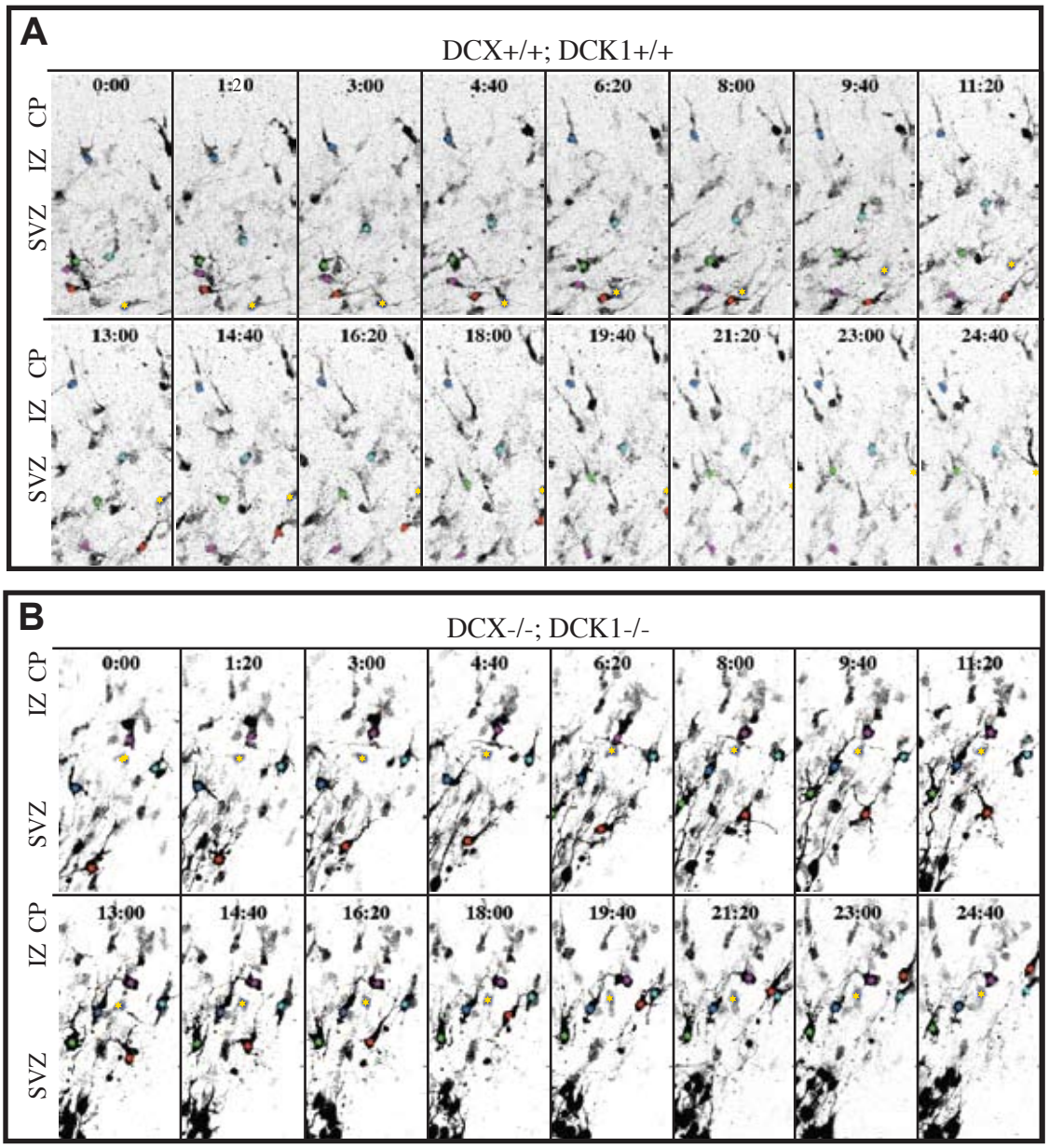

Figure IV.8: Timelapse images of radial cell migration in E16.5 slice. Individual cells are marked with colored stars. (A) Wild-type slice. Dark blue cell migrates radially then pauses in the CP. Light blue cell migrates radially and pauses below CP with multipolar morphology. Green cell exits multipolar stage (18:00) and migrates radially. Purple cell migrates tangentially then becomes multipolar (11:20). Yellow cell transitions from a bipolar to multipolar morphology (6:20) before becoming bipolar again and resuming radial migration. Red cell migrates tangentially then turns radially. (B) DKO slice. Blue cell begins multipolar, then extends a leading process (9:40), which is subsequently lost (21:20). Purple, yellow and light blue cells remain multipolar. Green cell migrates radially before acquiring a highly branched leading process and ceases migration (9:40). Red cell exits the multipolar stage and migrates radially.

Supplementary Figure IV.1: DCX expression in RMS and RMS morphological defects in DCX null mice (a-c) Co-distribution of DCX and PSA-NCAM in the SVZa/RMS (arrows) and proximal olfactory bulb (asterisk). There was a thin stream of cells expressing both DCX and PSA-NCAM that expanded over the caudal-rostral dimension of the bulb. Scale bar 2mm, (d) Abnormally thickened RMS in DCX–/y mice as analyzed by serial section. Top and bottom panels show every third 50 _m sections from the rostral to caudal RMS in 7-week old DCX+/y and DCX–/y mice. Note that the large dark blue region of the RMS (*) is significantly larger in sections through the mutant. (e) RMS defect was fully expressive in DCX–/– but not DCX+/– female mice. Cresyl violet-staining showing adult DCX+/y males, DCX+/– females and DCX–/y males. Note that the RMS in the DCX+/– female is not different in appearance from DCX+/y males (arrows). Thickened RMS in DCX–/– female was indistinguishable from DCX–/y male (arrow).

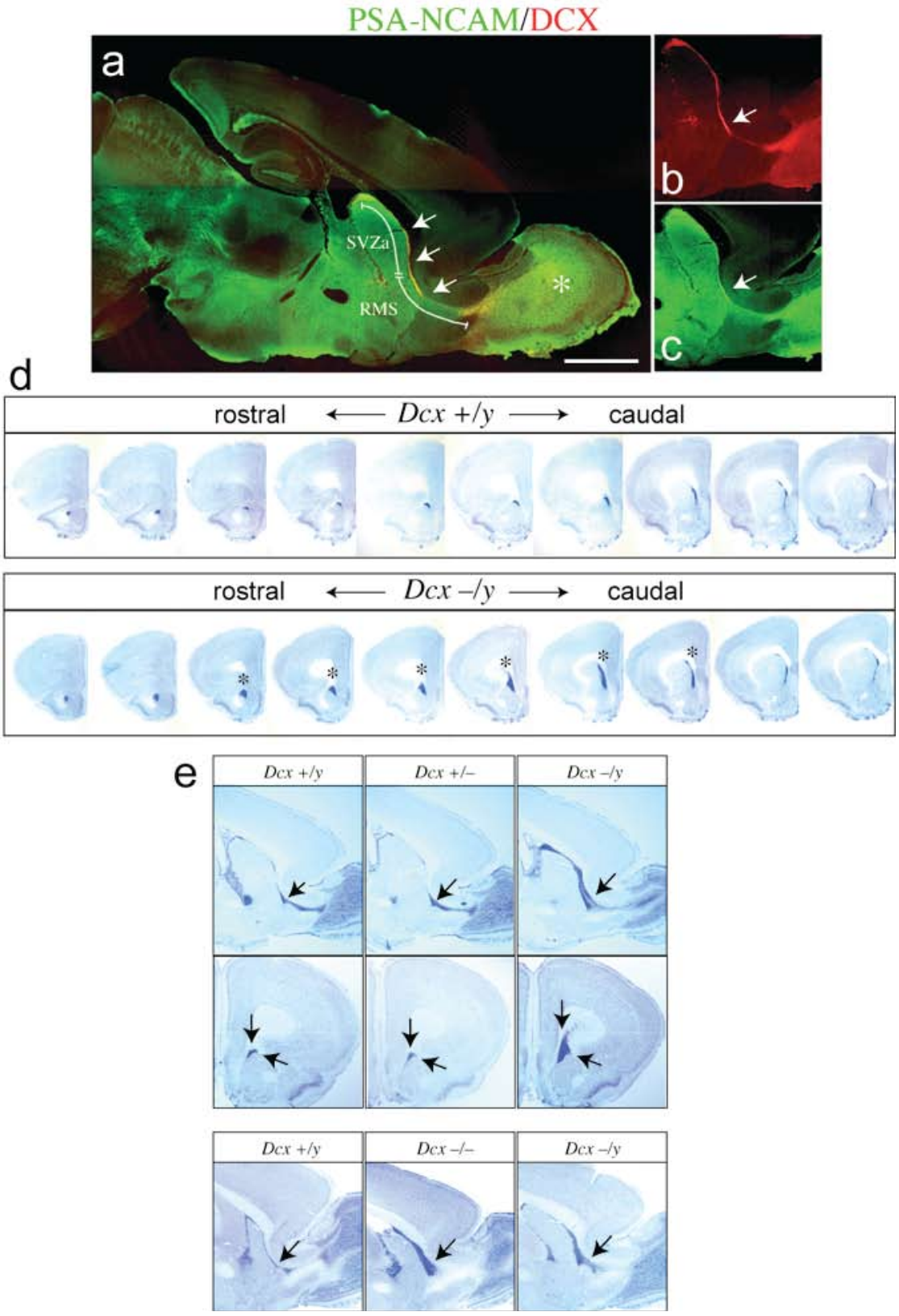
PSA-NCAM/DCX
a
b
c
SVZa
RMS
*
d
rostral
Dcx +/y
caudal
rostral
Dcx –/y
caudal
e
Dcx +/y
Dcx +/–
Dcx –/y
Dcx +/y
Dcx –/–
Dcx –/y

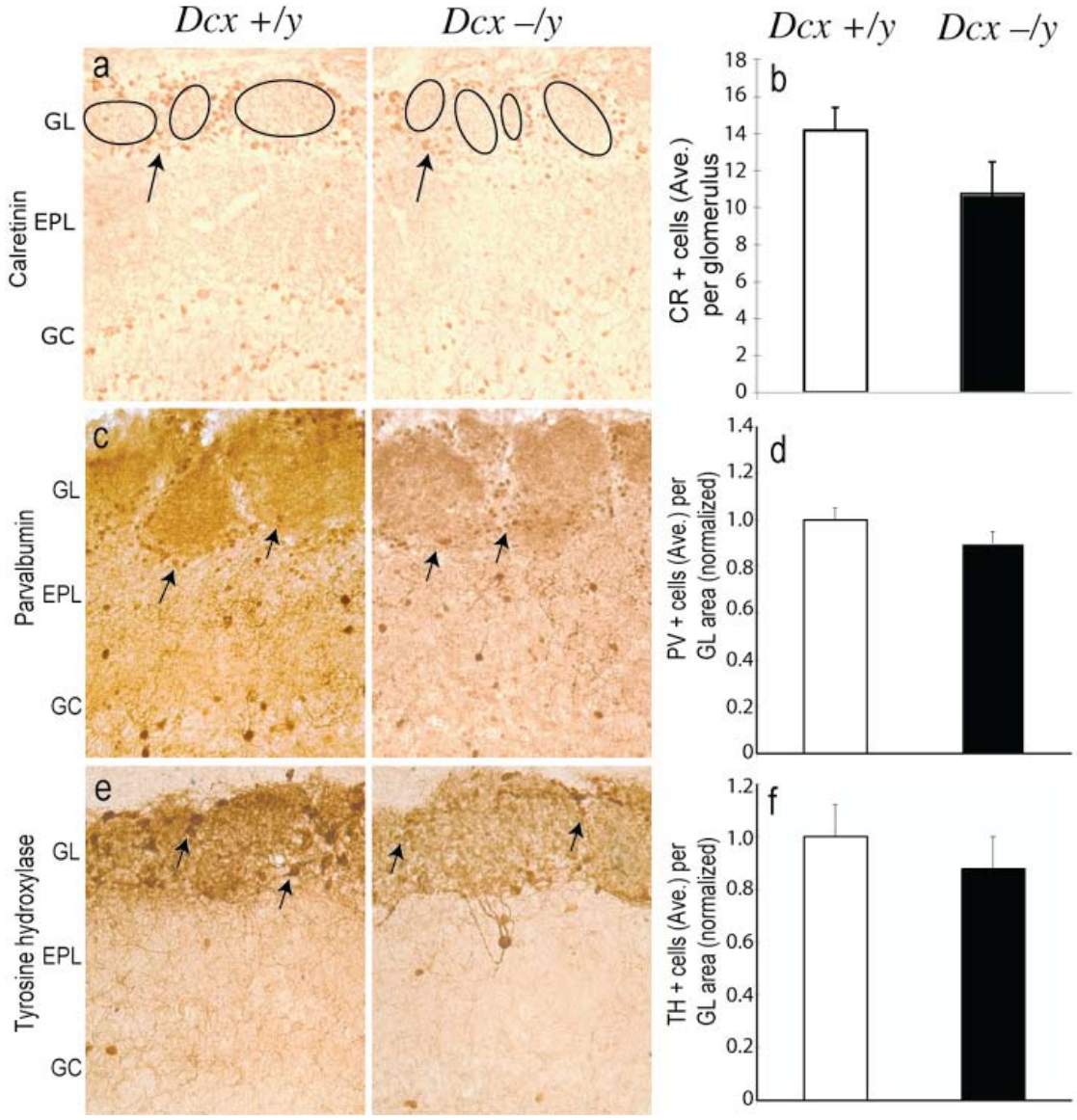

Supplementary Figure IV.2: No significant difference in numbers of calretinin (CR), parvalbumin (PV) or tyrosine hydroxylase (TH)-positive cells in the glomerular layer of Dcx–/y mice. (a) Sections from adult mice showed roughly equal numbers of CR (+) neurons (arrows) per glomerulus (circles). (c, e) PV and TH (+) neurons (arrows) were visible surrounding glomeruli, and no significant differences in numbers of labeled cells per normalized area were apparent. (b, d, f) Quantification showed slightly lower positive cells in mutant GL for each, but differences were not statistically significant. b, $n > 30$ glomeruli from each of three mice of each genotype from matched sections. $P < 0.05$, Student t-test. d, f, 3 serial matched sections from $n = 3$ mice for each genotype. $P > 0.05$, Student t-test. Error bar = s.e.m. GL = glomerular layer, EPL = external plexiform layer, GC = granule cell layer.

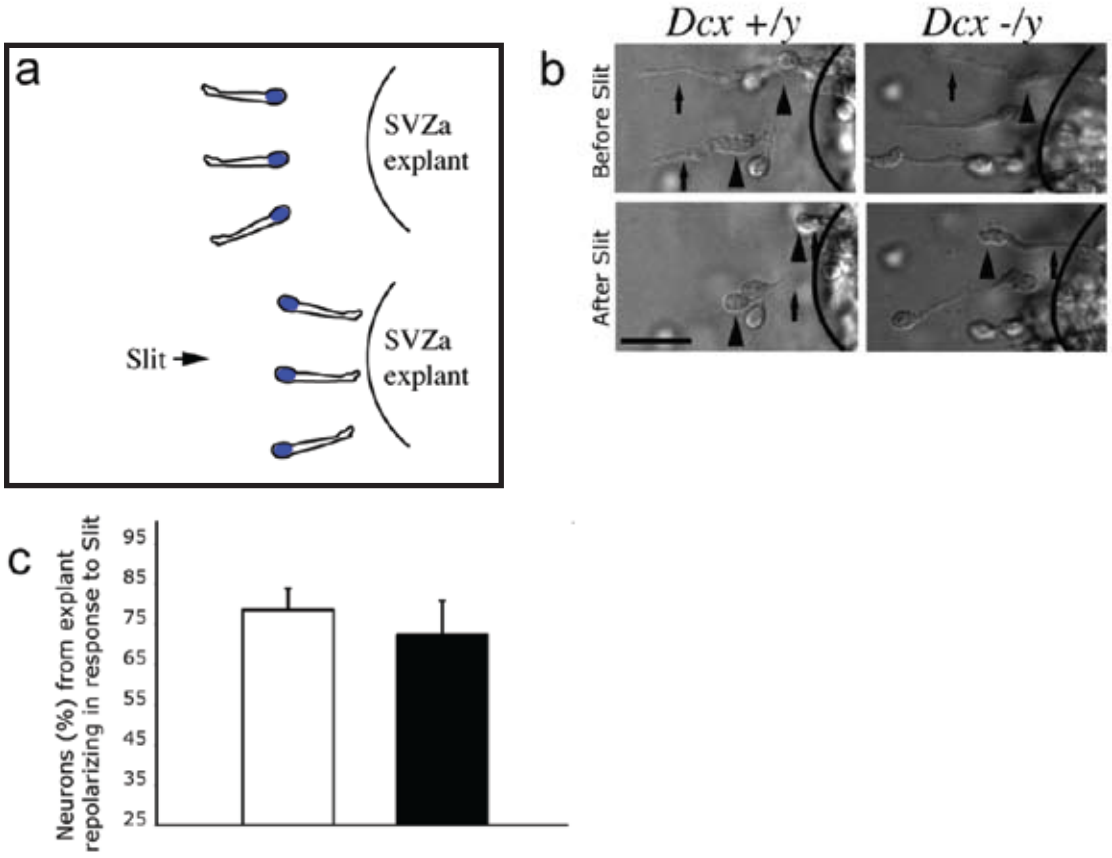

Supplementary Figure IV.3: No apparent defect in responsiveness of DCX DCX–/y neurons to Slit chemorepulsion. (a) Method for testing effect of Slit on neuronal reorientation. Explants were cultured in a collagen-Matrigel matrix for 12 hours to allow neurons to exit and begin migration, followed by bath application of Slit. Most cells reorient and migrate back into the explant in the subsequent 2 hours. (b, c) Mutant DCX–/y neurons had no apparent defect in re-polarization in response to Slit chemorepulsion. Neuronal morphology in DCX+/y (left) and DCX–/y (right) neurons before Slit application oriented away from explant (outlined in black) with leading process (arrow) in front of cell soma (arrowhead). Following Slit application neuronal repolarization was evident in DCX–/y and DCX+/y, with leading process oriented back towards the explant. Scale bar 50 _m. (d) No significant difference in proportion of neurons from explants that repolarize in response to Slit. n = 169 wt and 83 mutant cells imaged for 2 hours following Slit application, $P > 0.05$, Student t-test. Error bar = s.e.m.

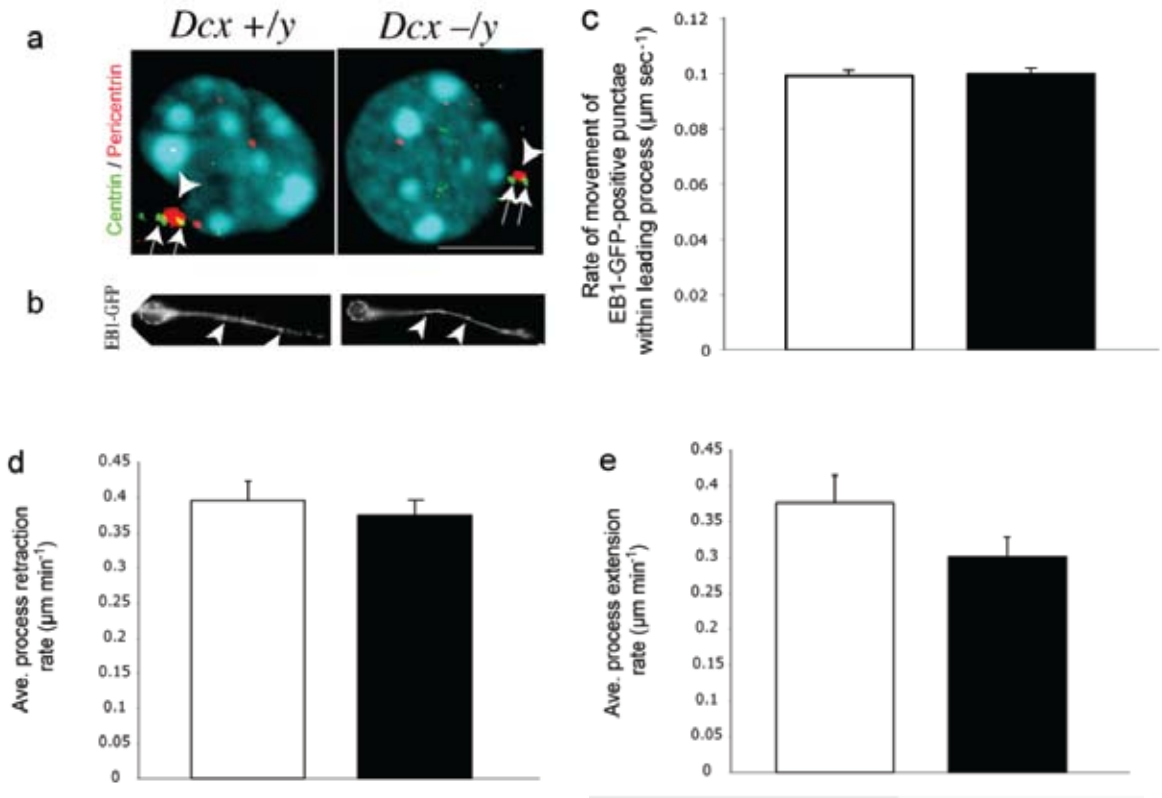

Supplementary Figure IV.4: No apparent defects in centrosome structure and microtubule polymerization dynamics in DCX–/y (a) No apparent defect in appearance of the centrosome in DCX–/y neurons. Dissociated migrating SVZa neurons were fixed and stained for centrosomal markers. Note the pair of centrioles seen with centrin labeling (green, pair of arrows) and the pericentriolar matrix seen with pericentrin labeling (redarrowhead). Hoechst stain (blue) shows nucleus. Scale bar 5 µm. (b, c) No apparent defect in plus-end microtubule dynamics in DCX–/y neurons. Migrating SVZa neurons were infected with a lentivirus encoding End-Binding protein 1 (EB1)-tagged GFP. Distinct punctate signals were observed in the leading process (b, arrowheads), and could be observed in time-lapse analysis to move away from the nucleus (dashed circle). Time-lapse analysis of each punctum for every 10 sec from 10 cells of each genotype (total n >240 from each genotype) showed no significant difference in this movement. $P > 0.05$, Student t-test. (d, e) No difference in leading process retraction or growth following acute application then washout of the microtubule depolymerizing agent nocodazole. Nocodazole was added at time zero, and time-lapse analysis was obtained for 50 min (every 5 min) to capture rate of process retraction. Subsequently, the drug was washed out and time-lapse analysis for 3-hours (every 5 min) to capture rate of process re-extension. No significant differences were noted. n = 33 wt and 61 mutant cells. Averaged from 2 trials. $P > 0.05$, Student t-test. Error bar = s.e.m.

REFERENCES

Abal, M., M. Piel, V. Bouckson-Castaing, M. Mogensen, J.B. Sibarita, and M. Bornens. 2002. Microtubule release from the centrosome in migrating cells. *J Cell Biol.* 159:731-7.

Ahmad, F.J., and P.W. Baas. 1995. Microtubules released from the neuronal centrosome are transported into the axon. *J Cell Sci.* 108 (Pt 8):2761-9.

Altman, J., and G.D. Das. 1966. Autoradiographic and histological studies of postnatal neurogenesis. I. A longitudinal investigation of the kinetics, migration and transformation of cells incorporating tritiated thymidine in neonate rats, with special reference to postnatal neurogenesis in some brain regions. *J Comp Neurol.* 126:337-89.

Alvarez-Buylla, A., and J.M. Garcia-Verdugo. 2002. Neurogenesis in adult subventricular zone. *J Neurosci.* 22:629-34.

Andrews, W.D., M. Barber, and J.G. Parnavelas. 2007. Slit-Robo interactions during cortical development. *J Anat.* 211:188-98.

Angevine, J.B., Jr., and R.L. Sidman. 1961. Autoradiographic study of cell migration during histogenesis of cerebral cortex in the mouse. *Nature.* 192:766-8.

Anthony, T.E., C. Klein, G. Fishell, and N. Heintz. 2004. Radial glia serve as neuronal progenitors in all regions of the central nervous system. *Neuron.* 41:881-90.

Anton, E.S., H.T. Ghashghaei, J.L. Weber, C. McCann, T.M. Fischer, I.D. Cheung, M. Gassmann, A. Messing, R. Klein, M.H. Schwab, K.C. Lloyd, and C. Lai. 2004. Receptor tyrosine kinase ErbB4 modulates neuroblast migration and placement in the adult forebrain. *Nat Neurosci.* 7:1319-28.

Anton, E.S., M.A. Marchionni, K.F. Lee, and P. Rakic. 1997. Role of GGF/neuregulin signaling in interactions between migrating neurons and radial glia in the developing cerebral cortex. *Development.* 124:3501-10.

Araki, M., C. Masutani, M. Takemura, A. Uchida, K. Sugasawa, J. Kondoh, Y. Ohkuma, and F. Hanaoka. 2001. Centrosome protein centrin 2/caltractin 1 is part of the xeroderma pigmentosum group C complex that initiates global genome nucleotide excision repair. *J Biol Chem.* 276:18665-72.

Azimzadeh, J., and M. Bornens. 2004. The centrosome in evolution. Wiley-VCH, Weinheim. 93-122 pp.

Azimzadeh, J., and M. Bornens. 2007. Structure and duplication of the centrosome. *J Cell Sci.* 120:2139-42.

Baas, P.W., and W. Yu. 1996. A composite model for establishing the microtubule arrays of the neuron. *Mol Neurobiol*. 12:145-61.

Bai, J., R.L. Ramos, J.B. Ackman, A.M. Thomas, R.V. Lee, and J.J. LoTurco. 2003. RNAi reveals doublecortin is required for radial migration in rat neocortex. *Nat Neurosci*. 6:1277-83.

Baird, D.H., K.A. Myers, M. Mogensen, D. Moss, and P.W. Baas. 2004. Distribution of the microtubule-related protein ninein in developing neurons. *Neuropharmacology*. 47:677-83.

Barnes, A.P., D. Solecki, and F. Polleux. 2008. New insights into the molecular mechanisms specifying neuronal polarity in vivo. *Curr Opin Neurobiol*. 18:44-52.

Baron, A.T., T.M. Greenwood, C.W. Bazinet, and J.L. Salisbury. 1992. Centrin is a component of the pericentriolar lattice. *Biol Cell*. 76:383-8.

Battye, R., A. Stevens, and J.R. Jacobs. 1999. Axon repulsion from the midline of the Drosophila CNS requires slit function. *Development*. 126:2475-81.

Beisson, J., and M. Wright. 2003. Basal body/centriole assembly and continuity. *Curr Opin Cell Biol*. 15:96-104.

Bellanger, J.M., J.C. Carter, J.B. Phillips, C. Canard, B. Bowerman, and P. Gonczy. 2007. ZYG-9, TAC-1 and ZYG-8 together ensure correct microtubule function throughout the cell cycle of C. elegans embryos. *J Cell Sci*. 120:2963-73.

Bellion, A., J.P. Baudoin, C. Alvarez, M. Bornens, and C. Metin. 2005. Nucleokinesis in tangentially migrating neurons comprises two alternating phases: forward migration of the Golgi/centrosome associated with centrosome splitting and myosin contraction at the rear. *J Neurosci*. 25:5691-9.

Bielas, S.L., and J.G. Gleeson. 2004. Cytoskeletal-associated proteins in the migration of cortical neurons. *J Neurobiol*. 58:149-59.

Bielas, S.L., F.F. Serneo, M. Chechlacz, T.J. Deerinck, G.A. Perkins, P.B. Allen, M.H. Ellisman, and J.G. Gleeson. 2007. Spinophilin facilitates dephosphorylation of doublecortin by PP1 to mediate microtubule bundling at the axonal wrist. *Cell*. 129:579-91.

Bobinnec, Y., A. Khodjakov, L.M. Mir, C.L. Rieder, B. Edde, and M. Bornens. 1998. Centriole disassembly in vivo and its effect on centrosome structure and function in vertebrate cells. *J Cell Biol*. 143:1575-89.

Bornens, M., and J. Azimzadeh. 2007. Origin and evolution of the centrosome. *Adv Exp Med Biol*. 607:119-29.

Briggs, M.W., and D.B. Sacks. 2003a. IQGAP1 as signal integrator: Ca2+, calmodulin, Cdc42 and the cytoskeleton. *FEBS Lett*. 542:7-11.

Briggs, M.W., and D.B. Sacks. 2003b. IQGAP proteins are integral components of cytoskeletal regulation. *EMBO Rep*. 4:571-4.

Brinon, J.G., J.R. Alonso, R. Arevalo, E. Garcia-Ojeda, J. Lara, and J. Aijon. 1992. Calbindin D-28k-positive neurons in the rat olfactory bulb. An immunohistochemical study. *Cell Tissue Res*. 269:289-97.

Brose, K., K.S. Bland, K.H. Wang, D. Arnott, W. Henzel, C.S. Goodman, M. Tessier-Lavigne, and T. Kidd. 1999. Slit proteins bind Robo receptors and have an evolutionarily conserved role in repulsive axon guidance. *Cell*. 96:795-806.

Brown, J.P., S. Couillard-Despres, C.M. Cooper-Kuhn, J. Winkler, L. Aigner, and H.G. Kuhn. 2003. Transient expression of doublecortin during adult neurogenesis. *J Comp Neurol*. 467:1-10.

Busson, S., D. Dujardin, A. Moreau, J. Dompierre, and J.R. De Mey. 1998. Dynein and dynactin are localized to astral microtubules and at cortical sites in mitotic epithelial cells. *Curr Biol*. 8:541-4.

Bystron, I., C. Blakemore, and P. Rakic. 2008. Development of the human cerebral cortex: Boulder Committee revisited. *Nat Rev Neurosci*. 9:110-22.

Causeret, F., M. Hidalgo-Sanchez, P. Fort, S. Backer, M.R. Popoff, C. Gauthier-Rouviere, and E. Bloch-Gallego. 2004. Distinct roles of Rac1/Cdc42 and Rho/Rock for axon outgrowth and nucleokinesis of precerebellar neurons toward netrin 1. *Development*. 131:2841-52.

Caviness, V.S., Jr. 1976. Patterns of cell and fiber distribution in the neocortex of the reeler mutant mouse. *J Comp Neurol*. 170:435-47.

Chae, T.H., and C.A. Walsh. 2007. Genes that control the size of the cerebral cortex. *Novartis Found Symp*. 288:79-90; discussion 91-8.

Charron, F., and M. Tessier-Lavigne. 2007. The Hedgehog, TGF-beta/BMP and Wnt families of morphogens in axon guidance. *Adv Exp Med Biol*. 621:116-33.

Chazal, G., P. Durbec, A. Jankovski, G. Rougon, and H. Cremer. 2000. Consequences of neural cell adhesion molecule deficiency on cell migration in the rostral migratory stream of the mouse. *J Neurosci*. 20:1446-57.

Chen, G., J. Sima, M. Jin, K.Y. Wang, X.J. Xue, W. Zheng, Y.Q. Ding, and X.B. Yuan. 2008. Semaphorin-3A guides radial migration of cortical neurons during development. *Nat Neurosci*. 11:36-44.

Chenn, A., Y.A. Zhang, B.T. Chang, and S.K. McConnell. 1998. Intrinsic polarity of mammalian neuroepithelial cells. *Mol Cell Neurosci*. 11:183-93.

Chretien, D., B. Buendia, S.D. Fuller, and E. Karsenti. 1997. Reconstruction of the centrosome cycle from cryoelectron micrographs. *J Struct Biol*. 120:117-33.

Connolly, J.A., B.W. Kiosses, and V.I. Kalnins. 1986. Centrioles are lost as embryonic myoblasts fuse into myotubes in vitro. *Eur J Cell Biol*. 39:341-5.

Cooper, J.A. 2008. A mechanism for inside-out lamination in the neocortex. *Trends Neurosci*. 31:113-9.

Corbo, J.C., T.A. Deuel, J.M. Long, P. LaPorte, E. Tsai, A. Wynshaw-Boris, and C.A. Walsh. 2002. Doublecortin is required in mice for lamination of the hippocampus but not the neocortex. *J Neurosci*. 22:7548-57.

Corfas, G., K. Roy, and J.D. Buxbaum. 2004. Neuregulin 1-erbB signaling and the molecular/cellular basis of schizophrenia. *Nat Neurosci*. 7:575-80.

D'Assoro, A.B., F. Stivala, S. Barrett, G. Ferrigno, and J.L. Salisbury. 2001. GFP-centrin as a marker for centriole dynamics in the human breast cancer cell line MCF-7. *Ital J Anat Embryol*. 106:103-10.

Dang, L., K. Yoon, M. Wang, and N. Gaiano. 2006. Notch3 signaling promotes radial glial/progenitor character in the mammalian telencephalon. *Dev Neurosci*. 28:58-69.

Danowski, B.A., A. Khodjakov, and P. Wadsworth. 2001. Centrosome behavior in motile HGF-treated PtK(2) cells expressing GFP-gamma tubulin. *Cell Motil Cytoskeleton*. 50:59-68.

Davies, S.P., H. Reddy, M. Caivano, and P. Cohen. 2000. Specificity and mechanism of action of some commonly used protein kinase inhibitors. *Biochem J*. 351:95-105.

de Anda, F.C., G. Pollarolo, J.S. Da Silva, P.G. Camoletto, F. Feiguin, and C.G. Dotti. 2005. Centrosome localization determines neuronal polarity. *Nature*. 436:704-8.

de Carlos, J.A., L. Lopez-Mascaraque, and F. Valverde. 1996. Dynamics of cell migration from the lateral ganglionic eminence in the rat. *J Neurosci*. 16:6146-56.

de Saint Phalle, B., and W. Sullivan. 1998. Spindle assembly and mitosis without centrosomes in parthenogenetic Sciara embryos. *J Cell Biol*. 141:1383-91.

Debec, A., C. Detraves, C. Montmory, G. Geraud, and M. Wright. 1995. Polar organization of gamma-tubulin in acentriolar mitotic spindles of Drosophila melanogaster cells. *J Cell Sci.* 108 (Pt 7):2645-53.

Dehay, C., and H. Kennedy. 2007. Cell-cycle control and cortical development. *Nat Rev Neurosci.* 8:438-50.

Del Rio, J.A., C. Gonzalez-Billault, J.M. Urena, E.M. Jimenez, M.J. Barallobre, M. Pascual, L. Pujadas, S. Simo, A. La Torre, F. Wandosell, J. Avila, and E. Soriano. 2004. MAP1B is required for Netrin 1 signaling in neuronal migration and axonal guidance. *Curr Biol.* 14:840-50.

Deng, C.X. 2002. Roles of BRCA1 in centrosome duplication. *Oncogene.* 21:6222-7.

des Portes, V., J.M. Pinard, P. Billuart, M.C. Vinet, A. Koulakoff, A. Carrie, A. Gelot, E. Dupuis, J. Motte, Y. Berwald-Netter, M. Catala, A. Kahn, C. Beldjord, and J. Chelly. 1998. A novel CNS gene required for neuronal migration and involved in X-linked subcortical laminar heterotopia and lissencephaly syndrome. *Cell.* 92:51-61.

Deuel, T.A., J.S. Liu, J.C. Corbo, S.Y. Yoo, L.B. Rorke-Adams, and C.A. Walsh. 2006. Genetic interactions between doublecortin and doublecortin-like kinase in neuronal migration and axon outgrowth. *Neuron.* 49:41-53.

Di Cristo, G. 2007. Development of cortical GABAergic circuits and its implications for neurodevelopmental disorders. *Clin Genet.* 72:1-8.

Dickson, B.J. 2002. Molecular mechanisms of axon guidance. *Science.* 298:1959-64.

Dictenberg, J.B., W. Zimmerman, C.A. Sparks, A. Young, C. Vidair, Y. Zheng, W. Carrington, F.S. Fay, and S.J. Doxsey. 1998. Pericentrin and gamma-tubulin form a protein complex and are organized into a novel lattice at the centrosome. *J Cell Biol.* 141:163-74.

Diviani, D., and J.D. Scott. 2001. AKAP signaling complexes at the cytoskeleton. *J Cell Sci.* 114:1431-7.

Doetsch, F., and A. Alvarez-Buylla. 1996. Network of tangential pathways for neuronal migration in adult mammalian brain. *Proc Natl Acad Sci U S A.* 93:14895-900.

Doetsch, F., I. Caille, D.A. Lim, J.M. Garcia-Verdugo, and A. Alvarez-Buylla. 1999. Subventricular zone astrocytes are neural stem cells in the adult mammalian brain. *Cell.* 97:703-16.

Doetsch, F., J.M. Garcia-Verdugo, and A. Alvarez-Buylla. 1997. Cellular composition and three-dimensional organization of the subventricular germinal zone in the adult mammalian brain. *J Neurosci*. 17:5046-61.

Dominguez, I., K. Itoh, and S.Y. Sokol. 1995. Role of glycogen synthase kinase 3 beta as a negative regulator of dorsoventral axis formation in Xenopus embryos. *Proc Natl Acad Sci U S A*. 92:8498-502.

Dotti, C.G., and G.A. Banker. 1987. Experimentally induced alteration in the polarity of developing neurons. *Nature*. 330:254-6.

Doxsey, S. 2001. Re-evaluating centrosome function. *Nat Rev Mol Cell Biol*. 2:688-98.

Doxsey, S.J., P. Stein, L. Evans, P.D. Calarco, and M. Kirschner. 1994. Pericentrin, a highly conserved centrosome protein involved in microtubule organization. *Cell*. 76:639-50.

Drescher, U. 2005. A no-Wnt situation: SFRPs as axon guidance molecules. *Nat Neurosci*. 8:1281-2.

Dujardin, D.L., L.E. Barnhart, S.A. Stehman, E.R. Gomes, G.G. Gundersen, and R.B. Vallee. 2003. A role for cytoplasmic dynein and LIS1 in directed cell movement. *J Cell Biol*. 163:1205-11.

Edelman, A.M., W.Y. Kim, D. Higgins, E.G. Goldstein, M. Oberdoerster, and W. Sigurdson. 2005. Doublecortin kinase-2, a novel doublecortin-related protein kinase associated with terminal segments of axons and dendrites. *J Biol Chem*. 280:8531-43.

Edmondson, J.C., and M.E. Hatten. 1987. Glial-guided granule neuron migration in vitro: a high-resolution time-lapse video microscopic study. *J Neurosci*. 7:1928-34.

Elias, L.A., D.D. Wang, and A.R. Kriegstein. 2007. Gap junction adhesion is necessary for radial migration in the neocortex. *Nature*. 448:901-7.

Endo, Y., and J.S. Rubin. 2007. Wnt signaling and neurite outgrowth: insights and questions. *Cancer Sci*. 98:1311-7.

Eriksson, P.S., E. Perfilieva, T. Bjork-Eriksson, A.M. Alborn, C. Nordborg, D.A. Peterson, and F.H. Gage. 1998. Neurogenesis in the adult human hippocampus. *Nat Med*. 4:1313-7.

Errabolu, R., M.A. Sanders, and J.L. Salisbury. 1994. Cloning of a cDNA encoding human centrin, an EF-hand protein of centrosomes and mitotic spindle poles. *J Cell Sci*. 107 (Pt 1):9-16.

Etienne-Manneville, S., and A. Hall. 2001. Integrin-mediated activation of Cdc42 controls cell polarity in migrating astrocytes through PKCzeta. *Cell*. 106:489-98.

Etienne-Manneville, S., and A. Hall. 2003a. Cdc42 regulates GSK-3beta and adenomatous polyposis coli to control cell polarity. *Nature*. 421:753-6.

Etienne-Manneville, S., and A. Hall. 2003b. Cell polarity: Par6, aPKC and cytoskeletal crosstalk. *Curr Opin Cell Biol*. 15:67-72.

Faulkner, N.E., D.L. Dujardin, C.Y. Tai, K.T. Vaughan, C.B. O'Connell, Y. Wang, and R.B. Vallee. 2000. A role for the lissencephaly gene LIS1 in mitosis and cytoplasmic dynein function. *Nat Cell Biol*. 2:784-91.

Feierbach, B., and F. Chang. 2001. Cytokinesis and the contractile ring in fission yeast. *Curr Opin Microbiol*. 4:713-9.

Feng, Y., E.C. Olson, P.T. Stukenberg, L.A. Flanagan, M.W. Kirschner, and C.A. Walsh. 2000. LIS1 regulates CNS lamination by interacting with mNudE, a central component of the centrosome. *Neuron*. 28:665-79.

Francis, F., A. Koulakoff, D. Boucher, P. Chafey, B. Schaar, M.C. Vinet, G. Friocourt, N. McDonnell, O. Reiner, A. Kahn, S.K. McConnell, Y. Berwald-Netter, P. Denoulet, and J. Chelly. 1999. Doublecortin is a developmentally regulated, microtubule-associated protein expressed in migrating and differentiating neurons. *Neuron*. 23:247-56.

Frantz, G.D., and S.K. McConnell. 1996. Restriction of late cerebral cortical progenitors to an upper-layer fate. *Neuron*. 17:55-61.

Friocourt, G., A. Koulakoff, P. Chafey, D. Boucher, F. Fauchereau, J. Chelly, and F. Francis. 2003. Doublecortin functions at the extremities of growing neuronal processes. *Cereb Cortex*. 13:620-6.

Fukata, M., T. Watanabe, J. Noritake, M. Nakagawa, M. Yamaga, S. Kuroda, Y. Matsuura, A. Iwamatsu, F. Perez, and K. Kaibuchi. 2002. Rac1 and Cdc42 capture microtubules through IQGAP1 and CLIP-170. *Cell*. 109:873-85.

Gaiano, N., J.S. Nye, and G. Fishell. 2000. Radial glial identity is promoted by Notch1 signaling in the murine forebrain. *Neuron*. 26:395-404.

Gambello, M.J., D.L. Darling, J. Yingling, T. Tanaka, J.G. Gleeson, and A. Wynshaw-Boris. 2003. Multiple dose-dependent effects of Lis1 on cerebral cortical development. *J Neurosci*. 23:1719-29.

Gdalyahu, A., I. Ghosh, T. Levy, T. Sapir, S. Sapoznik, Y. Fishler, D. Azoulai, and O. Reiner. 2004. DCX, a new mediator of the JNK pathway. *Embo J*. 23:823-32.

Glantz, S.A. 1996. Primer of biostatistics, 4th ed. McGraw-Hill, New York.

Gleeson, J.G., K.M. Allen, J.W. Fox, E.D. Lamperti, S. Berkovic, I. Scheffer, E.C. Cooper, W.B. Dobyns, S.R. Minnerath, M.E. Ross, and C.A. Walsh. 1998. Doublecortin, a brain-specific gene mutated in human X-linked lissencephaly and double cortex syndrome, encodes a putative signaling protein. *Cell*. 92:63-72.

Gleeson, J.G., P.T. Lin, L.A. Flanagan, and C.A. Walsh. 1999. Doublecortin is a microtubule-associated protein and is expressed widely by migrating neurons. *Neuron*. 23:257-71.

Goldstein, B., H. Takeshita, K. Mizumoto, and H. Sawa. 2006. Wnt signals can function as positional cues in establishing cell polarity. *Dev Cell*. 10:391-6.

Gong, S., C. Zheng, M.L. Doughty, K. Losos, N. Didkovsky, U.B. Schambra, N.J. Nowak, A. Joyner, G. Leblanc, M.E. Hatten, and N. Heintz. 2003. A gene expression atlas of the central nervous system based on bacterial artificial chromosomes. *Nature*. 425:917-25.

Goold, R.G., R. Owen, and P.R. Gordon-Weeks. 1999. Glycogen synthase kinase 3beta phosphorylation of microtubule-associated protein 1B regulates the stability of microtubules in growth cones. *J Cell Sci*. 112 (Pt 19):3373-84.

Gotz, M., and W.B. Huttner. 2005. The cell biology of neurogenesis. *Nat Rev Mol Cell Biol*. 6:777-88.

Gould, E., A.J. Reeves, M.S. Graziano, and C.G. Gross. 1999. Neurogenesis in the neocortex of adult primates. *Science*. 286:548-52.

Graham, M.E., P. Ruma-Haynes, A.G. Capes-Davis, J.M. Dunn, T.C. Tan, V.A. Valova, P.J. Robinson, and P.L. Jeffrey. 2004. Multisite phosphorylation of doublecortin by cyclin-dependent kinase 5. *Biochem J*. 381:471-81.

Gregory, W.A., J.C. Edmondson, M.E. Hatten, and C.A. Mason. 1988. Cytology and neuron-glial apposition of migrating cerebellar granule cells in vitro. *J Neurosci*. 8:1728-38.

Grove, E.A., S. Tole, J. Limon, L. Yip, and C.W. Ragsdale. 1998. The hem of the embryonic cerebral cortex is defined by the expression of multiple Wnt genes and is compromised in Gli3-deficient mice. *Development*. 125:2315-25.

Gschwendt, M., S. Dieterich, J. Rennecke, W. Kittstein, H.J. Mueller, and F.J. Johannes. 1996. Inhibition of protein kinase C mu by various inhibitors. Differentiation from protein kinase c isoenzymes. *FEBS Lett*. 392:77-80.

Guan, C.B., H.T. Xu, M. Jin, X.B. Yuan, and M.M. Poo. 2007. Long-range Ca2+ signaling from growth cone to soma mediates reversal of neuronal migration induced by slit-2. *Cell*. 129:385-95.

Gupta, A., K. Sanada, D.T. Miyamoto, S. Rovelstad, B. Nadarajah, A.L. Pearlman, J. Brunstrom, and L.H. Tsai. 2003. Layering defect in p35 deficiency is linked to improper neuronal-glial interaction in radial migration. *Nat Neurosci*. 6:1284-91.

Hack, I., M. Bancila, K. Loulier, P. Carroll, and H. Cremer. 2002. Reelin is a detachment signal in tangential chain-migration during postnatal neurogenesis. *Nat Neurosci*. 5:939-45.

Hacker, G. 2000. The morphology of apoptosis. *Cell Tissue Res*. 301:5-17.

Hart, P.E., G.M. Poynter, C.M. Whitehead, J.D. Orth, J.N. Glantz, R.C. Busby, S.L. Barrett, and J.L. Salisbury. 2001. Characterization of the X-linked murine centrin Cetn2 gene. *Gene*. 264:205-13.

Hartfuss, E., E. Forster, H.H. Bock, M.A. Hack, P. Leprince, J.M. Luque, J. Herz, M. Frotscher, and M. Gotz. 2003. Reelin signaling directly affects radial glia morphology and biochemical maturation. *Development*. 130:4597-609.

Hatanaka, Y., S. Hisanaga, C.W. Heizmann, and F. Murakami. 2004. Distinct migratory behavior of early- and late-born neurons derived from the cortical ventricular zone. *J Comp Neurol*. 479:1-14.

Hatten, M.E. 1993. The role of migration in central nervous system neuronal development. *Curr Opin Neurobiol*. 3:38-44.

Hatten, M.E. 2002. New directions in neuronal migration. *Science*. 297:1660-3.

Rivas, R.J., and M.E. Hatten. 1995. Motility and cytoskeletal organization of migrating cerebellar granule neurons. *J Neurosci*. 15:981-9.

He, X., J.P. Saint-Jeannet, J.R. Woodgett, H.E. Varmus, and I.B. Dawid. 1995. Glycogen synthase kinase-3 and dorsoventral patterning in Xenopus embryos. *Nature*. 374:617-22.

Higginbotham, H., S. Bielas, T. Tanaka, and J.G. Gleeson. 2004. Transgenic mouse line with green-fluorescent protein-labeled Centrin 2 allows visualization of the centrosome in living cells. *Transgenic Res*. 13:155-64.

Hinchcliffe, E.H., F.J. Miller, M. Cham, A. Khodjakov, and G. Sluder. 2001. Requirement of a centrosomal activity for cell cycle progression through G1 into S phase. *Science*. 291:1547-50.

Hinds, J.W., and T.L. Ruffett. 1971. Cell proliferation in the neural tube: an electron microscopic and golgi analysis in the mouse cerebral vesicle. *Z Zellforsch Mikrosk Anat*. 115:226-64.

Hu, H. 1999. Chemorepulsion of neuronal migration by Slit2 in the developing mammalian forebrain. *Neuron*. 23:703-11.

Jiang, H., W. Guo, X. Liang, and Y. Rao. 2005. Both the establishment and the maintenance of neuronal polarity require active mechanisms: critical roles of GSK-3beta and its upstream regulators. *Cell*. 120:123-35.

Jiang, M., C.L. Lee, K.L. Smith, and J.W. Swann. 1998. Spine loss and other persistent alterations of hippocampal pyramidal cell dendrites in a model of early-onset epilepsy. *J Neurosci*. 18:8356-68.

Joberty, G., C. Petersen, L. Gao, and I.G. Macara. 2000. The cell-polarity protein Par6 links Par3 and atypical protein kinase C to Cdc42. *Nat Cell Biol*. 2:531-9.

Kawauchi, T., and M. Hoshino. 2008. Molecular pathways regulating cytoskeletal organization and morphological changes in migrating neurons. *Dev Neurosci*. 30:36-46.

Keays, D.A., G. Tian, K. Poirier, G.J. Huang, C. Siebold, J. Cleak, P.L. Oliver, M. Fray, R.J. Harvey, Z. Molnar, M.C. Pinon, N. Dear, W. Valdar, S.D. Brown, K.E. Davies, J.N. Rawlins, N.J. Cowan, P. Nolan, J. Chelly, and J. Flint. 2007. Mutations in alpha-tubulin cause abnormal neuronal migration in mice and lissencephaly in humans. *Cell*. 128:45-57.

Kerjan, G., and J.G. Gleeson. 2007. Genetic mechanisms underlying abnormal neuronal migration in classical lissencephaly. *Trends Genet*. 23:623-30.

Kidd, T., K.S. Bland, and C.S. Goodman. 1999. Slit is the midline repellent for the robo receptor in Drosophila. *Cell*. 96:785-94.

Kidd, T., K. Brose, K.J. Mitchell, R.D. Fetter, M. Tessier-Lavigne, C.S. Goodman, and G. Tear. 1998. Roundabout controls axon crossing of the CNS midline and defines a novel subfamily of evolutionarily conserved guidance receptors. *Cell*. 92:205-15.

Klein, P.S., and D.A. Melton. 1996. A molecular mechanism for the effect of lithium on development. *Proc Natl Acad Sci U S A*. 93:8455-9.

Klotz, C., N. Garreau de Loubresse, F. Ruiz, and J. Beisson. 1997. Genetic evidence for a role of centrin-associated proteins in the organization and dynamics of the infraciliary lattice in Paramecium. *Cell Motil Cytoskeleton*. 38:172-86.

Knoblich, J.A. 2008. Mechanisms of asymmetric stem cell division. *Cell*. 132:583-97.

Koizumi, H., H. Higginbotham, T. Poon, T. Tanaka, B.C. Brinkman, and J.G. Gleeson. 2006a. Doublecortin maintains bipolar shape and nuclear translocation during migration in the adult forebrain. *Nat Neurosci*. 9:779-86.

Koizumi, H., T. Tanaka, and J.G. Gleeson. 2006b. Doublecortin-like kinase functions with doublecortin to mediate fiber tract decussation and neuronal migration. *Neuron*. 49:55-66.

Komuro, H., and T. Kumada. 2005. Ca2+ transients control CNS neuronal migration. *Cell Calcium*. 37:387-93.

Komuro, H., and P. Rakic. 1998. Orchestration of neuronal migration by activity of ion channels, neurotransmitter receptors, and intracellular Ca2+ fluctuations. *J Neurobiol*. 37:110-30.

Koonce, M.P., R.A. Cloney, and M.W. Berns. 1984. Laser irradiation of centrosomes in newt eosinophils: evidence of centriole role in motility. *J Cell Biol*. 98:1999-2010.

Kosaka, K., Y. Aika, K. Toida, C.W. Heizmann, W. Hunziker, D.M. Jacobowitz, I. Nagatsu, P. Streit, T.J. Visser, and T. Kosaka. 1995. Chemically defined neuron groups and their subpopulations in the glomerular layer of the rat main olfactory bulb. *Neurosci Res*. 23:73-88.

Laoukili, J., E. Perret, S. Middendorp, O. Houcine, C. Guennou, F. Marano, M. Bornens, and F. Tournier. 2000. Differential expression and cellular distribution of centrin isoforms during human ciliated cell differentiation in vitro. *J Cell Sci*. 113 (Pt 8):1355-64.

Leclerc, S., M. Garnier, R. Hoessel, D. Marko, J.A. Bibb, G.L. Snyder, P. Greengard, J. Biernat, Y.Z. Wu, E.M. Mandelkow, G. Eisenbrand, and L. Meijer. 2001. Indirubins inhibit glycogen synthase kinase-3 beta and CDK5/p25, two protein kinases involved in abnormal tau phosphorylation in Alzheimer's disease. A property common to most cyclin-dependent kinase inhibitors? *J Biol Chem*. 276:251-60.

Lee, S.M., S. Tole, E. Grove, and A.P. McMahon. 2000. A local Wnt-3a signal is required for development of the mammalian hippocampus. *Development*. 127:457-67.

Li, H.S., J.H. Chen, W. Wu, T. Fagaly, L. Zhou, W. Yuan, S. Dupuis, Z.H. Jiang, W. Nash, C. Gick, D.M. Ornitz, J.Y. Wu, and Y. Rao. 1999. Vertebrate slit, a secreted ligand for the transmembrane protein roundabout, is a repellent for olfactory bulb axons. *Cell*. 96:807-18.

Li, Z., D.E. McNulty, K.J. Marler, L. Lim, C. Hall, R.S. Annan, and D.B. Sacks. 2005. IQGAP1 promotes neurite outgrowth in a phosphorylation-dependent manner. *J Biol Chem*. 280:13871-8.

Lian, G., and V. Sheen. 2006. Cerebral developmental disorders. *Curr Opin Pediatr*. 18:614-20.

Lim, D.A., and A. Alvarez-Buylla. 1999. Interaction between astrocytes and adult subventricular zone precursors stimulates neurogenesis. *Proc Natl Acad Sci U S A*. 96:7526-31.

Lin, P.T., J.G. Gleeson, J.C. Corbo, L. Flanagan, and C.A. Walsh. 2000. DCAMKL1 encodes a protein kinase with homology to doublecortin that regulates microtubule polymerization. *J Neurosci*. 20:9152-61.

Liu, G., and Y. Rao. 2003. Neuronal migration from the forebrain to the olfactory bulb requires a new attractant persistent in the olfactory bulb. *J Neurosci*. 23:6651-9.

Lledo, P.M., and A. Saghatelyan. 2005. Integrating new neurons into the adult olfactory bulb: joining the network, life-death decisions, and the effects of sensory experience. *Trends Neurosci*. 28:248-54.

Lois, C., and A. Alvarez-Buylla. 1994. Long-distance neuronal migration in the adult mammalian brain. *Science*. 264:1145-8.

Lois, C., J.M. Garcia-Verdugo, and A. Alvarez-Buylla. 1996. Chain migration of neuronal precursors. *Science*. 271:978-81.

LoTurco, J.J., and J. Bai. 2006. The multipolar stage and disruptions in neuronal migration. *Trends Neurosci*. 29:407-13.

Lyuksyutova, A.I., C.C. Lu, N. Milanesio, L.A. King, N. Guo, Y. Wang, J. Nathans, M. Tessier-Lavigne, and Y. Zou. 2003. Anterior-posterior guidance of commissural axons by Wnt-frizzled signaling. *Science*. 302:1984-8.

Machon, O., C.J. van den Bout, M. Backman, R. Kemler, and S. Krauss. 2003. Role of beta-catenin in the developing cortical and hippocampal neuroepithelium. *Neuroscience*. 122:129-43.

Marin-Padilla, M. 1998. Cajal-Retzius cells and the development of the neocortex. *Trends Neurosci*. 21:64-71.

Marshall, W.F., Y. Vucica, and J.L. Rosenbaum. 2001. Kinetics and regulation of de novo centriole assembly. Implications for the mechanism of centriole duplication. *Curr Biol*. 11:308-17.

McConnell, S.K., and C.E. Kaznowski. 1991. Cell cycle dependence of laminar determination in developing neocortex. *Science*. 254:282-5.

McManus, M.F., I.M. Nasrallah, M.M. Pancoast, A. Wynshaw-Boris, and J.A. Golden. 2004. Lis1 is necessary for normal non-radial migration of inhibitory interneurons. *Am J Pathol*. 165:775-84.

Meads, T., and T.A. Schroer. 1995. Polarity and nucleation of microtubules in polarized epithelial cells. *Cell Motil Cytoskeleton*. 32:273-88.

Meijer, L., A.L. Skaltsounis, P. Magiatis, P. Polychronopoulos, M. Knockaert, M. Leost, X.P. Ryan, C.A. Vonica, A. Brivanlou, R. Dajani, C. Crovace, C. Tarricone, A. Musacchio, S.M. Roe, L. Pearl, and P. Greengard. 2003. GSK-3-selective inhibitors derived from Tyrian purple indirubins. *Chem Biol*. 10:1255-66.

Meraldi, P., J. Lukas, A.M. Fry, J. Bartek, and E.A. Nigg. 1999. Centrosome duplication in mammalian somatic cells requires E2F and Cdk2-cyclin A. *Nat Cell Biol*. 1:88-93.

Merkle, F.T., Z. Mirzadeh, and A. Alvarez-Buylla. 2007. Mosaic organization of neural stem cells in the adult brain. *Science*. 317:381-4.

Merkle, F.T., A.D. Tramontin, J.M. Garcia-Verdugo, and A. Alvarez-Buylla. 2004. Radial glia give rise to adult neural stem cells in the subventricular zone. *Proc Natl Acad Sci U S A*. 101:17528-32.

Metin, C., D. Deleglise, T. Serafini, T.E. Kennedy, and M. Tessier-Lavigne. 1997. A role for netrin-1 in the guidance of cortical efferents. *Development*. 124:5063-74.

Mimori-Kiyosue, Y., N. Shiina, and S. Tsukita. 2000. The dynamic behavior of the APC-binding protein EB1 on the distal ends of microtubules. *Curr Biol*. 10:865-8.

Miyoshi, H., U. Blomer, M. Takahashi, F.H. Gage, and I.M. Verma. 1998. Development of a self-inactivating lentivirus vector. *J Virol*. 72:8150-7.

Moberg, P.J., R. Agrin, R.E. Gur, R.C. Gur, B.I. Turetsky, and R.L. Doty. 1999. Olfactory dysfunction in schizophrenia: a qualitative and quantitative review. *Neuropsychopharmacology*. 21:325-40.

Mogensen, M.M., A. Malik, M. Piel, V. Bouckson-Castaing, and M. Bornens. 2000. Microtubule minus-end anchorage at centrosomal and non-centrosomal sites: the role of ninein. *J Cell Sci*. 113 (Pt 17):3013-23.

Molyneaux, B.J., P. Arlotta, J.R. Menezes, and J.D. Macklis. 2007. Neuronal subtype specification in the cerebral cortex. *Nat Rev Neurosci*. 8:427-37.

Moya, F., and M. Valdeolmillos. 2004. Polarized increase of calcium and nucleokinesis in tangentially migrating neurons. *Cereb Cortex*. 14:610-8.

Murase, S., and A.F. Horwitz. 2004. Directions in cell migration along the rostral migratory stream: the pathway for migration in the brain. *Curr Top Dev Biol*. 61:135-52.

Mussman, J.G., H.F. Horn, P.E. Carroll, M. Okuda, P. Tarapore, L.A. Donehower, and K. Fukasawa. 2000. Synergistic induction of centrosome hyperamplification by loss of p53 and cyclin E overexpression. *Oncogene*. 19:1635-46.

Nacher, J., C. Crespo, and B.S. McEwen. 2001. Doublecortin expression in the adult rat telencephalon. *Eur J Neurosci*. 14:629-44.

Nadarajah, B., J.E. Brunstrom, J. Grutzendler, R.O. Wong, and A.L. Pearlman. 2001. Two modes of radial migration in early development of the cerebral cortex. *Nat Neurosci*. 4:143-50.

Nguyen-Ba-Charvet, K.T., N. Picard-Riera, M. Tessier-Lavigne, A. Baron-Van Evercooren, C. Sotelo, and A. Chedotal. 2004. Multiple roles for slits in the control of cell migration in the rostral migratory stream. *J Neurosci*. 24:1497-506.

Ninkovic, J., and M. Gotz. 2007. Signaling in adult neurogenesis: from stem cell niche to neuronal networks. *Curr Opin Neurobiol*. 17:338-44.

Nobes, C.D., and A. Hall. 1999. Rho GTPases control polarity, protrusion, and adhesion during cell movement. *J Cell Biol*. 144:1235-44.

Noctor, S.C., A.C. Flint, T.A. Weissman, R.S. Dammerman, and A.R. Kriegstein. 2001. Neurons derived from radial glial cells establish radial units in neocortex. *Nature*. 409:714-20.

Noctor, S.C., V. Martinez-Cerdeno, L. Ivic, and A.R. Kriegstein. 2004. Cortical neurons arise in symmetric and asymmetric division zones and migrate through specific phases. *Nat Neurosci*. 7:136-44.

Noctor, S.C., V. Martinez-Cerdeno, and A.R. Kriegstein. 2008. Distinct behaviors of neural stem and progenitor cells underlie cortical neurogenesis. *J Comp Neurol*. 508:28-44.

Noritake, J., T. Watanabe, K. Sato, S. Wang, and K. Kaibuchi. 2005. IQGAP1: a key regulator of adhesion and migration. *J Cell Sci*. 118:2085-92.

O'Brien, J., and S.C. Lummis. 2004. Biolistic and diolistic transfection: using the gene gun to deliver DNA and lipophilic dyes into mammalian cells. *Methods*. 33:121-5.

Ogawa, M., T. Miyata, K. Nakajima, K. Yagyu, M. Seike, K. Ikenaka, H. Yamamoto, and K. Mikoshiba. 1995. The reeler gene-associated antigen on Cajal-Retzius neurons is a crucial molecule for laminar organization of cortical neurons. *Neuron*. 14:899-912.

Ohno, S. 2001. Intercellular junctions and cellular polarity: the PAR-aPKC complex, a conserved core cassette playing fundamental roles in cell polarity. *Curr Opin Cell Biol*. 13:641-8.

Ohshima, T., M. Hirasawa, H. Tabata, T. Mutoh, T. Adachi, H. Suzuki, K. Saruta, T. Iwasato, S. Itohara, M. Hashimoto, K. Nakajima, M. Ogawa, A.B. Kulkarni, and K. Mikoshiba. 2007. Cdk5 is required for multipolar-to-bipolar transition during radial neuronal migration and proper dendrite development of pyramidal neurons in the cerebral cortex. *Development*. 134:2273-82.

Okabe, M., M. Ikawa, K. Kominami, T. Nakanishi, and Y. Nishimune. 1997. 'Green mice' as a source of ubiquitous green cells. *FEBS Lett*. 407:313-9.

Palazzo, A.F., H.L. Joseph, Y.J. Chen, D.L. Dujardin, A.S. Alberts, K.K. Pfister, R.B. Vallee, and G.G. Gundersen. 2001. Cdc42, dynein, and dynactin regulate MTOC reorientation independent of Rho-regulated microtubule stabilization. *Curr Biol*. 11:1536-41.

Pang, T., R. Atefy, and V. Sheen. 2008. Malformations of cortical development. *Neurologist*. 14:181-91.

Paoletti, A., M. Moudjou, M. Paintrand, J.L. Salisbury, and M. Bornens. 1996. Most of centrin in animal cells is not centrosome-associated and centrosomal centrin is confined to the distal lumen of centrioles. *J Cell Sci*. 109 (Pt 13):3089-102.

Patel, S., L. Yenush, P.L. Rodriguez, R. Serrano, and T.L. Blundell. 2002. Crystal structure of an enzyme displaying both inositol-polyphosphate-1-phosphatase and 3'-phosphoadenosine-5'-phosphate phosphatase activities: a novel target of lithium therapy. *J Mol Biol*. 315:677-85.

Piel, M., P. Meyer, A. Khodjakov, C.L. Rieder, and M. Bornens. 2000. The respective contributions of the mother and daughter centrioles to centrosome activity and behavior in vertebrate cells. *J Cell Biol*. 149:317-30.

Piel, M., J. Nordberg, U. Euteneuer, and M. Bornens. 2001. Centrosome-dependent exit of cytokinesis in animal cells. *Science*. 291:1550-3.

Polleux, F., and A. Ghosh. 2002. The slice overlay assay: a versatile tool to study the influence of extracellular signals on neuronal development. *Sci STKE*. 2002:PL9.

Polleux, F., R.J. Giger, D.D. Ginty, A.L. Kolodkin, and A. Ghosh. 1998. Patterning of cortical efferent projections by semaphorin-neuropilin interactions. *Science*. 282:1904-6.

Polleux, F., T. Morrow, and A. Ghosh. 2000. Semaphorin 3A is a chemoattractant for cortical apical dendrites. *Nature*. 404:567-73.

Pombero, A., L. Valdes, C. Vieira, and S. Martinez. 2007. Developmental mechanisms and experimental models to understand forebrain malformative diseases. *Genes Brain Behav*. 6 Suppl 1:45-52.

Rakic, P. 1971. Guidance of neurons migrating to the fetal monkey neocortex. *Brain Res*. 33:471-6.

Rakic, P. 1972. Mode of cell migration to the superficial layers of fetal monkey neocortex. *J Comp Neurol*. 145:61-83.

Rakic, P. 1974. Neurons in rhesus monkey visual cortex: systematic relation between time of origin and eventual disposition. *Science*. 183:425-7.

Rakic, P. 2002. Neurogenesis in adult primate neocortex: an evaluation of the evidence. *Nat Rev Neurosci*. 3:65-71.

Rakic, P., E. Knyihar-Csillik, and B. Csillik. 1996. Polarity of microtubule assemblies during neuronal cell migration. *Proc Natl Acad Sci U S A*. 93:9218-22.

Ralston, E. 1993. Changes in architecture of the Golgi complex and other subcellular organelles during myogenesis. *J Cell Biol*. 120:399-409.

Ramos, R.L., J. Bai, and J.J. LoTurco. 2006. Heterotopia formation in rat but not mouse neocortex after RNA interference knockdown of DCX. *Cereb Cortex*. 16:1323-31.

Rasin, M.R., V.R. Gazula, J.J. Breunig, K.Y. Kwan, M.B. Johnson, S. Liu-Chen, H.S. Li, L.Y. Jan, Y.N. Jan, P. Rakic, and N. Sestan. 2007. Numb and Numbl are required for maintenance of cadherin-based adhesion and polarity of neural progenitors. *Nat Neurosci*. 10:819-27.

Richards, L.J., S.E. Koester, R. Tuttle, and D.D. O'Leary. 1997. Directed growth of early cortical axons is influenced by a chemoattractant released from an intermediate target. *J Neurosci*. 17:2445-58.

Ridley, A.J., M.A. Schwartz, K. Burridge, R.A. Firtel, M.H. Ginsberg, G. Borisy, J.T. Parsons, and A.R. Horwitz. 2003. Cell migration: integrating signals from front to back. *Science*. 302:1704-9.

Rivas, R.J., and M.E. Hatten. 1995. Motility and cytoskeletal organization of migrating cerebellar granule neurons. *J Neurosci*. 15:981-9.

Rosenblatt, J., L.P. Cramer, B. Baum, and K.M. McGee. 2004. Myosin II-dependent cortical movement is required for centrosome separation and positioning during mitotic spindle assembly. *Cell*. 117:361-72.

Ross, M.E. 2002. Full circle to cobbled brain. *Nature*. 418:376-7.

Rothberg, J.M., J.R. Jacobs, C.S. Goodman, and S. Artavanis-Tsakonas. 1990. slit: an extracellular protein necessary for development of midline glia and commissural axon pathways contains both EGF and LRR domains. *Genes Dev*. 4:2169-87.

Rubinson, D.A., C.P. Dillon, A.V. Kwiatkowski, C. Sievers, L. Yang, J. Kopinja, D.L. Rooney, M. Zhang, M.M. Ihrig, M.T. McManus, F.B. Gertler, M.L. Scott, and L. Van Parijs. 2003. A lentivirus-based system to functionally silence genes in primary mammalian cells, stem cells and transgenic mice by RNA interference. *Nat Genet*. 33:401-6.

Salisbury, J.L., K.M. Suino, R. Busby, and M. Springett. 2002. Centrin-2 is required for centriole duplication in mammalian cells. *Curr Biol*. 12:1287-92.

Sameshima, M., Y. Imai, and Y. Hashimoto. 1988. The position of the microtubule-organizing center relative to the nucleus is independent of the direction of cell migration in Dictyostelium discoideum. *Cell Motil Cytoskeleton*. 9:111-6.

Sanchez, C., M. Perez, and J. Avila. 2000. GSK3beta-mediated phosphorylation of the microtubule-associated protein 2C (MAP2C) prevents microtubule bundling. *Eur J Cell Biol*. 79:252-60.

Schaar, B.T., K. Kinoshita, and S.K. McConnell. 2004. Doublecortin microtubule affinity is regulated by a balance of kinase and phosphatase activity at the leading edge of migrating neurons. *Neuron*. 41:203-13.

Schaar, B.T., and S.K. McConnell. 2005. Cytoskeletal coordination during neuronal migration. *Proc Natl Acad Sci U S A*. 102:13652-7.

Schliwa, M., U. Euteneuer, R. Graf, and M. Ueda. 1999. Centrosomes, microtubules and cell migration. *Biochem Soc Symp*. 65:223-31.

Schliwa, M., K.B. Pryzwansky, and U. Euteneuer. 1982. Centrosome splitting in neutrophils: an unusual phenomenon related to cell activation and motility. *Cell*. 31:705-17.

Schmechel, D.E., and P. Rakic. 1979. A Golgi study of radial glial cells in developing monkey telencephalon: morphogenesis and transformation into astrocytes. *Anat Embryol (Berl)*. 156:115-52.

Selemon, L.D., A. Begovic, P.S. Goldman-Rakic, and S.A. Castner. 2007. Amphetamine sensitization alters dendritic morphology in prefrontal cortical pyramidal neurons in the non-human primate. *Neuropsychopharmacology*. 32:919-31.

Shen, Q., Y. Wang, J.T. Dimos, C.A. Fasano, T.N. Phoenix, I.R. Lemischka, N.B. Ivanova, S. Stifani, E.E. Morrisey, and S. Temple. 2006. The timing of cortical neurogenesis is encoded within lineages of individual progenitor cells. *Nat Neurosci*. 9:743-51.

Shi, S.H., T. Cheng, L.Y. Jan, and Y.N. Jan. 2004. APC and GSK-3beta are involved in mPar3 targeting to the nascent axon and establishment of neuronal polarity. *Curr Biol*. 14:2025-32.

Shi, S.H., L.Y. Jan, and Y.N. Jan. 2003. Hippocampal neuronal polarity specified by spatially localized mPar3/mPar6 and PI 3-kinase activity. *Cell*. 112:63-75.

Shoukimas, G.M., and J.W. Hinds. 1978. The development of the cerebral cortex in the embryonic mouse: an electron microscopic serial section analysis. *J Comp Neurol*. 179:795-830.

Shu, T., R. Ayala, M.D. Nguyen, Z. Xie, J.G. Gleeson, and L.H. Tsai. 2004. Ndel1 operates in a common pathway with LIS1 and cytoplasmic dynein to regulate cortical neuronal positioning. *Neuron*. 44:263-77.

Shu, T., H.C. Tseng, T. Sapir, P. Stern, Y. Zhou, K. Sanada, A. Fischer, F.M. Coquelle, O. Reiner, and L.H. Tsai. 2006. Doublecortin-like kinase controls neurogenesis by regulating mitotic spindles and M phase progression. *Neuron*. 49:25-39.

Sluder, G., F.J. Miller, and C.L. Rieder. 1989. Reproductive capacity of sea urchin centrosomes without centrioles. *Cell Motil Cytoskeleton*. 13:264-73.

Solecki, D.J., L. Model, J. Gaetz, T.M. Kapoor, and M.E. Hatten. 2004. Par6alpha signaling controls glial-guided neuronal migration. *Nat Neurosci*. 7:1195-203.

Standaert, M.L., G. Bandyopadhyay, M.P. Sajan, L. Cong, M.J. Quon, and R.V. Farese. 1999. Okadaic acid activates atypical protein kinase C (zeta/lambda) in rat and 3T3/L1 adipocytes. An apparent requirement for activation of Glut4 translocation and glucose transport. *J Biol Chem*. 274:14074-8.

Standaert, M.L., L. Galloway, P. Karnam, G. Bandyopadhyay, J. Moscat, and R.V. Farese. 1997. Protein kinase C-zeta as a downstream effector of

phosphatidylinositol 3-kinase during insulin stimulation in rat adipocytes. Potential role in glucose transport. *J Biol Chem*. 272:30075-82.

Stearns, T., L. Evans, and M. Kirschner. 1991. Gamma-tubulin is a highly conserved component of the centrosome. *Cell*. 65:825-36.

Stevenson, V.A., J. Kramer, J. Kuhn, and W.E. Theurkauf. 2001. Centrosomes and the Scrambled protein coordinate microtubule-independent actin reorganization. *Nat Cell Biol*. 3:68-75.

Tabata, H., and K. Nakajima. 2001. Efficient in utero gene transfer system to the developing mouse brain using electroporation: visualization of neuronal migration in the developing cortex. *Neuroscience*. 103:865-72.

Tabata, H., and K. Nakajima. 2003. Multipolar migration: the third mode of radial neuronal migration in the developing cerebral cortex. *J Neurosci*. 23:9996-10001.

Takahashi, H., and F.C. Liu. 2006. Genetic patterning of the mammalian telencephalon by morphogenetic molecules and transcription factors. *Birth Defects Res C Embryo Today*. 78:256-66.

Tanaka, T., F.F. Serneo, C. Higgins, M.J. Gambello, A. Wynshaw-Boris, and J.G. Gleeson. 2004a. Lis1 and doublecortin function with dynein to mediate coupling of the nucleus to the centrosome in neuronal migration. *J Cell Biol*. 165:709-21.

Tanaka, T., F.F. Serneo, H.C. Tseng, A.B. Kulkarni, L.H. Tsai, and J.G. Gleeson. 2004b. Cdk5 phosphorylation of doublecortin ser297 regulates its effect on neuronal migration. *Neuron*. 41:215-27.

Tassin, A.M., B. Maro, and M. Bornens. 1985a. Fate of microtubule-organizing centers during myogenesis in vitro. *J Cell Biol*. 100:35-46.

Tassin, A.M., M. Paintrand, E.G. Berger, and M. Bornens. 1985b. The Golgi apparatus remains associated with microtubule organizing centers during myogenesis. *J Cell Biol*. 101:630-8.

Tramontin, A.D., J.M. Garcia-Verdugo, D.A. Lim, and A. Alvarez-Buylla. 2003. Postnatal development of radial glia and the ventricular zone (VZ): a continuum of the neural stem cell compartment. *Cereb Cortex*. 13:580-7.

Tsai, J.W., Y. Chen, A.R. Kriegstein, and R.B. Vallee. 2005. LIS1 RNA interference blocks neural stem cell division, morphogenesis, and motility at multiple stages. *J Cell Biol*. 170:935-45.

Tsai, L.H., and J.G. Gleeson. 2005. Nucleokinesis in neuronal migration. *Neuron*. 46:383-8.

Tuy, F.P., Y. Saillour, C. Kappeler, J. Chelly, and F. Francis. 2008. Alternative transcripts of Dclk1 and Dclk2 and their expression in doublecortin knockout mice. *Dev Neurosci*. 30:171-86.

Uchida, Y., T. Ohshima, Y. Sasaki, H. Suzuki, S. Yanai, N. Yamashita, F. Nakamura, K. Takei, Y. Ihara, K. Mikoshiba, P. Kolattukudy, J. Honnorat, and Y. Goshima. 2005. Semaphorin3A signalling is mediated via sequential Cdk5 and GSK3beta phosphorylation of CRMP2: implication of common phosphorylating mechanism underlying axon guidance and Alzheimer's disease. *Genes Cells*. 10:165-79.

Ueda, M., R. Graf, H.K. MacWilliams, M. Schliwa, and U. Euteneuer. 1997. Centrosome positioning and directionality of cell movements. *Proc Natl Acad Sci U S A*. 94:9674-8.

Vaughan, K.T., S.H. Tynan, N.E. Faulkner, C.J. Echeverri, and R.B. Vallee. 1999. Colocalization of cytoplasmic dynein with dynactin and CLIP-170 at microtubule distal ends. *J Cell Sci*. 112 (Pt 10):1437-47.

Vreugdenhil, E., S.M. Kolk, K. Boekhoorn, C.P. Fitzsimons, M. Schaaf, T. Schouten, A. Sarabdjitsingh, R. Sibug, and P.J. Lucassen. 2007. Doublecortin-like, a microtubule-associated protein expressed in radial glia, is crucial for neuronal precursor division and radial process stability. *Eur J Neurosci*. 25:635-48.

Wang, K.H., K. Brose, D. Arnott, T. Kidd, C.S. Goodman, W. Henzel, and M. Tessier-Lavigne. 1999. Biochemical purification of a mammalian slit protein as a positive regulator of sensory axon elongation and branching. *Cell*. 96:771-84.

Wang, S., T. Watanabe, J. Noritake, M. Fukata, T. Yoshimura, N. Itoh, T. Harada, M. Nakagawa, Y. Matsuura, N. Arimura, and K. Kaibuchi. 2007. IQGAP3, a novel effector of Rac1 and Cdc42, regulates neurite outgrowth. *J Cell Sci*. 120:567-77.

Ward, M., C. McCann, M. DeWulf, J.Y. Wu, and Y. Rao. 2003. Distinguishing between directional guidance and motility regulation in neuronal migration. *J Neurosci*. 23:5170-7.

Ward, M.E., H. Jiang, and Y. Rao. 2005. Regulated formation and selection of neuronal processes underlie directional guidance of neuronal migration. *Mol Cell Neurosci*. 30:378-87.

Weiss, K.H., C. Johanssen, A. Tielsch, J. Herz, T. Deller, M. Frotscher, and E. Forster. 2003. Malformation of the radial glial scaffold in the dentate gyrus of reeler mice, scrambler mice, and ApoER2/VLDLR-deficient mice. *J Comp Neurol*. 460:56-65.

Weissman, T.A., P.A. Riquelme, L. Ivic, A.C. Flint, and A.R. Kriegstein. 2004. Calcium waves propagate through radial glial cells and modulate proliferation in the developing neocortex. *Neuron*. 43:647-61.

White, R.A., Z. Pan, and J.L. Salisbury. 2000. GFP-centrin as a marker for centriole dynamics in living cells. *Microsc Res Tech*. 49:451-7.

Whitford, K.L., V. Marillat, E. Stein, C.S. Goodman, M. Tessier-Lavigne, A. Chedotal, and A. Ghosh. 2002. Regulation of cortical dendrite development by Slit-Robo interactions. *Neuron*. 33:47-61.

Wichterle, H., J.M. Garcia-Verdugo, D.G. Herrera, and A. Alvarez-Buylla. 1999. Young neurons from medial ganglionic eminence disperse in adult and embryonic brain. *Nat Neurosci*. 2:461-6.

Winner, B., C.M. Cooper-Kuhn, R. Aigner, J. Winkler, and H.G. Kuhn. 2002. Long-term survival and cell death of newly generated neurons in the adult rat olfactory bulb. *Eur J Neurosci*. 16:1681-9.

Wolf, A.M., A.I. Lyuksyutova, A.G. Fenstermaker, B. Shafer, C.G. Lo, and Y. Zou. 2008. Phosphatidylinositol-3-kinase-atypical protein kinase C signaling is required for Wnt attraction and anterior-posterior axon guidance. *J Neurosci*. 28:3456-67.

Wolfrum, U., A. Giessl, and A. Pulvermuller. 2002. Centrins, a novel group of Ca2+-binding proteins in vertebrate photoreceptor cells. *Adv Exp Med Biol*. 514:155-78.

Wong, K., X.R. Ren, Y.Z. Huang, Y. Xie, G. Liu, H. Saito, H. Tang, L. Wen, S.M. Brady-Kalnay, L. Mei, J.Y. Wu, W.C. Xiong, and Y. Rao. 2001. Signal transduction in neuronal migration: roles of GTPase activating proteins and the small GTPase Cdc42 in the Slit-Robo pathway. *Cell*. 107:209-21.

Wu, W., K. Wong, J. Chen, Z. Jiang, S. Dupuis, J.Y. Wu, and Y. Rao. 1999. Directional guidance of neuronal migration in the olfactory system by the protein Slit. *Nature*. 400:331-6.

Xie, Z., L.Y. Moy, K. Sanada, Y. Zhou, J.J. Buchman, and L.H. Tsai. 2007. Cep120 and TACCs control interkinetic nuclear migration and the neural progenitor pool. *Neuron*. 56:79-93.

Xu, H.T., X.B. Yuan, C.B. Guan, S. Duan, C.P. Wu, and L. Feng. 2004. Calcium signaling in chemorepellant Slit2-dependent regulation of neuronal migration. *Proc Natl Acad Sci U S A*. 101:4296-301.

Xu, X., Z. Weaver, S.P. Linke, C. Li, J. Gotay, X.W. Wang, C.C. Harris, T. Ried, and C.X. Deng. 1999. Centrosome amplification and a defective G2-M cell cycle

checkpoint induce genetic instability in BRCA1 exon 11 isoform-deficient cells. *Mol Cell*. 3:389-95.

Yan, X., F. Li, Y. Liang, Y. Shen, X. Zhao, Q. Huang, and X. Zhu. 2003. Human Nudel and NudE as regulators of cytoplasmic dynein in poleward protein transport along the mitotic spindle. *Mol Cell Biol*. 23:1239-50.

Yoon, K., S. Nery, M.L. Rutlin, F. Radtke, G. Fishell, and N. Gaiano. 2004. Fibroblast growth factor receptor signaling promotes radial glial identity and interacts with Notch1 signaling in telencephalic progenitors. *J Neurosci*. 24:9497-506.

Yoshihara, S., K. Omichi, M. Yanazawa, K. Kitamura, and Y. Yoshihara. 2005. Arx homeobox gene is essential for development of mouse olfactory system. *Development*. 132:751-62.

Yoshimura, T., Y. Kawano, N. Arimura, S. Kawabata, A. Kikuchi, and K. Kaibuchi. 2005. GSK-3beta regulates phosphorylation of CRMP-2 and neuronal polarity. *Cell*. 120:137-49.

Young, K.M., M. Fogarty, N. Kessaris, and W.D. Richardson. 2007. Subventricular zone stem cells are heterogeneous with respect to their embryonic origins and neurogenic fates in the adult olfactory bulb. *J Neurosci*. 27:8286-96.

Yu, W., V.E. Centonze, F.J. Ahmad, and P.W. Baas. 1993. Microtubule nucleation and release from the neuronal centrosome. *J Cell Biol*. 122:349-59.

Yvon, A.M., J.W. Walker, B. Danowski, C. Fagerstrom, A. Khodjakov, and P. Wadsworth. 2002. Centrosome reorientation in wound-edge cells is cell type specific. *Mol Biol Cell*. 13:1871-80.

Zhao, C., W. Deng, and F.H. Gage. 2008. Mechanisms and functional implications of adult neurogenesis. *Cell*. 132:645-60.

Zheng, Y., M.K. Jung, and B.R. Oakley. 1991. Gamma-tubulin is present in Drosophila melanogaster and Homo sapiens and is associated with the centrosome. *Cell*. 65:817-23.

Zhou, C.J., C. Zhao, and S.J. Pleasure. 2004a. Wnt signaling mutants have decreased dentate granule cell production and radial glial scaffolding abnormalities. *J Neurosci*. 24:121-6.

Zhou, F.Q., J. Zhou, S. Dedhar, Y.H. Wu, and W.D. Snider. 2004b. NGF-induced axon growth is mediated by localized inactivation of GSK-3beta and functions of the microtubule plus end binding protein APC. *Neuron*. 42:897-912.

Zmuda, J.F., and R.J. Rivas. 1998. The Golgi apparatus and the centrosome are localized to the sites of newly emerging axons in cerebellar granule neurons in vitro. *Cell Motil Cytoskeleton*. 41:18-38.

Zmuda, J.F., and R.J. Rivas. 2000. Actin filament disruption blocks cerebellar granule neurons at the unipolar stage of differentiation in vitro. *J Neurobiol*. 43:313-28.

Zumbrunn, J., K. Kinoshita, A.A. Hyman, and I.S. Nathke. 2001. Binding of the adenomatous polyposis coli protein to microtubules increases microtubule stability and is regulated by GSK3 beta phosphorylation. *Curr Biol*. 11:44-9.